2007

Highly Correlated Lanthanide Intermetallic And Oxide Phases: Crystal Growth And Structure-Property Relationships

Jasmine N. Millican
Louisiana State University and Agricultural and Mechanical College, jmilli1@lsu.edu

HIGHLY CORRELATED LANTHANIDE INTERMETALLIC AND OXIDE PHASES: CRYSTAL GROWTH AND STRUCTURE - PROPERTY RELATIONSHIPS

A Dissertation

Submitted to the Graduate Faculty of the
Louisiana State University and
Agricultural and Mechanical College
in partial fulfillment of the
requirements for the degree of
Doctor of Philosophy

in

The Department of Chemistry

by
Jasmine N. Millican
B.S., Southern University and A&M College, 2002
May 2007

DEDICATION

This document is dedicated to those that came before me, made a difference, and passed to the great beyond before they could fully realize the fruits of their labors. Thank you, for supporting me, inspiring me, and leading me either in spirit or by example. Your positive impacts and contributions to society will not be forgotten.

- ✧ **Nathaniel Henry Millican** (Maternal Great Grandfather) - Started the human relations division for improving employee relations at ESSO (EXXON Corporation), Baton Rouge, Louisiana
- ✧ **Frank B. Millican, Sr.** (Maternal Great uncle) - School Board Member, East Baton Rouge Parish
- ✧ **Steve B. Millican, Sr.** (Maternal Grandfather) -1st Black police officer in East Baton Rouge Parish
- ✧ **Kemp Thomas, Jr.** (Paternal Grandfather) - The Airport Kid- Boxer- Baton Rouge, Louisiana
- ✧ **Nettie Millican** (Maternal Great Aunt) – Secretary of the NAACP, 2 Governor Appointed Positions: Louisiana Pardon Board and Port Commissioner
- ✧ **John W. Millican** (Maternal Uncle) - City Court Judge, Chattanooga, TN

ACKNOWLEDGEMENTS

I would like to first thank God for his blessings, for sustaining me, and for directing my paths. Once again I realize that "through him, all things are possible".

Professionally, I would like to thank the Department of Chemistry at Louisiana State University, my committee members, colleagues, and collaborators for your words of scientific wisdom, advice, and encouragement. I would also like the funding agencies that have funded my research: NSF Career (DMR-0237664), PRF# 38274-G5, and the Alfred P. Sloan Foundation.

Thank you, to my research advisor, Dr. Julia Y. Chan, for your guidance, understanding, and for always going beyond the call of duty (even if that means having a student like me harass you at home). You have given me creative freedom as a scientist to try new things experimentally, which has greatly enhanced my scientific knowledge and abilities (no matter how much it cost you in Pd and Pt). Your "boot camp" tactics and dedication to making your students successful scientists is remarkable, and you have taught me the importance of hard work and how to even find knowledge where most people would least expect it (failed experiments).

To Dr. George Stanley, thank you for your good advice, great example of service in the scientific community, cheerful spirit, humor, and M&Ms. Thank you, Dr. Andrew Maverick, for asking the tough questions and challenging me to think "outside the box". Thank you, Dr. David Young for always putting time aside to explain (sometimes more than one time) complex physical behavior and phenomena, such as Kondo and RKKY interactions and also for managing to keep a straight face, when I occasionally tried to pronounce the Japanese scientists' names (Ruderman, Kittel, Kasuya, and Yosida).

Thank you, to my collaborators, David P. Young and Monica Moldovan (Department of Physics and Astronomy, LSU), Meigan Aronson (Brookhaven National Laboratory, NY), and

Satoru Nakatsujii (University of Tokyo, Japan), whom without, none of this work would be possible. I would also like to thank Dr. Frank Fronczek for sharing his wealth of knowledge and love of crystallography with me.

Personally, I would like to first thank God for blessing me with a wonderful mother, Shermaine M. Thomas, who could stand as an example to all mothers. She is the smartest woman that I have encountered in this life, and I strive to become half the woman that she is. She has been a constant protector, provider, strict disciplinarian, and friend. Thank you, for always making me take the road less traveled rather than the road of least resistance; whether by encouraging words or by "brute force" and for making the hard decisions even if and when they were unpopular. You have taught me that "the world is full of smart and talented people", but hard work and determination are just as important (if not more important) in discovering true success. Against all odds (and the statistics), you have managed to successfully raise three "young, black, female scientists"- a 100% success rate. I could not imagine getting to this level without your unconditional love, self sacrifice, perseverance, and gentle nudges in the right direction. I am eternally grateful for your guidance and love.

To my fathers, Kemp Thomas, III and Tyronne Perry, I would like to thank each of you for investing in me, whether it was emotionally, spiritually, or financially. You have both contributed in my upbringing and taken over the role of father at different stages in my life without hesitation.

To my "daddy", Kemp Thomas, III, thanks for raising me up from a baby, when you used to take me fishing and hunting (on your shoulders). From your shoulders, I learned to view the world from a new perspective- always looking up. You have always taught me to respect the Lord and to put him first in all my endeavors. You have continued to pray for me even when I

forgot to pray for myself. You also taught me the importance of self discipline, tough love, good moral values, and knowing how to skin a catfish.

To my "step-daddy," Tyronne Perry, thank you for supporting me even at the point "when I thought I was all grown up." You have tremendously enhanced the quality of life in our family. Thank you, for always supporting me whether that meant putting me in my place, keeping me mobile, or teaching me the importance of putting oil in my car (Who would have thought that a motor would blow up without it?). You are greatly appreciated.

I would also like to thank my "little" sisters and closest friends, Kandace R. Thomas and Angela C. Thomas, for always keeping me on my "P's and Q's" and giving me a reason to strive to do my best because I always wanted to be a positive role model for you both. In turn, I can now actually look to both of you for advice and encouragement. Thank you, for your support, unconditional love, and shoulders to lean on.

I would be amiss if I failed to mention the great support and love that I have received from my maternal grandmother, Ms. Augustine Millican. We have shared a special bond since before I can remember, and she has been a great influence on my life and has taught me how to be strong in the midst of despair. Because of her, failure was not an option for me- I live to make her proud and to let her know that her hard work and belief in me has not been in vain. Throughout this long journey, I could always count on her for unchanging love, encouragement, heart to heart conversations, and a hot meal or two. I would also like to thank my maternal aunt, Ms. Mary Millican, for her support- even if that meant struggling to read and understand some of my "scientific materials".

I have also been blessed with many memorable mentors throughout my life, who have believed in me and guided me in my quest for understanding and knowledge. The first of these

mentors was Mr. Lafayette Harrison, who was my fifth grade teacher; his alacrity for reaching students has made an indelible difference in my life and enjoyment of learning. I would also like to acknowledge my mentors, Dr. Mildred Smalley, Dr. Ella Kelley, and Dr. Diola Bagayoko at Southern University and A&M College, who were relentless in making sure that I pursued an advanced degree. They made sure that I obtained all the research and training experiences necessary for me to be well prepared for the next stage in my life.

I would also like to express my gratitude to all of my friends, who have been my personal pep squad through out it all. My research group members, who are more like family to me, have also been constant source of support. Dr. Robin Macaluso, Dr. Willa Williams, Dr. Evan Thomas, Edem Okudzeto, Dixie Gautreaux, and Jung Young Cho, you are greatly appreciated.

In particular, I would like to give special thanks to Dr. Evan L. Thomas, who has been a good friend to me for over 14 years (even though he will only admit to about 9). He has endured this long journey with me and shared my many triumphs and disappointments. Thanks for always being a very good listener, maintaining a sense of humor, contributing to our "little philosophical discussions", and helping me to maintain my sanity.

I would also like to thank my dear friend, Frankline C. Kimbeng, who has greatly enhanced my quality of life and encouraged me to broaden my horizons and to become a more well- rounded individual. Thanks for explaining the past 300 years of history and politics to me (Why don't we take classes for that sort of thing?). Your perseverance, work ethic, and relentless pursuit of knowledge has been an inspiration to me and has made me re-evaluate what I truly consider doing my personal best.

I would like to thank all of the other countless colleagues, family members, and friends, who have helped me to accomplish my goals. Although you may not have been acknowledged here specifically, you are also greatly appreciated.

TABLE OF CONTENTS

ABSTRACT

Our primary research goals are to synthesize, characterize, and study the structure, dimensionality, and physical properties of new highly correlated electron materials. Intermetallic lanthanide and oxide phases are of great interest due to their fascinating array of structural features and physical property phenomena, such as heavy fermion behavior, superconductivity, and magnetism. The crystal growth, structure, and physical properties of several different classes of materials, such as the *Ln*-*M*-Ga (*Ln* = La, Ce, Pr, *M* = Ni, Pd), Yb_5Pt_9, and $R_2Ir_2O_7$ (R = Pr, Eu) compounds, will be highlighted within. The *Ln*-*M*-Ga phases allow us to examine the influence of the lanthanide environments, dimensionality and layering on the magnetic and transport properties in these compounds. For example, $CePdGa_6$ is a heavy fermion with $\gamma \sim 230$ mJ mol^{-1} K^{-2} and exhibits an anisotropic magnetism with $T_N \sim 5.5$ K. The structurally related compound, Ce_2PdGa_{10}, also shows enhanced mass behavior ($\gamma \sim 220$ mJ/mol-K^2), exhibits paramagnetic behavior down to 2 K, and has a large positive *MR* > 200 % at 2 K and 9 T. Also bearing a striking resemblance to the $CePdGa_6$ phase, Ce_2PdGa_{12} is an antiferromagnetic heavy fermion with $\gamma \sim 170$ mJ mol^{-1} K^{-2} and a magnetic transition at $T_N \sim 11$ K. The crystal structures and physical properties of several new Ln_2NiGa_{10} (Ln = La, Ce, Pr) and Ln_2NiGa_{12} (*Ln* = La, Ce, Pr) compounds will also be discussed and compared to determine the role of the lanthanide and transition metal environments. The oxide pyrochlores, $R_2Ir_2O_7$ (*R* = Pr, Eu), which show geometrically frustrated magnetism, may also offer insight into the structure-property relationships in three dimensional materials.

CHAPTER I. INTRODUCTION

1.1. Overview

Highly correlated electronic materials, which exhibit strong conduction and *f*-electron correlations, are of considerable interest due to the exotic physical phenomena that they may exhibit, such as magnetism, superconductivity (SC), and heavy fermion behavior (HF).[1-4] In HF materials, there is a strong coupling of the *f*-electrons and conduction electrons at low temperatures resulting in a large effective mass of the electrons (10^2-10^3 times that of a free electron).[1-4] Highly correlated materials, which exhibit the unusual co-existence of two or more physical phenomena, such as HF behavior[3, 5, 6] and SC,[7] are ideal to study quantum critical behavior—an area of instability that lies between two stable states of matter.[8-10] In general, a quantum critical point occurs when the ordering temperature of a cooperative phase, such as magnetic order, approaches absolute zero. In materials near a quantum critical point (QCP), as the temperature approaches absolute zero, two unstable quantum phases may be in competition, often leading to new exotic physical behavior. To

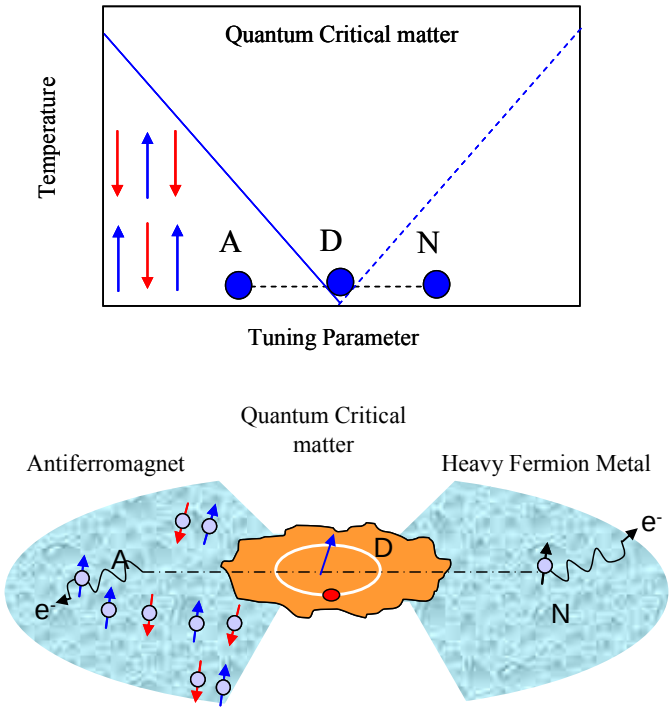

Adapted from: Coleman, P. and Schofield, A. J., Nature, Vol. 433, 2005, pp. 227.

Figure 1. Quantum critical phase diagram. *A* represents antiferomagnetically ordered (AFM) region, *N* represents a normal metal, and *D* represents the quantum critical region.

prevent this instability, superconductivity is often the escape route.[8] Subsequently, new physical behavior can be found once materials are driven close to a QCP.[9-11] As shown in Figure 1, materials that lie near a QCP can be altered by adjusting tuning parameters, such as magnetic field,[12-14] chemical pressure (doping),[15, 16] or external pressure.[10, 17] Quantum criticality in the heavy fermion Ce_nMIn_{3n+2} (M = Co, Rh, and Ir; n = 1, 2, ∞) compounds has been extensively studied.[18-23] For instance, while the $CeCoIn_5$[23-25] and $CeIrIn_5$[25, 26] compounds were found to become superconducting at T_c = 2.3 and 0.4 K, respectively, under ambient pressure, in the $CeRhIn_5$[8, 19] (T_c = 2.1 K) and Ce_2RhIn_8[18, 22, 27] (T_c = 2.0 K) compounds, the co-existence of superconductivity and antiferromagnetic (AFM) behavior is achieved by applying pressures of 16 and 25 kbar, respectively. It has been suggested that quantum critical behavior has also been found in new materials with unconventional behavior, such as $PrOs_4Sb_{12}$, which is the only Pr-based superconducting (Tc ~1.85 K) heavy fermion.[28, 29]

In order to better understand the relationship between the structure and physical property behavior of highly correlated materials, we have studied several different types of materials, such as lanthanide intermetallic and oxide phases. In our exploration to find new heavy fermion materials, we have been able to synthesize several layered ternary Ce-Pd-Ga compounds: $CePdGa_6$,[30] Ce_2PdGa_{10},[31] and Ce_2PdGa_{12}.[32] $CePdGa_6$ is a heavy fermion material with γ ~ 230 mJ mol^{-1} K^{-2} and exhibits an anisotropic magnetism with T_N ~ 5.5 K.[30] Ce_2PdGa_{10} also shows enhanced mass behavior and has a large positive magnetoresistance (MR) greater than 200 % at 2 K and 9 T.[31] Ce_2PdGa_{12} is an antiferromagnetic heavy fermion with γ ~ 170 mJ mol^{-1} K^{-2} and a magnetic transition at T_N ~ 11 K.[32] These Ce-Pd-Ga phases allow us to examine the influence of the Ce environment, dimensionality and layering on the magnetic and transport properties. Two competing mechanisms, Kondo and RKKY interactions, have been used to rationalize ordering

temperatures in this family of Ce-Pd-Ga phases.[33-35] The Kondo effect results from the introduction of a magnetic impurity into a metallic host.[36, 37] This causes the local moments to be screened by the conduction electrons below a Kondo coherence temperature (T_K), resulting in a minimum in the resistivity of the material.[37] The RKKY (Ruderman, Kittel, Kasuya, and Yosida) interaction is a consequence of exchange coupling between the magnetic ions and conduction electrons- resulting in the magnetization of the conduction electrons.[36] This causes an indirect exchange between two distant magnetic ions, which ultimately increases the magnetic interactions.

In our desire to further investigate quantum criticality, we have determined the crystal structure of a new unconventional heavy fermion, Yb_5Pt_9, which exhibits ferromagnetic behavior. We have also studied frustrated magnetism in the oxide pyrochlore, $R_2Ir_2O_7$ (R = Pr, Eu) phases as a function of temperature. The structure of the oxide pyrochlore may give further insight as to how structural features can directly affect the property behavior in materials.

1.2. Crystal Growth

In order to synthesize high quality, phase pure single crystals of lanthanide intermetallic compounds for physical property measurements, we have employed flux growth methods. Typically, stoichiometric ratios of 1:1:20 of lanthanide (*Ln*), transition metal (*M*), and main group elements (*X*), respectively, are combined and placed into an alumina crucible. The low melting point of the main group element is used to lower the melting point of the lanthanide and transition metal elements, which typically have higher melting points. Quartz wool is placed over the sample and acts as a filter. The sample is then sealed in an evacuated fused silica tube to avoid exposure and oxidation. A high temperature furnace is then used to heat the sample according to a temperature profile. A typical profile consists of heating the sample in the

temperature range of 1273 K to 1423 K and then slowly cooling the sample to a target temperature at rates of 2-8 K/h. After the sample is allowed to cool to a preferred temperature above the melting point of the flux used, the ampoule is inverted and centrifuged to remove excess flux. Typically, metallic single crystals ranging in size from 0.25 x 0.25 x 0.25 mm^3 to 5 x 5 x 5 mm^3, are retrieved, as shown in Figure 1.2.

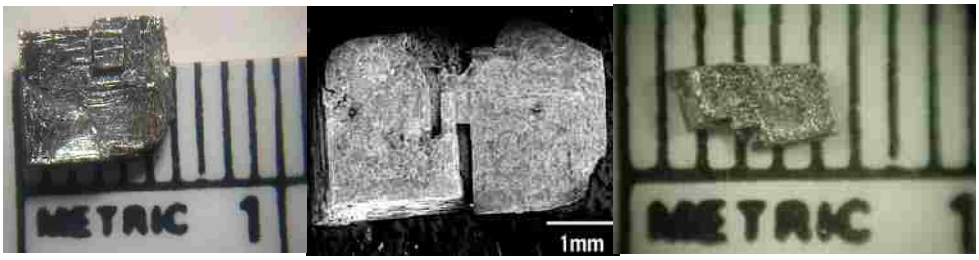

(a) (b) (c)

Figure 1.2. Aggregates of single crystals of (a) $CePdGa_6$, (b) Ce_2PdGa_{10}, and (c) Ce_2PdGa_{12}.

1.3. Characterization Techniques

1.3.1. X-ray Diffraction. Single crystal X-ray diffraction is the main characterization tool that we employ to characterize and determine the crystal structure of crystalline solids. The overall goal of diffraction is to create a picture of the crystal structure at an atomic level, as if looking through a very powerful microscope.[38] Powder X-ray diffraction is a complementary tool that can be used to obtain a characteristic powder pattern, which serves as a "fingerprint" for each material and allows for the determination of the homogeneity of a polycrystalline sample.[39] Crystallographic parameters, such as reflection intensities, lattice parameters, atomic positions, and displacement parameters, are obtained from X-ray diffraction experiments.

For X-ray diffraction to occur, a source material, such as tungsten filament is heated, which provokes the emission of electrons. The charged particles or electrons bombard the surface of a metal target, such as Cu, which emits X-rays. X-rays then hit the surface of the

sample, which results in the absorption of some X-rays and the diffraction at certain crystallographic planes within the sample.[39] As shown in Figure 1.3 (a), these special planes in the crystalline sample, denoted as *hkl*, act as pseudo-mirrors, which reflect and scatter the X-rays at special positions within the sample. The diffracted X-rays then hit a scintillation counter, Geiger counter, or photographic film detector, which is used to intercept the diffracted beams for electronic measurements.[40]

The relationship between diffracted beams incident with the crystallographic planes and the distance between these adjacent planes can be described using Bragg's Law of the form: $2d \sin\theta = n\lambda$, where d is the perpendicular distance between the two planes and θ represents the Bragg angle of diffraction, as shown in Figure 1.3 (b).[39] In order for diffraction to occur, Bragg's Law must be satisfied (diffracted waves interfere constructively).

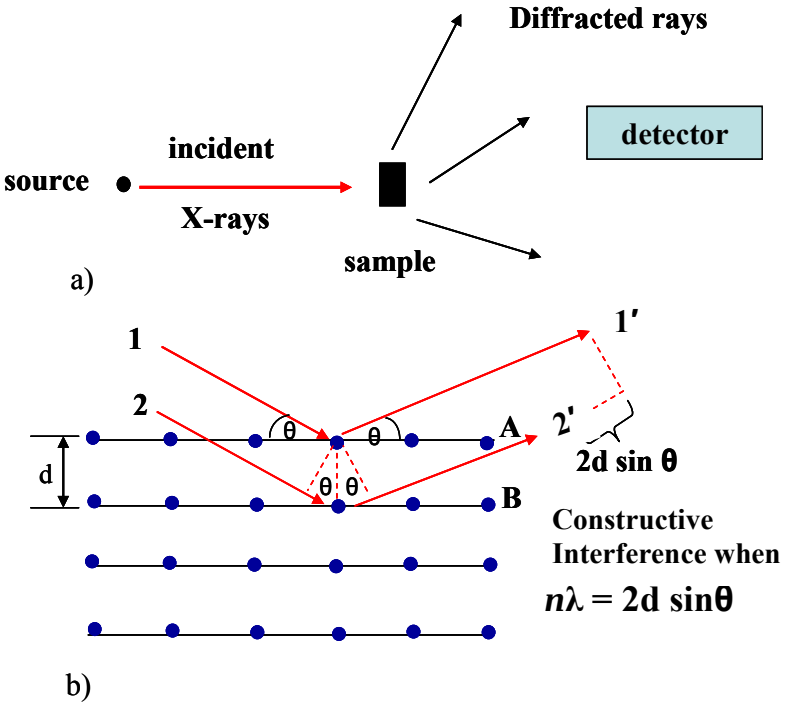

Adapted from: West, A. R., *Basic Solid State Chemistry*. 2nd ed.; John Wiley & Sons: New York, 1999, pp. 134-135.

Figure 1.3. Schematic of a) the X-ray diffraction experiment and b) the constructive interference between two diffractive waves that satisfy Bragg's Law, where nλ = 2d sinθ.

X-ray powder diffraction can be used on various different materials, such as nanoparticles, thin films, or powders. However, X-ray diffraction is not effective for scattering "light atoms" that do not possess a large number of electrons in their outer shell. In addition to

this problem, determining the atomic positions or occupancies of compounds containing elements with similar numbers of electrons, such as Ni^{28} and Ga^{31}, may be quite challenging because of the slight three electron difference between these elements.

1.3.2. Neutron Diffraction. We have employed neutron diffraction as a complementary tool in characterizing the chemical and/or magnetic structure of several materials, such as the *Ln*-M-Ga $CePdGa_6$ and Yb_5Pt_9 compounds at the National Institute of Standards and Technology (NIST). Using neutron diffraction, it is possible to determine the structures of compounds containing elements with similar atomic numbers and elements with large mass absorption coefficients, depending on the neutron cross-section scattering lengths for each element. Due to the presence of a magnetic dipole moment in neutrons, they interact with the nuclei and unpaired electrons in a material. This allows for determination of the magnetic structure in these materials.[39] For single crystal neutron diffraction experiments, large single crystals of a material, at least 2-5 mm^3, are required. When it is difficult to obtain large single crystals for some materials, neutron powder diffraction allows for structure determinations, if an initial model is known.

1.3.3. Physical Property Measurements. Measuring magnetic and transport properties, such as magnetic susceptibility, specific heat capacity, and resistivity, of highly correlated electron materials, enables us to investigate structure-property correlations in these materials, which may ultimately allow us to better understand what drives exotic behavior in complex materials.

The electrical resistivity of a material is decribed by the relationship in Equation 1.1,

$$\rho = R\frac{A}{L} \tag{1.1}$$

where R = resistance of the material, A = the cross sectional area of the sample, and L = length of the sample. The resistivity of a typical metal increases linearly with temperature. However, in a superconductive material, there is a characteristic drop to absolute zero in the resistivity at a

critical temperature (T_c). A broad shoulder in the resistivity as temperature approaches absolute zero, followed by a drop in the magnitude of the resistivity, is indicative of the onset of Kondo coherence in a material. Likewise, if a substantial drop in the resistivity is observed, magnetoresistance (MR (%) = [(ρ(H) - ρ(0)) / ρ(0)] x 100%) measurements are obtained for the material to determine the behavior of the resistivity with the application of magnetic field. Materials with large MR exhibit large changes in resistivity with the application of external field. Several of our layered intermetallic materials, exhibit large MR, such as Ce_2PdGa_{10} (MR >300%)[31] and La_2NiGa_{12} (MR > 200%)[41] at 3 K and fields of 9 T.

The magnetic susceptibility ($\chi = M/H$) of a material describes its magnetization in the presence of a magnetic field. The Curie Weiss Law (Equation 1.2) can be used to fit the paramagnetic region of a material in a linear form, where C is the Curie Constant, T is the

$$\chi = \frac{M}{H} = \frac{C}{T - \theta} \tag{1.2}$$

temperature, and θ is the Weiss Constant. From this fit, it is possible to determine the magnetic moment for the material by the relationship, $C = \frac{N\mu^2}{k_B}$, where N = Avogadro's number, μ = magnetic moment, and k_B = Boltzmann's constant..

The specific heat of a typical metal can be described as: $C_p = \gamma T + \alpha T^3$, where γ is the electronic contribution to the specific heat, α is the phonon contribution to the specific heat, and T is temperature.[36, 42] This relationship can be shown in a linear form, $\frac{C_P}{T} = \gamma + \alpha T^2$, and by plotting the specific heat as C_p/T as a function of T^2, γ (y-intercept) can be determined, which is proportional to the effective mass of the electrons. Heavy fermion materials typically exhibit γ ≥100 mJ/mol- K^2.[42]

In this dissertation, the crystal growth and structure-property relationships of several different classes of highly correlated materials, such as the *Ln*-*M*-Ga (*Ln* = La, Ce, Pr, *M* = Ni, Pd), Yb_5Pt_9, and $R_2Ir_2O_7$ (R = Pr, Eu) compounds, will be discussed. By investigating the structure-property relationships of these materials in the quantum critical regions of the magnetic phase diagram, ultimately, it may be possible to predict complex behavior in materials, as well as the design of new materials with desired properties.

CHAPTER II. CORRELATING THE STRUCTURE AND PROPERTY RELATIONSHIPS IN THE TERNARY Ce-Pd-Ga PHASES[1]

2.1. Introduction

Heavy fermion compounds are of particular interest because of the interplay between their local magnetic moments and conduction electrons, which yields large effective masses, long-range magnetic order, and in rare cases even superconductivity.[1-3, 43] Several ternary Ce-*M*-*X* (*M* = transition metal, *X* = main group element) compounds are of notable interest due to their interesting structural and physical properties. It has been shown that Ce_nMIn_{3n+2} (n = 1, 2, ∞ ; *M* = Co, Rh, or Ir)[44, 45] are heavy fermion compounds, where $CeCoIn_5$ exhibits the highest superconducting transition temperature (T_c = 2.3 K) of any Ce-based heavy fermion material.[44] Although the origin of superconductivity in heavy fermion materials remains an unresolved issue, there is growing evidence that the superconductivity found in $CeCoIn_5$ may be magnetically mediated.[44] Ce_nRhIn_{3n+2} (n = 1, 2) and $CeIn_3$ (n = ∞) compounds comprise a homologous series that display both antiferromagnetic and superconducting behavior.[46-48] The fact that both antiferromagnetism and superconductivity occur simultaneously in the Ce_nRhIn_{3n+2} (n = 1, 2) and $CeIn_3$ (n = ∞) compounds has been correlated with minimal distortions in the $CeIn_3$ cuboctahedra layer. Although distortions have been found for the *M* = Co or Ir in the Ce_nMIn_{3n+2} analogues,[49] they exhibit superconductivity at ambient pressure.[44, 45] $CePdGa_6$, a layered compound with structural similarities to the Ce_nRhIn_{3n+2} (n = 1, 2) compounds, was found to be a heavy fermion compound with $\gamma \sim 300$ mJ/mol K^2.[30] $CePdGa_6$ exhibits an antiferromagnetic

[1] Reprinted from J. Solid State Chem., 178, Macaluso, R. T.; Millican, J.N.; Nakatsuji, S.: Lee, H.O.; Carter, B.; Moreno, N. O.; Fisk.; Chan, J.Y., Copyright (2005), with permission from Elsevier
Reprinted from J. Solid State Chem., 177, Millican, J. N.; Macaluso, R. T.; Young, D. P.; Moldovan, M.; Chan, J.Y., Copyright (2004), with permission from Elsevier
Reprinted from Comments Inorg. Chem. (Review Article), 27, Thomas, E. L.; Millican, J. N.; Okudzeto, E. Chan, J. Y., Copyright (2006), with permission from Taylor and Francis Group.

transition along its *c*-axis at T_N = 5.5 K. Its structure consists of a periodic stacking of $CeGa_{8/4}$ layers and $PdGa_{8/2}$ layers along the *c*-axis.

In our exploration of structurally related Ce compounds, we have also synthesized two new ternary phases, Ce_2PdGa_{12}[32] and Ce_2PdGa_{10}.[31] The structure and physical properties of Ce_2PdGa_{12} and Ce_2PdGa_{10} will be presented and compared to $CePdGa_6$ to determine the relationships between the structure and physical property behavior in these compounds.

2.2. Experimental

2.2.1. Synthesis. Single crystals of Ce_2PdGa_{12} and Ce_2PdGa_{10} were synthesized using the flux growth method. In synthesizing a wide range of different ternary intermetallic compounds by flux growth, the starting stoichiometric ratios are often quite similar. In order to synthesize phase-pure single crystals of these Ce-Pd-Ga compounds for physical property measurements, it was necessary to first determine optimal crystal growth conditions in which to isolate each phase. In our attempts to obtain single crystals of homogeneous phases from each growth, we have observed that in addition to modifying the stoichiometric ratios of the starting materials, the heat treatment employed, in particular the final dwell temperature, also plays a major role in

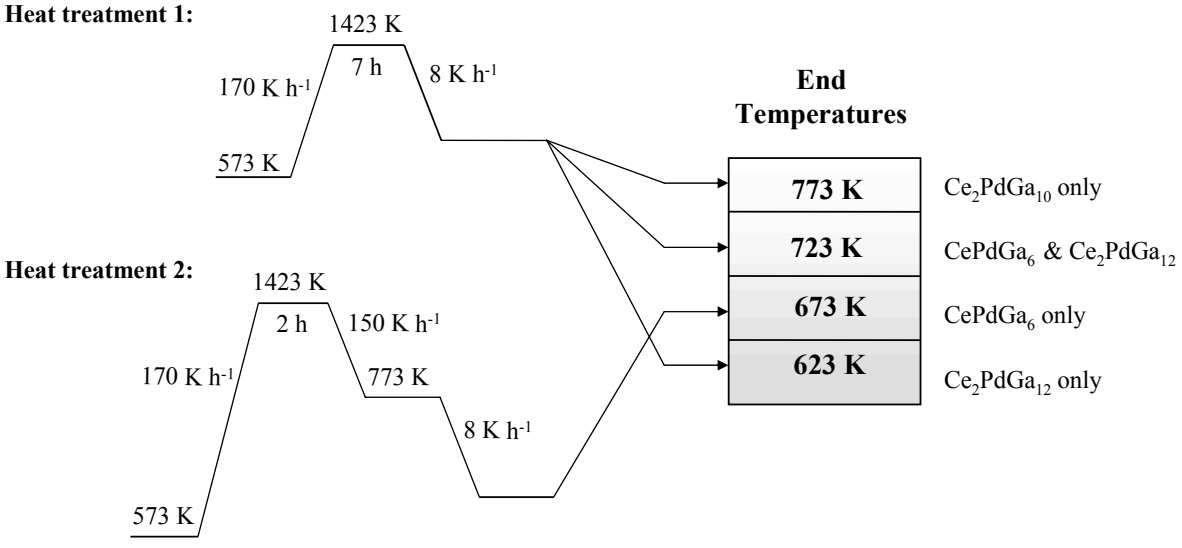

Figure 2.1. Crystal growth conditions for $CePdGa_6$, Ce_2PdGa_{12} and Ce_2PdGa_{10}.

determining which phase forms. While manipulating these synthetic variables, we found that $CePdGa_6$ and Ce_2PdGa_{12} coexist with the use of identical growth conditions, as shown in heat treatment 1 of Figure 2.1. For example, growing phase-pure single crystals of $CePdGa_6$ required not only a change in synthetic variables, such as the starting stoichiometric ratios of the reactants, but also in the heat treatment.[32] The successful growth of $CePdGa_6$ was only made possible by combining stoichiometric Ce:Pd:Ga ratios of 1:1.5:15 and following heat treatment 2 (See Figure 2.1).[32, 50] Interestingly, Ce_2PdGa_{10} also has the same starting stoichiometric ratio and a similar heat treatment as Ce_2PdGa_{12}.[30] However, the final dwell temperatures are varied to isolate each phase.

We were able to grow single crystals of La_2PdGa_{12} and Ce_2PdGa_{12} using excess Ga flux as shown in heat treatment 1.[32, 50] Stoichiometric ratios of 1:1:20 of La or Ce (3N, Ames Laboratory), Pd powder (5N, Alfa Aesar), and Ga shot (5N, Alfa Aesar) were combined in alumina crucibles and sealed in evacuated fused silica tubes. Each sample was then heated to 1423 K for 2 h and allowed to cool to 723 K at a rate of 8 K/h, at which point the sample was inverted and centrifuged. Silver, plate-like single crystals were retrieved with crystal size ranging from 0.125 x 0.25 x 0.25 to 0.5 x 0.5 x 1 cm^3.

To synthesize phase pure single crystals of La_2PdGa_{10} and Ce_2PdGa_{10}, the starting materials, La or Ce ingot (3N, Ames Laboratory), Pd powder (5N, Alfa Aesar), and Ga shot (5N, Alfa Aesar) were placed in a 5-mL alumina crucible in a 1:1:20 ratio. The samples were sealed in evacuated silica tubes and heated at 1423 K for 7 hours. Upon slow cooling to a final dwell temperature of 773 K at a rate of 281 K/ h, the sample tubes were then inverted and centrifuged for 5 minutes to remove excess Ga flux. Silver, plate-shaped crystals were found, and typical

crystal size ranged from 1 x 2 x 2 to 1 x 5 x 5 mm^3, as shown in Figure 2.2. The single crystalline samples were not observed to decompose in air over a period of months.

Figure 2.2. Aggregate of Ce_2PdGa_{10}.

2.2.2. X-ray Diffraction of Ce_2PdGa_{10}. Fragments of single crystals of La_2PdGa_{10} and Ce_2PdGa_{10} of size 0.03 x 0.03 x 0.05 mm^3 and 0.025 x 0.05 x 0.05 mm^3, respectively, were mounted onto the goniometer of a Nonius Kappa CCD diffractometer equipped with a MoK_α radiation (λ = 0.71073 Å) X-ray tube. Data were collected, and the structural models were refined using SHELXL97.[51] Because of the similarity of the crystal system and unit cell dimensions, the atomic positions from the Ce_2NiGa_{10} structure type[52] were used as an initial structural model in determining the atomic positions for La_2PdGa_{10} and Ce_2PdGa_{10}. Corrections were made for extinction, and the data were refined with anisotropic displacement parameters. Selected crystallographic parameters for La_2PdGa_{10} and Ce_2PdGa_{10} are presented in Table 2.1. To ensure sample homogeneity, three separate batches of Ce_2PdGa_{10} crystals were characterized by single crystal X-ray diffraction.

2.2.3. X-ray Diffraction for Ce_2PdGa_{12}. A suitable 0.03 x 0.03 x 0.08 mm^3 silver-colored fragment of Ce_2PdGa_{12} was mounted onto the goniometer of a Nonius KappaCCD diffractometer equipped with Mo K_α radiation (λ = 0.71073 Å). Data were collected up to θ = 30.0° at 293 K. A similar treatment was applied to a 0.05 x 0.08 x 0.08 mm^3 silver-colored fragment of La_2PdGa_{12}. The space group and atomic positions of Sm_2NiGa_{12} were used to construct an initial model for the structure determinations of both La_2PdGa_{12} and Ce_2PdGa_{12} compounds. The structural models were refined using SHELXL97.[51] Data were corrected for extinction and refined with anisotropic displacement parameters. Data were also corrected for absorption by a

multi-scan method using HKL Scalepack. Selected crystallographic parameters for La_2PdGa_{12} and Ce_2PdGa_{12} are provided in Table 2.2.

Table 2.1. Crystallographic Parameters for La_2PdGa_{10} and Ce_2PdGa_{10}

Crystal Data		
Formula	La_2PdGa_{10}	Ce_2PdGa_{10}
a (Å)	4.3560(3)	4.3230(3)
c (Å)	26.514(3)	26.536(3)
V (Å^3)	503.10(7)	495.91(7)
Z	2	2
Crystal Dimension (mm^3)	0.03 x 0.03 x 0.05	0.005 x 0.025 x 0.050
Crystal System	Tetragonal	Tetragonal
Space Group	*I*4/*mmm*	*I*4/*mmm*
θ range (º)	3.07-30.05	2.55-32.03
μ(mm^{-1})	58.343	59.47
Data Collection		
Measured Reflections	624	1182
Independent Reflections	273	296
Reflections with I > 3σ(I)	243	198
R_{int}	0.0477	0.025
h	−6 → 6	−5 → 5
k	−4 → 4	−3 → 3
l	−23 → 36	−28 → 34
Refinement		
[a]R[F^2>2σ(F^2)]	0.0452	0.0271
[b]wR(F^2)	0.1056	0.0629
Reflections	323	490
Parameters	19	19
$\Delta\rho_{max}$ (e Å^{-3})	2.731	1.384
$\Delta\rho_{min}$ (e Å^{-3})	−2.902	−1.384
Extinction coefficient	0.0036(5)	0.001(17)

[a] $R_1 = \sum||F_o| - |F_c||/\sum|F_o|$
[b] $wR_2 = [\sum[w(F_o^2 - F_c^2)^2]/ \sum[w(F_o^2)^2]]^{1/2}$

Table 2.2. Crystallographic Parameters of La_2PdGa_{12} and Ce_2PdGa_{12}

Crystal Data		
Formula	**La_2PdGa_{12}**	**Ce_2PdGa_{12}**
a (Å)	6.1080(6)	6.1040(2)
c (Å)	15.5540(9)	15.5490(9)
V (Å^3)	580.28(9)	579.64(5)
Z	2	2
Crystal Dimension (mm^3)	0.05 x 0.08 x 0.08	0.03 x 0.03 x 0.08
Crystal System	Tetragonal	Tetragonal
Space Group	*P4/nbm*	*P4/nbm*
θ range(°)	2.62 - 30.00	2.62 – 29.97
μ (mm^{-1})	50.582	50.906
Data Collection		
Measured reflections	1474	1537
Independent reflections	483	487
Reflections with $I > 2\sigma(I)$	366	387
R_{int}	0.0626	0.0419
h	$-8 \rightarrow 8$	$-8 \rightarrow 8$
k	$-6 \rightarrow 6$	$-6 \rightarrow 6$
l	$-21 \rightarrow 17$	$-21 \rightarrow 21$
Refinement		
[a]$R_1[F^2 > 2\sigma(F^2)]$	0.0415	0.0380
[b]$wR_2(F^2)$	0.1030	0.1064
Reflections	483	487
Parameters	26	26
$\Delta\rho_{max}$ (e Å^{-3})	2.925	3.778
$\Delta\rho_{min}$ (e Å^{-3})	−1.618	−2.375

[a] $R_1 = \sum||F_o| - |F_c||/\sum|F_o|$
[b] $wR_2 = [\sum[w(F_o^2 - F_c^2)^2]/ \sum[w(F_o^2)^2]]^{1/2}$

2.2.4. Physical Property Measurements. The electrical resistivity and magnetoresistance of Ce_2PdGa_{10} were measured by the standard 4-probe AC technique at 27 Hz. Pt wires (0.002 inch diameter) were attached to the sample with Epotech silver epoxy. The sample was vapor cooled

in a Quantum Design cryostat. The bulk magnetic susceptibility and magnetization versus field were also measured in a PPMS system from Quantum Design in fields up to 9 Tesla.

Magnetization data for Ce_2PdGa_{12} were obtained using a Quantum Design Magnetic Property Measurement System SQUID magnetometer. The temperature-dependent magnetization data were obtained first under zero-field cooled (ZFC) conditions from 2 K to 330 K under a field of 1000 G. Magnetization was then measured upon heating to obtain field-cooled (FC) data after cooling to 2 K under field. Field (H)-dependent measurements were collected at 2 K with H swept between 0 and 5.5 Tesla. These procedures were followed for crystallographic ab – plane of the crystal aligned parallel and perpendicular to the magnetic field. Specific heat was measured by a thermal relaxation method from 20 K to 0.35 K at zero magnetic field and ambient pressure using a Quantum Design Physical Property Measurement system. The entropy was obtained by integrating the specific heat divided by the temperature with respect to the temperature.

2.3. Results and Discussion

2.3.1. Structure of Ce_2PdGa_{10}. Ce_2PdGa_{10} crystallizes in the tetragonal $I4/mmm$ space group (No. 139) with the Ce, Pd, Ga1, Ga2, Ga3, and Ga4 atoms occupying the 4*e*, 2*b*, 4*d*, 8*g*, 4*e* and 4*e* Wyckoff symmetry sites, respectively. Ce_2PdGa_{10} has lattice parameters of a = 4.3230(3) Å and c = 26.536(3) Å, Z = 2. Atomic positions and related structural information for Ce_2PdGa_{10} are provided in Table 2.3. Ce_2PdGa_{10} is

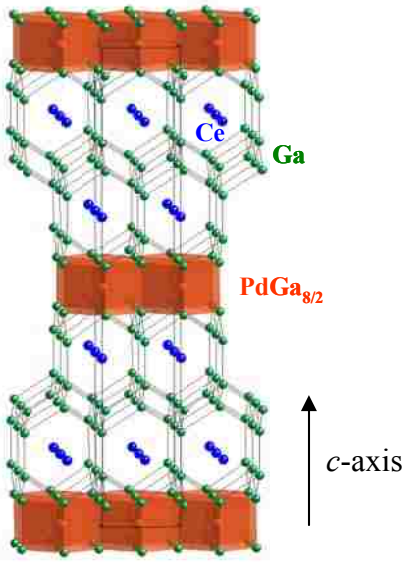

Figure 2.3. The crystal structure of Ce_2PdGa_{10}. Ce atoms are shown in blue; Pd polyhedra are shown in orange; and Ga atoms are shown in green.

isostructural to Ce_2NiGa_{10} [52] and $Ce_2NiAl_{6-x}Ge_{4-y}$.[53] The overall structure of Ce_2MGa_{10} (M = Ni or Pd), as shown in Figure 2.3, can be viewed as a periodic stacking of alternating staggered rare-earth bilayers and Ga3/Ga2/*M*/Ga2/Ga3 layers, forming a "sandwich" structure along the *c*-axis. Ga1-Ga4 tetrahedral slabs separate each Ce bilayer along the *c* -axis. The Ga2 atoms of the edge-sharing $PdGa_{8/2}$ rectangular prisms are capped by Ga3 atoms above and below to form Ga3/Ga2/Pd/Ga2/Ga3 slabs. These Ga3/Ga2/Pd/Ga2/Ga3 slabs are between staggered bilayers of Ce atoms along the *c*-axis.

Table 2.3. Atomic Positions and Displacement Parameters for La_2PdGa_{10} and Ce_2PdGa_{10}

Atom	Wyckoff Position	*x*	*y*	*z*	U_{eq} (Å^2)[a]
La	4*e*	0	0	0.35311(4)	0.0067(4)
Pd	2*b*	0	0	½	0.0058(5)
Ga1	4*d*	0	½	¼	0.0095(6)
Ga2	8*g*	½	0	0.44905(5)	0.0080(5)
Ga3	4*e*	0	0	0.10532(9)	0.0110(6)
Ga4	4*e*	0	0	0.19779(8)	0.0062(5)
Ce	4e	0	0	0.35289(3)	0.0108(3)
Pd	2b	0	0	½	0.0097(4)
Ga1	4d	0	½	¼	0.0124(5)
Ga2	8g	½	0	0.448564(4)	0.0114(4)
Ga3	4e	0	0	0.106093(7)	0.0165(5)
Ga4	4e	0	0	0.197678(6)	0.0115(5)

[a] U_{eq} is defined as one-third of the trace of the orthogonalized U_{ij} tensor.

With a bonding cutoff of 3.25 Å, these Ce atoms are coordinated to four Ga3 atoms with an interatomic distance of 3.2448(7) Å. However, the Ce···Ga1 and Ce···Ga4 interatomic distances of 3.4823(7) Å and 3.3384(8) Å, respectively, are too long to be considered bonding when compared to the expected interatomic distance of 3.17 Å, projected by the sum of the Ce (1.82 Å) and Ga (1.35 Å) covalent radii.[54] Thus, the Ce···Ga1 and Ce···Ga4 may represent weak bonding interactions. The Ga3···Ga3 interatomic distance of 4.323(1) Å found within these Ce layers is also too long to be considered bonding when compared to the sum of covalent radii of

Ga (1.35 Å).[54] However, the Ce-Ga3 interatomic distances are 3.2448(7) Å and within the 3.111 – 3.299 Å range found in the binary compounds $CeGa_6$,[55] $CeGa_2$,[56] and Ce_5Ga_3.[56] These distances are slightly larger than the expected Ce-Ga inter-atomic distance of 3.17 Å, projected by the sum of the Ce (1.82 Å) and Ga (1.35 Å) covalent radii.[54] Selected interatomic bond distances and bond angles for La_2PdGa_{10} and Ce_2PdGa_{10} are provided in Table 2.4.

Table 2.4. Selected Interatomic Distances (Å) and Bond Angles (°) of La_2PdGa_{10} and Ce_2PdGa_{10}

La_2PdGa_{10}		Ce_2PdGa_{10}	
La-Ga3 layer		*Ce-Ga3 layer*	
La-Ga3 (x4)	3.2714(9)	Ce-Ga3 (x4)	3.2448(7)
$PdGa_{8/4}$ segment		*$PdGa_{8/4}$ segment*	
$PdGa_{8/4}$ (x8)	2.5630(8)	$PdGa_{8/4}$ (x8)	2.5564(6)
Ga1-Ga4 slab layer		*Ga1-Ga4 slab layer*	
Ga1-Ga4 (x4)	2.5807(11)	Ga1-Ga4 (x4)	2.5690(9)
Ga4-Ga3 (x1)	2.452(3)	Ga4-Ga3 (x1)	2.430(3)
Angles		*Angles*	
Ga3 – *Ln* – Ga3	83.48(3)	Ga3 – *Ln* – Ga3	83.54(2)
Ga2 – Pd – Ga2	73.87(3)	Ga2 – Pd – Ga2	73.44 (2)
	116.38(5)		115.46 (4)
	63.62(5)		64.54 (4)
Ga1-Ga4-Ga1	73.28(4)	Ga1-Ga4-Ga1	73.02 (3)
Ga4-Ga1-Ga4	106.72(4)	Ga4-Ga1-Ga4	106.98 (3)
	115.13(8)		114.57 (6)

Pd atoms are located at the center of the rectangular prisms and are coordinated to Ga2 atoms at the vertices. The Pd-Ga2 interatomic distance is 2.5564(6) Å, which is consistent with other known Pd-Ga inter-atomic distances. In Pd_2Ga and $CePdGa_6$, for example, the Pd and Ga atoms are separated by 2.558 Å[57] and 2.5609(4) Å,[30] respectively. The Pd-Ga2 interatomic distances of 2.5564(6) Å in Ce_2PdGa_{10} are also within the expected interatomic distance of 2.72 Å based on

the summation of the covalent radii of Pd (1.37 Å) and Ga (1.35 Å).[54] In the $PdGa_{8/4}$ rectangular prisms of Ce_2PdGa_{10}, the Ga2-Ga2 distance along the *c*-axis is 2.730(2) Å, which is consistent with the expected Ga-Ga interatomic distance of 2.70 Å obtained from the sum of the covalent radii of Ga (1.35 Å).[54] This Ga2-Ga2 distance of 2.730(2) Å is also consistent with the Ga–Ga bond of 2.7039(15) Å and 2.46(2) -2.792(11) Å in $CePdGa_6$ and elemental Ga, respectively.[58]

2.3.2. Structure of Ce_2PdGa_{12}. The structure of Ce_2PdGa_{12} (shown in Figure 2.4), is isostructural to Sm_2NiGa_{12}[59] and has similar structural units to the $CePdGa_6$ and Ce_2PdGa_{10} compounds. Ce_2PdGa_{12} crystallizes in the tetragonal space group, *P*4/*nbm* (No. 125 with origin choice 2), $Z = 2$. The Ce, Pd, Ga1, Ga2, Ga3, and Ga4 atoms occupy the 4*h*, 2*c*, 4*g*, 4*g,* 8*m*, and 8*m* Wyckoff symmetry sites, respectively. The atomic positions and displacement parameters for La_2PdGa_{12} and Ce_2PdGa_{12} are provided in Table 2.5. Selected inter-atomic distances and bond angles for La_2PdGa_{12} and Ce_2PdGa_{12} are provided in Table 2.6.

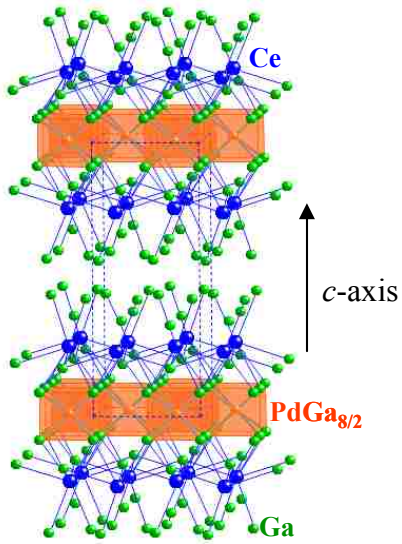

Figure 2.4. The crystal structure of Ce_2PdGa_{12}. The Ce atoms are shown in blue; the PdGa8/2 rectangular prisms are shown in orange; and the Ga atoms are shown in green.

The structure of Ce_2PdGa_{12}, as shown in Figure 2.4, can be viewed as a three-dimensional network of Ce atoms residing in Ga cavities of a with slightly distorted $PdGa_{8/2}$ rectangular prisms, where the Pd atom is coordinated to eight Ga atoms: four Ga3 atoms with interatomic distances of 2.5512(10) Å and four other Ga3 atoms by 2.5558(10) Å. These distances are typical of Pd-Ga bonds in Pd_5Ga_3,[60] $PdGa_5$, Pd_2Ga,[61]and in $CePdGa_6$ [62] where the bonding distances range between 2.388 Å – 2.701 Å. In addition, the sum of the two covalent radii of Ga (1.22 Å) and Pd (1.37 Å) is 2.59 Å,[63] which is close to our

experimental Pd - Ga distances in Ce_2PdGa_{12}. The Ga3 – Ga3 interatomic distance along the *ab* – plane is 3.0501(9) Å, too long to be considered a bond according to the 1.22 Å van der Waal radius of Ga. These distances in the $PdGa_{8/2}$ rectangular prisms are similar to the $PdGa_{8/2}$ prisms in $CePdGa_6$ where the Ga – Ga interatomic distance is shorter along the *c* – axis [2.7299(19) Å] and longer across the *ab* – plane [3.076(1) Å].

Table 2.5. Atomic Positions and Displacement Parameters in La_2PdGa_{12} and Ce_2PdGa_{12}

Atom	Wyckoff Position	*x*	*y*	*z*	U_{eq} (Å^2)[a]
La	4*h*	3/4	1/4	0.2465(5)	0.0105(3)
Pd	2*c*	3/4	1/4	0	0.0105(3)
Ga1	4*g*	3/4	3/4	0.1840(1)	0.0170(4)
Ga2	4*g*	3/4	3/4	0.3418(1)	0.0134(4)
Ga3	8*m*	0.5004(2)	0.0004(2)	−0.0877(7)	0.0135(4)
Ga4	8*m*	0.5704(2)	0.0704(2)	0.4289(8)	0.0268(5)
Ce	4*h*	3/4	1/4	0.2466(4)	0.0098(3)
Pd	2*c*	3/4	1/4	0	0.0098(4)
Ga1	4*g*	3/4	3/4	0.1840(1)	0.0117(4)
Ga2	4*g*	3/4	3/4	0.3417 (9)	0.0149(4)
Ga3	8*m*	0.5003(1)	0.0003(1)	−0.0878(6)	0.0116(3)
Ga4	8*m*	0.5702(2)	0.0702(1)	0.4286(7)	0.0253(4)

[a] U_{eq} is defined as one-third of the trace of the orthogonalized U_{ij} tensor.

The Ga-only segment consists of two Ga layers; one layer is composed of Ga2 and the other of Ga4. The Ga2 sheet includes Ga2 – Ga2 contact distances ranging between 4.3176(3) – 6.1060(4) Å, indicating that the Ga2 atoms are isolated from each other. The Ga4-Ga4 atoms, however, are separated by 2.5290(2) Å, similar to 2.44 Å, the bonding distance by summing two Ga covalent radii (1.22 Å).[63] The Ga4 atoms also form interatomic distances of 2.6173(10) Å with Ga2 atoms, falling within the range of 2.297 – 2.930 Å found in $CeGa_6$,[64] $CeGa_2$,[64] and $PdGa_5$.[61]

Figure 2.5 shows the local Ce coordination of Ce_2PdGa_{12}. Using a Ce-Ga bonding cutoff

of ~ 3.3 Å, which is larger than the projected sum of 2.9 Å of the Ce (1.65 Å) and Ga (1.25 Å) covalent radii,[65] the Ce atom is coordinated to 10 Ga atoms: 4 Ga1, 4 Ga3, and, 2 Ga4. All of these Ce-Ga distances are similar to Ce-Ga bond distances found in the binary compounds, $CeGa_2$[64] and $CeGa_6$,[64] which range between 3.252 Å – 3.299 Å.

Table 2.6. Selected Interatomic Distances (Å) of La_2PdGa_{12} and Ce_2PdGa_{12}

La_2PdGa_{12}		**Ce_2PdGa_{12}**	
La layer		*Ce layer*	
La-Ga1 (x4)	3.2047(6)	Ce-Ga1 (x4)	3.2033(5)
La-Ga4 (x2)	3.2331(15)	Ce-Ga4 (x2)	3.2286(13)
La-Ga3 (x2)	3.2784(13)	Ce-Ga3 (x2)	3.2772(11)
La-Ga3 (x2)	3.2824(13)	Ce-Ga3 (x2)	3.2808(11)
$PdGa_6$ Segment		*$PdGa_6$ Segment*	
Ga1-Ga3 (x4)	2.6283(10)	Ga1-Ga3 (x4)	2.6257(10)
Pd-Ga3 (x4)	2.5570(13)	Pd-Ga3 (x4)	2.5512(10)
(x4)	2.5519(12)	(x4)	2.5558(10)
Ga - only Segment		*Ga - only Segment*	
Ga2-Ga4 (x4)	2.6204(11)	Ga2-Ga4 (x4)	2.6173(10)
Ga4-Ga4 (x1)	2.5260(3)	Ga4-Ga4 (x1)	2.5290(2)

As shown in Figure 2.5, the Ce atom caps a rectangular anti-prism composed of Ga1 and Ga3 atoms. The Ce-Ga1 and Ce-Ga3 distances are 3.2034(5) Å (4x) and 3.2772(11) Å (4x), respectively. In addition, Ce is also bonded to two Ga4 atoms at an interatomic distance of 3.2286(13) Å. Rare-earth atoms can be found as the cap of other main group layers, such as in $CeNiSb_3$,[62, 66] $(RE)In_{1-x}Sb_2$ (RE = La – Nd),[67]

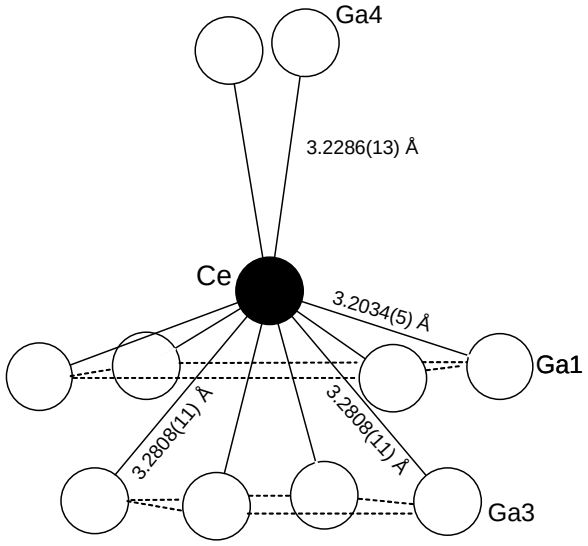

Figure 2.5. Ce environment (*CN* = 10) of Ce_2PdGa_{12}. Ce is shaded black and the Ga atoms are shown as white circles.

(RE)MSb_3 (M = V, Cr),[68] and $RESb_2$.[69, 70] The Ga1 and Ga3 atoms surrounding Ce can be viewed as two different layers, where the Ga4 layer also serves as the face of the $PdGa_{8/2}$ rectangular prisms. Although the Ga1– Ga1 interatomic distance is greater than 4 Å and indicates that *intra*layer Ga1 interactions are unlikely, the distance between Ga1 and Ga3 layers of 2.6257(10) Å implies that there may be some weak *inter*layer interactions.

2.3.3. Structural Comparisons. The layered Ce-Pd-Ga phases ($CePdGa_6$, Ce_2PdGa_{10}, and

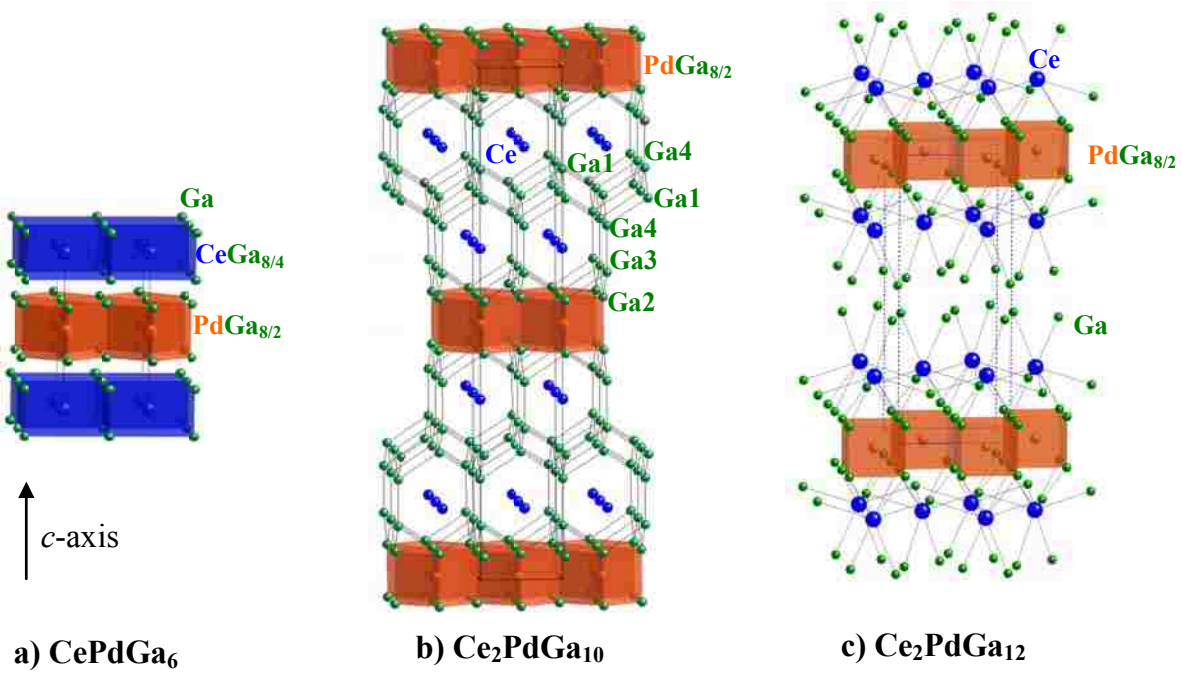

Figure 2.6. The crystal structures of (a) $CePdGa_6$, (b) Ce_2PdGa_{10}, and (c) Ce_2PdGa_{12} are shown along the *c*-axis. The Ce atoms or polyhedra are shown in blue; the Pd atoms or polyhedra are shown in orange, and the Ga atoms are shown in green.

Ce_2PdGa_{12}), as shown in Figure 2.6, offer a family of compounds for comparison due to similarities in their structures. The crystal structure of $CePdGa_6$ is layered with a striking resemblance to the Ce_nMIn_{3n+2} (T = Co, Rh, Ir; n = 1, 2, ∞)[44, 45, 71, 72] compounds. Both families of compounds crystallize in the tetragonal $P4/mmm$ (No. 123) space group. The structure of Ce_nMIn_{3n+2} consists of a periodic stacking of $CeIn_3$ cuboctahedra layers, and $MIn_{8/2}$ rectangular prisms along the *c*-axis. Although exhibiting a similar stacking in the *c*-direction, the structure

of $CePdGa_6$ consists of face-sharing $CeGa_{8/4}$ rectangular prisms and $PdGa_{8/2}$ rectangular prisms along the *c*-axis. At a glance, the crystal structures of Ce_2PdGa_{10} and Ce_2PdGa_{12}, also, both show a similar stacking to that of $CePdGa_6$ along the *c*-direction. In comparison, all of the structures have Ce-Ga contacts and face-sharing $PdGa_{8/2}$ rectangular prisms. However, the Ce environments in these compounds differ. While Ce is coordinated to 8 Ga atoms, forming $CeGa_{8/4}$ rectangular prisms in $CePdGa_6$, the Ce environment of Ce_2PdGa_{12} consists of Ce atoms coordinated to 10 Ga atoms. Moreover, the Ce atoms in Ce_2PdGa_{10} are coordinated to 4 Ga atoms. Two distinct Ce-Ce distances are present in the structures of all three Ce-Pd-Ga compounds: Ce-Ce distances along the *ab* – plane, $(Ce\text{-}Ce)_{ab,}$ and *c* – axis, $(Ce\text{-}Ce)_c$. In $CePdGa_6$, the Ce-Ce interatomic distances are 4.350(3) Å in the *ab* – plane and 7.922(6) Å along the *c* – axis.[62] As for Ce_2PdGa_{12}, since Ce atoms separate $PdGa_{8/2}$ and Ga-only segments that stack along the *c* – axis, there are two distinct $(Ce\text{-}Ce)_c$ distances along the *c*- axis. Thus, the $(Ce\text{-}Ce)_{ab}$ interatomic spacing in Ce_2PdGa_{12} is 4.318(6) Å, and $(Ce\text{-}Ce)_c$ distances measure 7.664(5) Å and 7.882(6) Å. In Ce_2PdGa_{10}, the $(Ce\text{-}Ce)_{ab}$ interatomic spacing is 4.323(6) Å and the $(Ce\text{-}Ce)_c$ distances measure 6.258(5) Å and 7.807(7) Å.

2.3.4. Physical Properties of Ce_2PdGa_{10}. Figure 2.7 shows the electrical resistivity as a function of temperature for a single crystal of Ce_2PdGa_{10}. The data are shown for current applied in the *ab*-plane. The sample is metallic ($d\rho/dT > 0$), with the resistance decreasing roughly linearly with temperature from 300 K down to 175 K. Below 50 K the slope of the resistivity begins to increase, and the value of the resistivity drops by a factor of 4 at low temperature. This broad shoulder in the resistivity is typical of Kondo compounds, where a drop in the resistivity indicates the onset of Kondo coherence (shielding of the conduction electrons). The electrical resistivity of single crystals of $CePdGa_6$ in the *ab*-plane also exhibits a similar

behavior.[73] We attempted to measure the resistivity with current applied along the *c*-axis, however, the samples were too small to do this accurately in conjunction with the usual difficulties in performing a 4-probe measurement on a thin flat sample perpendicular to the plane.

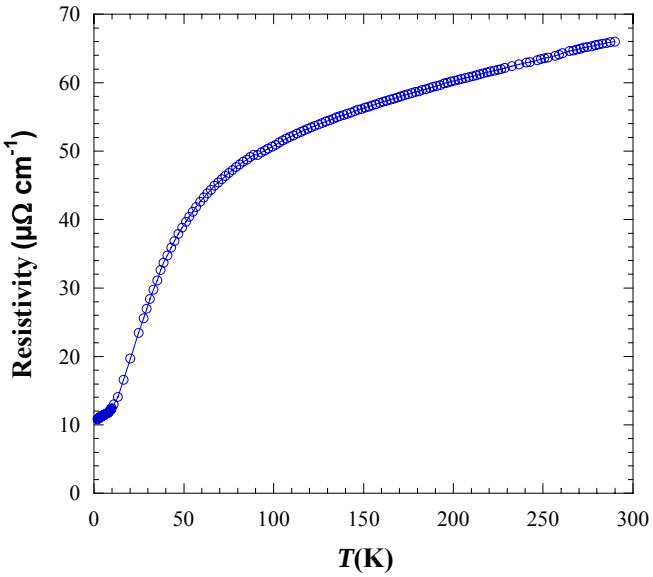

Figure 2.7. The normalized electrical resistivity of a single crystal of Ce_2PdGa_{10} as a function of temperature. The data are taken for the current parallel to the *ab*-plane.

Figure 2.8 shows the in-plane magnetoresistance (MR(%) = [(ρ(H) - ρ(0)) / ρ(0)] x 100) of a single crystal of Ce_2PdGa_{10} as a function of field at 2 K.[74] The MR is positive and large at 2 K, increasing by over 200% at 9 Tesla, which is quite unusual for most intermetallic compounds at low temperatures. Other intermetallics that exhibit large positive magnetoresistance are on the order of MR% ~ 120% at fields of 9 Tesla.[74-76] $SmPd_2Ga_2$ has a positive MR ~ 120% at 2 K and fields of 9 Tesla.[75] Although the magnitude of the magnetoresistance for Ce_2PdGa_{10} is unusual, a classical effect is

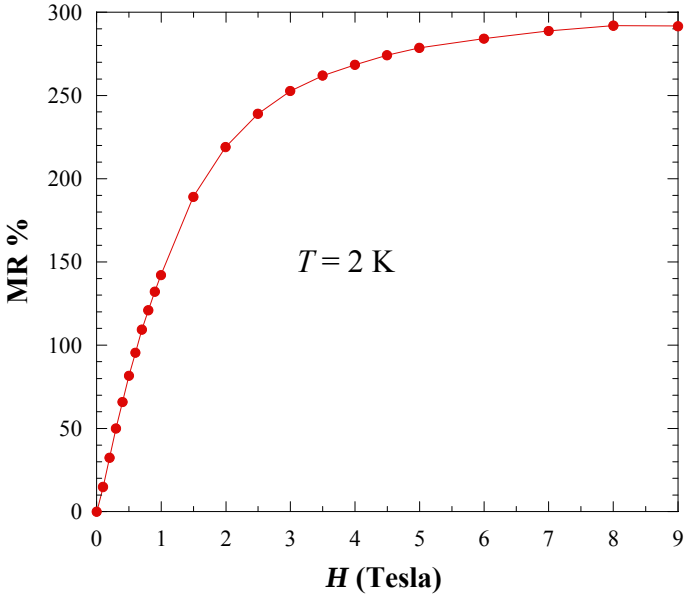

Figure 2.8. The magnetoresistance of a single crystal of Ce_2PdGa_{10} as a function of field at 2 K. The data are taken for the field parallel to the *ab*-plane.

observed as the MR saturates up to fields of 9 Tesla. The MR tends to follow the curve of a paramagnet induced with field as suggested by the magnetization data. The large MR may be attributed to increasing spin disorder scattering which is not uncommon in the paramagnetic systems, where electrons are scattered on entirely disordered magnetic moments.[77] In the main panel of Figure 2.9, the magnetic susceptibility of a single crystal of Ce_2PdGa_{10} is shown as a function of temperature for the field perpendicular to the *ab*-plane. The sample was zero field cooled (ZFC) and then warmed in a constant field of 0.1 Tesla. The data are well fit by the solid line in the main panel of Figure 2.9, which represents a modified Curie law of the form: $\chi = M/H = \chi_o + C/T$, where χ_o is some temperature-independent background susceptibility. From the fit, $\chi_o = 7.67 \times 10^{-4}$ μ_B/mol, and the Curie constant, C, has a value of 1.39×10^{-4} μ_B ·K/mol. This results in an effective magnetic moment of 2.5μ_B/mol Ce. This value is consistent with what one would expect for the full Hund's rule moment of 2.54 μ_B for Ce in its 3^+ state. The magnetic susceptibility of Ce_2PdGa_{10} is consistent with local moment paramagnetism, and no long-range magnetic order occurs down to 2 K. The inset of Figure 2.9 shows inverse susceptibility ($1/\chi$) as a function of field at 2 K. The data follow Curie Weiss behavior.

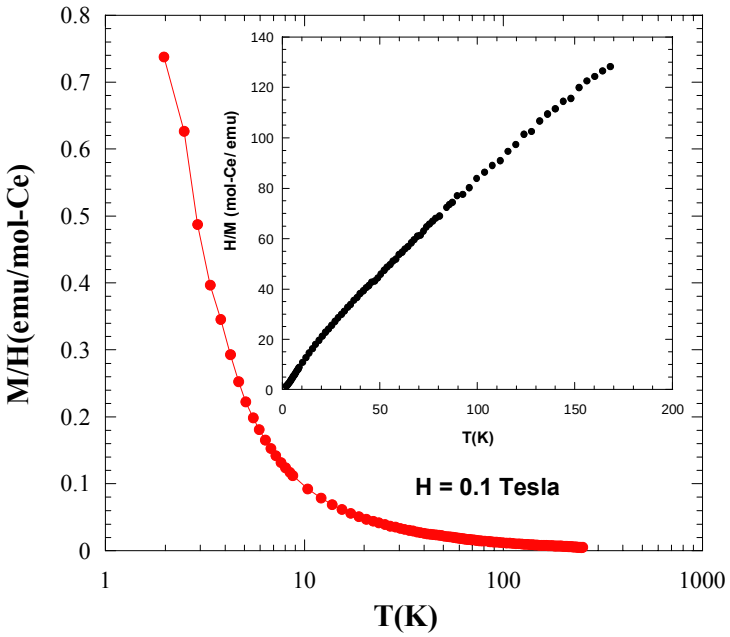

Figure 2.9. The magnetic susceptibility of a single crystal of Ce_2PdGa_{10} as a function of temperature for field perpendicular to the *ab*-plane. The inset shows inverse susceptibility with Curie-Weiss behavior as a function of temperature from 0 K to 170 K. The solid lines in the figures are a fit to the data as described in the text.

Plotted in Figure 2.10 is the magnetization of a single crystal of Ce_2PdGa_{10} at 2 K as a function of applied magnetic field. The open circles represent data for the field applied perpendicular to the *ab*-plane, and the solid circles are for the field parallel to the *ab*-plane. There is a small amount of magnetic anisotropy between the two field orientations at low field, with the magnetization being slightly larger for the field parallel to the *a*-*b* plane orientation, and essentially no anisotropy at higher fields. The data is again consistent with local-moment paramagnetism, and no hysteresis was observed in either field orientation. The magnetization in both field directions has not saturated even up to 9 Tesla.

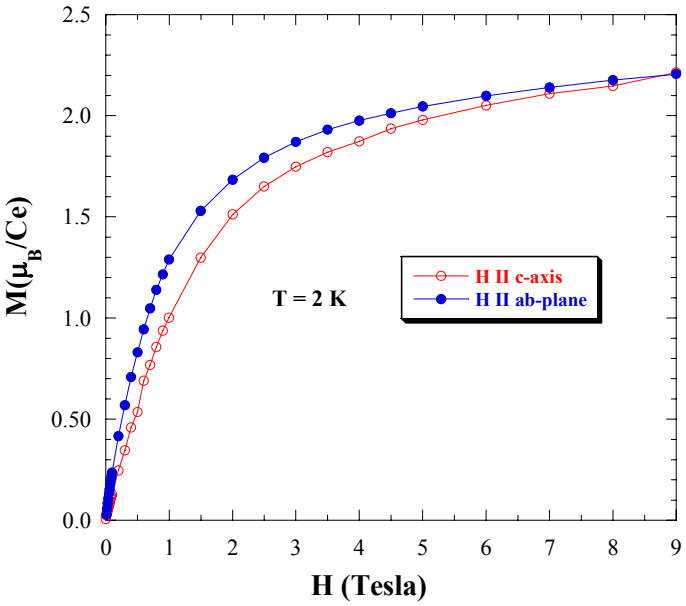

Figure 2.10. Magnetization versus field for a single crystal of Ce_2PdGa_{10} at 2 K. Closed blue and open red circles represent data for the field parallel to the *ab*-plane and *c*-axis, respectively.

Figure 2.11 shows the temperature dependency of the specific heat of Ce_2PdGa_{10}. The magnetic

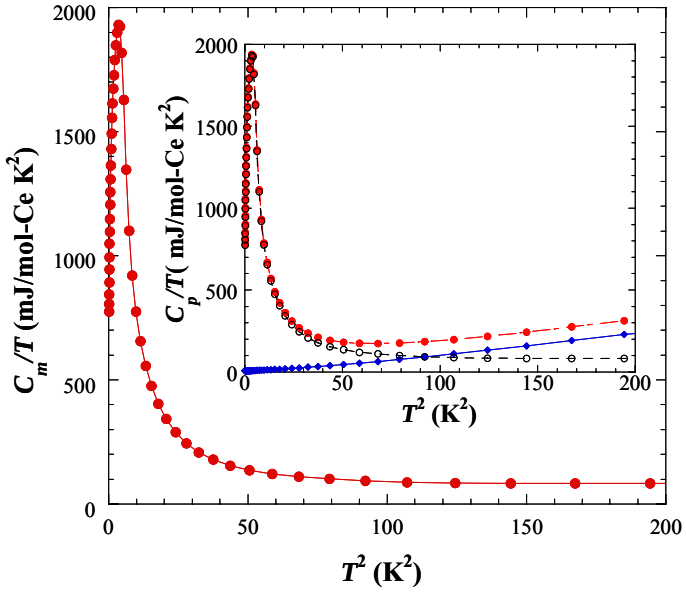

Figure 2.11. The magnetic portion of the specific heat, C_m/T, of Ce_2PdGa_{10} as a function of T^2 (K) is shown. C_m/T is obtained by subtracting the heat capacity of the La-analog (shown with blue diamonds in inset) from the total heat capacity of the compound (shown as red circles in inset).

contribution (C_m/T), which is estimated by subtracting the specific heat (C_P/T) of the La-analogue from the C_P/T of the Ce-compound, is shown as a function of T^2 (K^2). Although no magnetic transitions were observed from the *c*-axis magnetic susceptibility measurements down to 2 K, a broad peak is observed at 1.86 K, which is indicative of a magnetic transition, in the specific heat of this compound. The C_m/T shows an electronic specific heat coefficient (γ) of ~ 210 mJ/mol K^2 at T > 1.86 K for Ce_2PdGa_{10}. For clarity, we show C_P/T for both Ce and La-analogues in the inset of Figure 2.11.

2.3.5. Physical Properties of Ce_2PdGa_{12}. In order to compare the magnetic data of $CePdGa_6$ and Ce_2PdGa_{12}, we have re-measured the magnetization on phase pure single crystals of $CePdGa_6$ and Ce_2PdGa_{12}. Previous magnetic data of $CePdGa_6$[30] apparently has a Ce_2PdGa_{12} inclusion. The temperature dependence of the magnetic susceptibility (χ) is given for Ce_2PdGa_{12} and $CePdGa_6$ in Figures 2.12 and 2.13, respectively. The field of 0.1 T was applied along *ab*-plane and *c*-axis. In Ce_2PdGa_{12}, data for both orientations follow Curie-Weiss behavior above 100 K. The effective moments (μ_{eff}) are estimated to be 2.54 μ_B (*ab* – plane) and 2.59 μ_B (*c*–axis), which are very similar to the expected Ce $J = 5/2$ local moment, $\mu_{eff} = 2.54$ μ_B, with $\theta = -14.8$ K (*ab* – plane) and

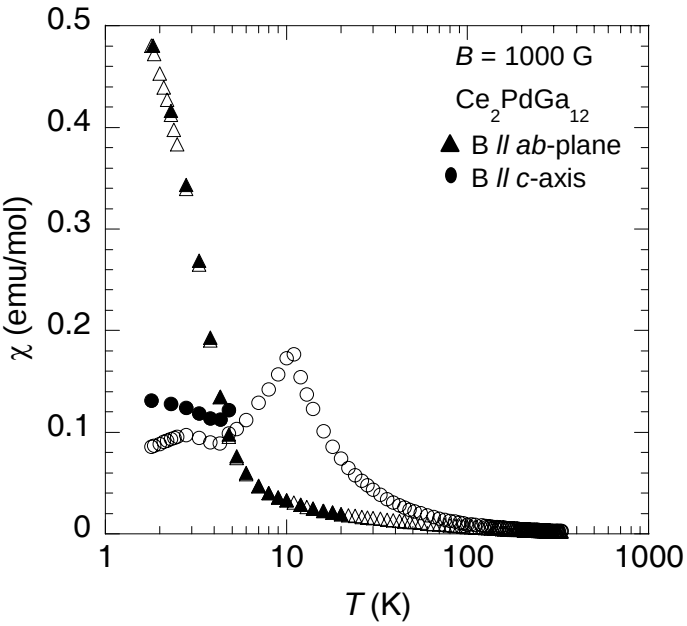

Figure 2.12. Magnetic susceptibility as a function of temperature of Ce_2PdGa_{12}. Triangles and circles represent data for B // crystallographic *ab* – plane and B // crystallographic *c* – axis, respectively; open and closed symbols represent field-cooled and zero-field cooled data, respectively.

18.2 K (c – axis). While a clear cusp in the c – axis component at 11 K is indicative of an antiferromagnetic transition, the *ab*-plane component shows a steep increase below about 3 K. A broad peak is also observed at 3 K in the C_P/T vs T plot. This suggests an appearance of a ferromagnetic component. This strong anisotropy is most likely due to the canting of spins in the Néel state below 11 K, creating a net ferromagnetic component along the *ab* – plane. The susceptibility of La_2PdGa_{12} (not shown) shows non-magnetic behavior (χ = -10^{-4} emu/mol at 273 K), indicating that the magnetic moments result only from the Ce *f*-electron, not from Pd *d*-electrons. $CePdGa_6$, on the other hand, shows an antiferromagnetic transition at 5 K with cusps in both the *ab*-plane and *c*-axis components. The Curie-Weiss analysis above 100 K yields the effective moments of μ_{eff} = 2.48μ_B (*ab*–plane) and 2.45 μ_B (*c*–axis), with θ = -12.9 K (*ab* – plane) and -1.17 K (*c* – axis), suggesting antiferromagnetic interactions. The field dependence of the magnetization (*M)* for Ce_2PdGa_{12}, as shown in Figure 2.14, was obtained with the crystal oriented along the *c* – axis and *ab* – plane in magnetic field. The *c* – axis magnetization shows a jump at 2.5 T, after showing a linear increase with the field. This indicates a metamagnetic transition, most likely due to a spin-flip transition from an antiferromagnetic to a ferromagnetic state. Along the crystallographic *ab* – plane, on the other

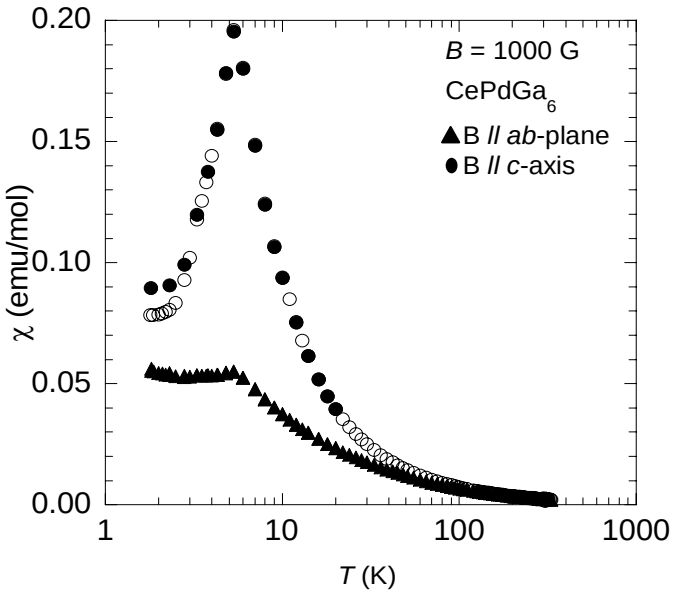

Figure 2.13. Magnetic susceptibility as a function of temperature of $CePdGa_6$. Triangles and circles represent data for B // crystallographic *ab* – plane and B // crystallographic *c* – axis, respectively; open and closed symbols represent field-cooled and zero-field cooled data, respectively.

hand, M increases rapidly up to B = 1 T and reaches the value ~ 0.2 μ_B at 5 T. A small hysteresis is observed below 0.1 T at 2 K, indicating the system has a ferromagnetic component in the *ab*-plane. The field dependence is similar to $CePdGa_6$,[62] where the magnetization shows a jump at 2 T, which is lower than the metamagnetic transition of Ce_2PdGa_{12}.

The temperature dependences of the specific heat of Ce_2PdGa_{12} and $CePdGa_6$ were measured and are shown in Figures 2.15 and 2.16, respectively. There are small deviations in the data from our previous report on $CePdGa_6$.[30] Because $CePdGa_6$ and Ce_2PdGa_{12} can coexist under a certain growth condition (see synthesis section), the previous report on the specific heat and magnetism of $CePdGa_6$ has minor effects from the inclusion of

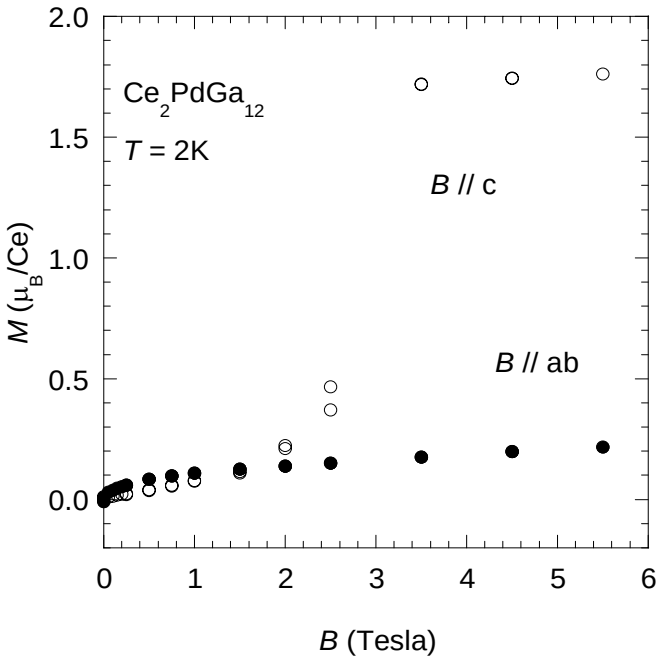

Figure 2.14. Magnetization of Ce_2PdGa_{12} as a function of field with $B \parallel ab$ – plane shown in black circles and $B \parallel c$ – axis in white circles.

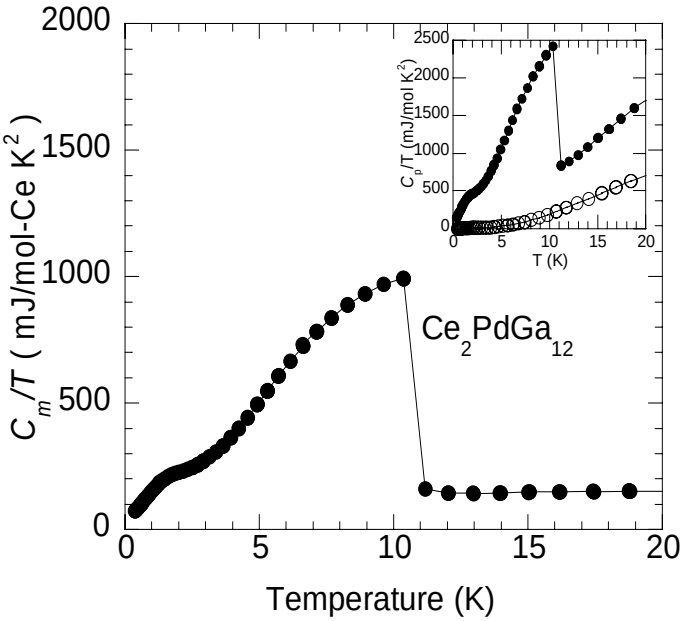

Figure 2.15. The magnetic portion of the specific heat, C_m/T, of Ce_2PdGa_{12} as a function of temperature (K) are shown. C_m/T is obtained by subtracting the heat capacity of the La-analog (shown as open circles in inset) from the total heat capacity of the compound (shown as black circles in inset).

Ce_2PdGa_{12}. [62] The magnetic part of the specific heat, C_m/T, for Ce_2PdGa_{12} (Figure 2.15) and $CePdGa_6$ (Figure 2.16) is estimated by subtracting the specific heat C_P/T of the La-analogue from the specific heat C_P/T of the Ce-compound. For clarity, we show C_P/T for both Ce and La-analogues in each inset. A sudden jump at 11 K, coincident with its antiferromagnetic transition, is observed in the C_m/T of Ce_2PdGa_{12}. Similarly a peak is observed in the heat capacity and is observed at the antiferromagnetic transition temperature of 5.5 K for $CePdGa_6$. The C_m/T of Ce_2PdGa_{12} shows electronic specific heat coefficient γ of ~ 72 mJ/mol K^2 at T close to 0 K and almost constant with ~ 140 mJ/mol K^2 at $T > T_N$, which is smaller than γ (~ 230- 400 mJ/mol K^2) for $CePdGa_6$. The corresponding entropies for the *f*-electron contribution can be estimated by integrating C_m/T for Ce_2PdGa_{12} and $CePdGa_6$. The entropy (S) released below T_N is about 6000 (mJ/mole-K) for Ce_2PdGa_{12}, while it is around 5000 (mJ/mole-K) for $CePdGa_6$. These values are roughly close to Rln2 (~5800 mJ/mole-K), which represents a doubly degenerate ground state in the paramagnetic regime. In addition, the suppressed entropy at T_N in $CePdGa_6$ is attributable to the Kondo effect.

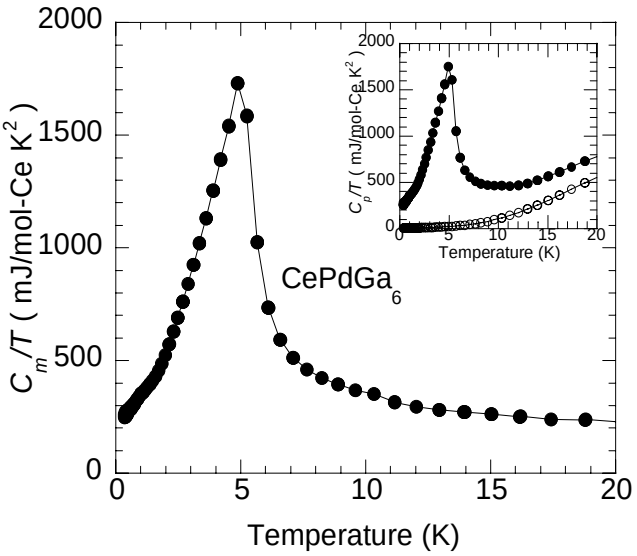

Figure 2.16. The magnetic portion of the specific heat, C_m/T, of $CePdGa_6$ as a function of temperature are shown. C_m/T is obtained by subtracting the heat capacity of the La-analog (shown as white circles in inset) from the total heat capacity of the compound (shown as black circles in the inset).

2.3.6. Powder Neutron Diffraction Experiments of $CePdGa_6$. Neutron powder diffraction experiments were conducted to determine the magnetic structure of $CePdGa_6$ at NIST. Single

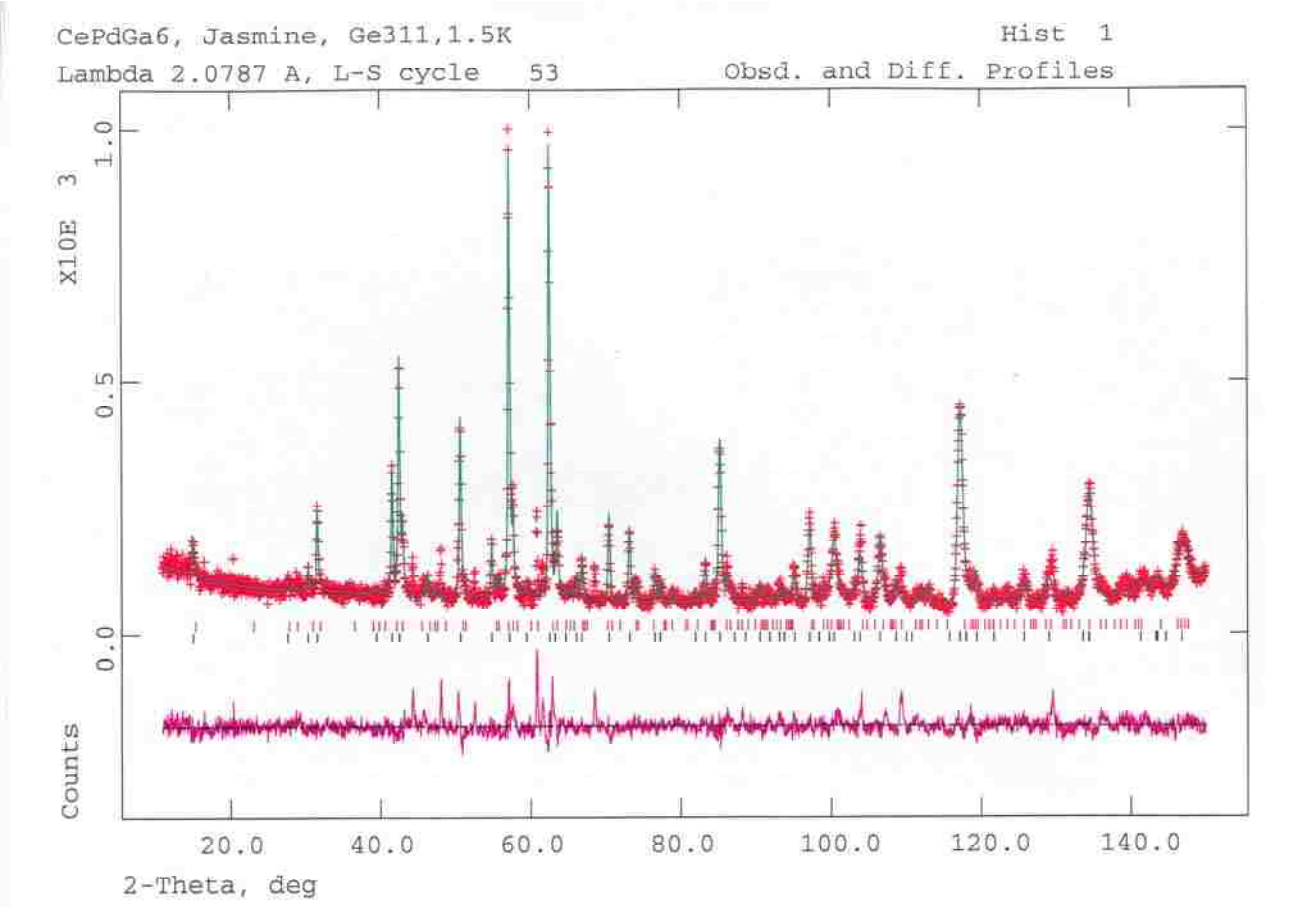

Figure 2.17. The neutron powder diffraction pattern of a sample containing $CePdGa_6$ and Ce_2PdGa_{12}. The calculated pattern for $CePdGa_6$ is shown with red tick marks; the calculated pattern for Ce_2PdGa_{12} is shown with black tick marks; and the difference pattern is shown in fuschia.

crystals of $CePdGa_6$ were crushed into a 4 gram powder sample. Neutron diffraction measurements were conducted on the sample using the BT-1 powder diffractometer, which is equipped with a Ge 311 vertically focusing monochromater ($\lambda = 2.079$ Å).

From the powder histogram, as shown in Figure 2.17, it was determined that the powder sample contained a mixture of $CePdGa_6$ (~ 70%), a secondary phase Ce_2PdGa_{12} (~ 20%), and a third unknown phase (~ 10%). By subtracting the peaks from the chemical cell, it is possible to

determine the magnetic contribution in the neutron diffraction pattern. A magnetic peak, which was observed at 33.15° in 2-theta, has been assigned to the impurity phase, Ce_2PdGa_{12}, which makes up approximately 20% of the total sample (shown in Figure 2.18). The powder neutron diffraction data shows a low signal to noise (S/N) ratio, which makes it difficult to determine magnetic peaks, which can be attributed to $CePdGa_6$. To overcome this problem by creating a larger S/N ratio, neutron diffraction experiments will be conducted on single crystals of $CePdGa_6$. Figure 2.19 shows proposed

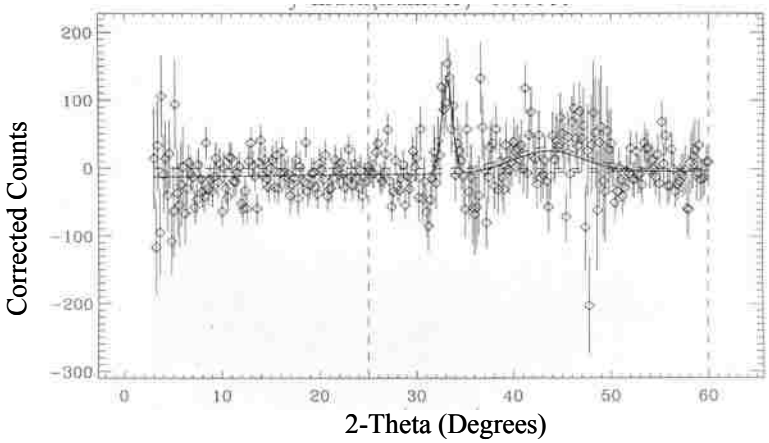

Figure 2.18. A fit of the neutron powder diffraction data a low 2-Theta. A magnetic peak occurs at 33.15°, which can be attributed to a Ce_2PdGa_{12} impurity.

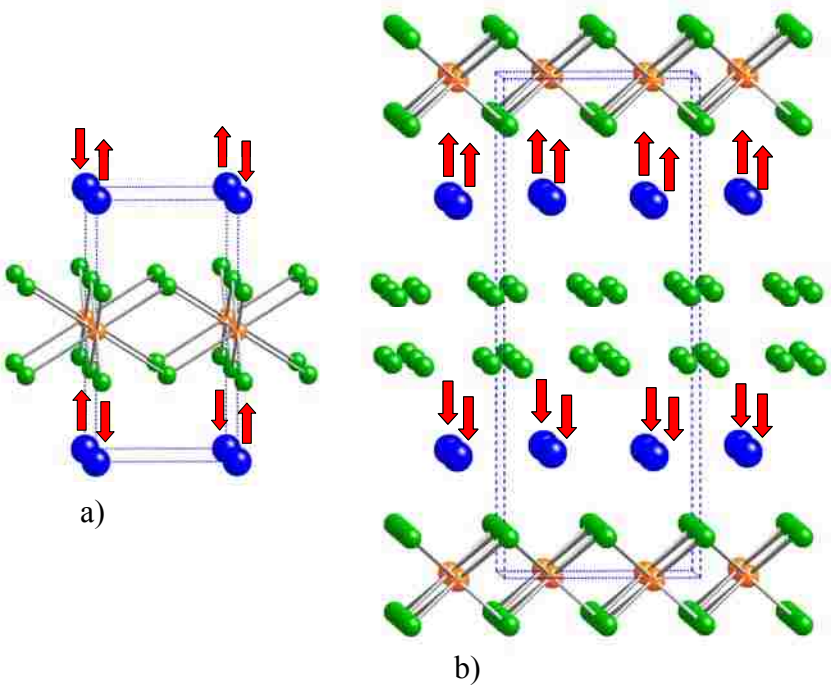

Figure 2.19. The proposed magnetic structures of a) $CePdGa_6$ and b) Ce_2PdGa_{12}, where Ce atoms are shown in blue, Pd atoms are shown in orange, and Ga atoms are shown in green.

magnetic structural models for $CePdGa_6$ and Ce_2PdGa_{12}. The proposed magnetic structure of $CePdGa_6$ (Figure 2.19a), the magnetic spins on the Ce atoms are aligned antiferromagnetically along the *a*-*b* plane and *c*-axis, which is consistent with the magnetic susceptibility of $CePdGa_6$ (Figure 2.13). However, in Ce_2PdGa_{12} (Figure 2.19b), the magnetic spins are aligned ferromagnetically along the *a*-*b* plane and antiferomagnetically along the *c*-axis, which is consistent with the magnetic susceptibility for this compound (Figure 2.12).

2.4. Conclusion

These layered Ce-Pd-Ga phases allow us to study the rare earth environment on the magnetism in each system. Two competing mechanisms, the RKKY (Ruderman-Kittel-Kasuya-Yosida) and Kondo interactions, can be used to describe the magnetism in these materials.[33-35] RKKY interactions exist when the exchange coupling between the magnetic ions and conduction electrons results in the magnetization of the conduction electrons, which in turn causes an indirect exchange between two distant magnetic ions.[36] We have observed that the higher magnetic ordering in Ce_2PdGa_{12} (T_N ~ 11 K) may be attributed to the existence of more Ce-Ga contacts (Ce *CN* = 10), where the magnetic Ce^{3+} ion can interact with additional conduction electron carriers. These stronger RKKY-like interactions cause the magnetic ordering observed in this compound to be more profound. However, the suppressed magnetism in $CePdGa_6$ (T_N ~ 5.5 K) and Ce_2PdGa_{10} (magnetic transition at 1.86 K), can be attributed to Kondo-like interactions.[31] The Kondo effect occurs as a result of the shielding of magnetic ions by conduction electrons in magnetic materials. This mechanism has been used to describe a minimum in the electrical resistivity of magnetic materials at a temperature, T_K. For example, in $CePdGa_6$ (Ce *CN* = 8) and Ce_2PdGa_{10} (Ce *CN* = 4), there are fewer Ce-Ga contacts, which leads to reduced hybridization, or less interaction between the Ce^{3+} ions and the conduction

electrons.[31] Fewer Ce – Ga contacts are found in Ce_2PdGa_{10}; Ce is coordinated to only 4 Ga atoms, whereas Ce is coordinated to 8 Ga atoms in $CePdGa_6$. Reduced Ce-Ce interactions that are inhibited by Ga1-Ga4 tetrahedral slab layers in the structure of Ce_2PdGa_{10} may also contribute to the suppressed magnetic ordering (magnetic transition at 1.86 K) in this compound. As a result of these reduced Ce-Ce interactions, the Ce moments may become more localized, and the Kondo effect to be more pronounced than RKKY interactions in this compound- leading to paramagnetic behavior. Evidence of this Kondo coherence is also observed in the resistivity data of Ce_2PdGa_{10}.

CHAPTER III. CRYSTAL GROWTH, STRUCTURE, AND PROPERTIES OF Ln_2NiGa_{10} AND Ln_2NiGa_{12} (*Ln* = La, Ce, Pr)

3.1. Introduction

Ternary Ce-Ni-*X* (*X* = main group element) intermetallic compounds are of interest due to their rich crystal chemistry and physical properties, such as magnetism, superconductivity, and heavy fermion behavior. For example, $CeNi_2Ge_2$,[78-81] which has been extensively studied due to its proximity to a quantum critical point, crystallizes in the $ThCr_2Si_2$[82] structure type and exhibits heavy fermion behavior ($\gamma \sim 350$ mJ/mol K^2) and superconductivity ($T_c \sim 0.22$ K) under pressure. $CeNi_2Sn_2$, which crystallizes in the $CaBe_2Ge_2$ structure type (derivative of the $ThCr_2Si_2$ structure type), also exhibits heavy fermion ($\gamma \sim 400$ mJ/mol K^2) and magnetic behavior (AFM, $T_N = 1.8$ K).[83-86]

In our interests to better understand the effect of rare earth atom and transition metal substitution in the heavy fermion materials, we have synthesized single crystals of Ln_2NiGa_{10} (*Ln* = Ce, Pr) and Ln_2NiGa_{12} (*Ln* = La, Ce, Pr), which are isostructural to the known Ce_2MGa_{10} (*M* = Ni, Pd)[31, 52] and Ln_2MGa_{12} (*Ln* = Ce, Sm; *M* = Ni, Pd) families of compounds, respectively.[32, 87] Although the structure of Ce_2NiGa_{10},[52] was previously reported for single crystalline materials, no physical properties have been reported to date. We will compare the structure and properties of the Ln_2NiGa_{10} (*Ln* = Ce, Pr) with Ce_2PdGa_{10}.[31] Recently, Cho et al., has also been successful in synthesizing Ce_2CuGa_{12}.[41] The Cu analogue allows for the systematic comparison of this family of compounds. We will also study the role of the lanthanide ion's influence among the La_2NiGa_{12}, Ce_2NiGa_{12}, and Pr_2NiGa_{12} compounds.

3.2. Experimental

3.2.1. Synthesis. Single crystals of the Ln_2NiGa_{10} (*Ln* = Ce, Pr) compounds were synthesized using excess Ga. Stoichiometric ratios of 1:1:20 of *Ln*, Ni, and Ga, respectively, were sealed in an evacuated fused silica tube. These samples were then heated up to 1423 K and allowed to dwell for 8 hours. The samples were then allowed to cool to 833 K at a rate of 8 K/h, at which point they were inverted and centrifuged. Silver metallic plate-shaped crystals were obtained. Typical crystal size ranged from 2 x 2 x 3 mm^3 to 3 x 3 x 5 mm^3.

The synthetic profile for the growth of the Ln_2NiGa_{12} (*Ln* = La, Ce, Pr) compounds is very similar to that used to make Ln_2NiGa_{10} (*Ln* = Ce, Pr). The only difference in the temperature profile for Ln_2NiGa_{10} (*Ln* = Ce, Pr) is the temperature of 623 K at which the sample was inverted and centrifuged. Silver, metallic plate-shaped crystals were retrieved with typical crystal size ranging from 3 x 3 x 6 to 5 x 5 x 6 mm^3.

3.2.2. Single Crystal X-ray Diffraction. The Ln_2NiGa_{10} (*Ln* = Ce, Pr) compounds were characterized via single crystal X-ray diffraction. Single crystal fragments of the Ln_2NiGa_{10} (*Ln* = Ce, Pr) and Ln_2NiGa_{12} (*Ln* = La, Ce, Pr) compounds were placed on glass fibers, which were mounted onto the goniometer of a Nonius KappaCCD diffractometer equipped with a MoKα radiation (λ = 0.71073 Å) X-ray tube. Data were collected, and structural models were obtained using SHELXL97.[51] Due to similarities in the crystal system and cell dimensions, the atomic positions of Ce_2PdGa_{10}[31] were used to construct initial structural models for the Pr_2NiGa_{10}. However, for the Ln_2NiGa_{12} (*Ln* = La, Ce, Pr) phases, the structure was solved using direct methods, and the atomic positions of Sm_2NiGa_{12}[87] were used for comparison. The data were corrected for extinction and refined using anisotropic displacement parameters. To ensure sample purity, powder X-ray diffraction was also performed. Selected crystallographic

parameters for the Ln_2NiGa_{10} (*Ln* = Ce, Pr) and Ln_2NiGa_{12} (*Ln* = La, Ce, Pr) compounds are provided in Tables 3.1 and 3.2, respectively.

Table 3.1. Crystallographic Parameters for Ce_2NiGa_{10} and Pr_2NiGa_{10}

Crystal Data		
Formula	Ce_2NiGa_{10}	Pr_2NiGa_{10}
a (Å)	4.2390(5)	4.2330(4)
c (Å)	26.386(4)	26.364(3)
V (Å^3)	474.13(10)	472.40(8)
Z	2	2
Crystal Dimension (mm^3)	0.05 x 0.05 x 0.075	0.025 x 0.030 x 0.045
Crystal System	Tetragonal	Tetragonal
Space Group	*I*4/*mmm*	*I*4/*mmm*
θ range (º)	0.998-30.034	0.998-30.034
μ(mm^{-1})	62.291	62.86
Data Collection		
Measured Reflections	472	1185
Independent Reflections	239	254
Reflections with I > 3σ(I)	225	244
R_{int}	0.0445	0.0385
h	−5 → 5	−5 → 5
k	−4 → 4	−4 → 4
l	−24 → 35	−25 → 36
Refinement		
$^aR_1$	0.0409	0.0585
$^bwR_2(F^2)$	0.1086	0.1315
Reflections	239	254
Parameters	19	9
$\Delta\rho_{max}$ (e Å^{-3})	2.689	6.275
$\Delta\rho_{min}$ (e Å^{-3})	−2.775	−1.700
Extinction coefficient	0.0076(10)	0.0015(8)

$^aR_1 = \sum||F_o| - |F_c||/\sum|F_o|$
$^bwR_2 = \sum[w(F_o^2 - F_c^2)]/ \sum[w(F_o^2)^2]^{1/2}$

Table 3.2. Crystallographic Parameters for Ce_2NiGa_{12} and Pr_2NiGa_{12}

Crystal Data		
Formula	Ce_2NiGa_{12}	Pr_2NiGa_{12}
a (Å)	6.0360(3)	6.0080(7)
c (Å)	15.5060(15)	15.454(3)
V (Å^3)	564.93(7)	557.83(13)
Z	2	2
Crystal Dimension (mm^3)	0.050 x 0.060 x 0.065	0.025 x 0.030 x 0.075
Crystal System	Tetragonal	Tetragonal
Space Group	*P*4/*nbm*	*P*4/*nbm*
θ range (º)	1.018-30.034	0.998-30.034
μ(mm^{-1})	52.279	53.231
Data Collection		
Measured Reflections	1120	933
Independent Reflections	456	346
Reflections with I > 4σ(I)	375	193
R_{int}	0.0307	0.1161
h	−8 → 8	−7 → 7
k	−6 → 6	−5 → 5
l	−21 → 11	−17 → 15
Refinement		
[a]R_1	0.0406	0.0496
[b]$wR_2(F^2)$	0.0710	0.1109
Reflections	456	346
Parameters	26	25
$\Delta\rho_{max}$ (e Å^{-3})	2.480	4.077
$\Delta\rho_{min}$ (e Å^{-3})	−1.397	−2.931
Extinction coefficient	0.0010(2)	0.0020(4)

[a] $R_1 = \sum||F_o| - |F_c||/\sum|F_o|$
[b] $wR_2 = \sum[w(F_o^2 - F_c^2)]/\sum[w(F_o^2)^2]^{1/2}$

3.2.3. Physical Property Measurements. The electrical resistivity and magnetoresistance of the Ln_2NiGa_{10} and Ln_2NiGa_{12} (*Ln* = La, Ce, Pr) compounds were measured by the standard 4-probe AC technique at 27 Hz. Pt wires (0.002 inch diameter) were attached to the sample with Epotech silver epoxy. The sample was vapor cooled in a Quantum Design cryostat. The bulk magnetic

susceptibility and magnetization versus field were also measured in a PPMS system from Quantum Design in fields up to 9 Tesla.

3.3. Results and Discussion

3.3.1. Structure of the Ln_2NiGa_{10} (*Ln* = Ce, Pr). The crystal structure of Pr_2NiGa_{10} is shown in Figure 3.1. Ln_2NiGa_{10} (*Ln* = Ce, Pr) crystallize in a tetragonal *I*4/*mmm* space group (no. 139) and have lattice parameters of a = 4.2390(5) Å, c = 26.3860(3) Å, Z = 2, V = 474.13 (11) Å^3, and a = 4.2330(4) Å, c = 26.364(3) Å, Z = 2, V = 472.40(8) Å^3, for Ce_2NiGa_{10} and Pr_2NiGa_{10}, respectively, with the *Ln*, Ni, Ga1, Ga2, Ga3, and Ga4 atoms occupying the 4*e*, 2*b*, 4*d*, 8*g*, 4*e*, and 4*e* Wyckoff symmetry sites, respectively. The atomic positions and displacement parameters for the Ln_2NiGa_{10} (*Ln* = Ce, Pr) compounds are provided in Table 3.3. Selected inter-atomic distances for the Ln_2NiGa_{10} (*Ln* = Ce, Pr) compounds are also shown in Table 3.4. The overall structure of the Ln_2NiGa_{10} (*Ln* = Ce, Pr) compounds consists of a periodic layering of face-sharing $NiGa_{8/2}$ rectangular prisms and *Ln* atoms, which are encapsulated in Ga-only cages. These cage-like encapsulations resemble the inverse PbO-type Cr_2Si_2 cages in the $ThCr_2Si_2$- type structure.[82]

Figure 3.1. The crystal structure of Ce_2NiGa_{10}. The Ce atoms are shown in blue, Ni polyhedra are shown in purple, and the Ga atoms are shown in green.

Each *Ln* atom of Ce_2NiGa_{10} and Pr_2NiGa_{10} is connected to Ga3 atoms with interatomic distances of 3.1775(9) Å (x4) and 3.1703(14) Å (x4), respectively. These distances are consistent with the expected *Ln*-Ga distances obtained from the summation of the covalent radii

of Ce or Pr (1.65 Å)[65] and Ga (1.25 Å).[65] These *Ln*-Ga3 distances are also consistent with the Ce-Ga3 distance of 3.2448(7) Å found in Ce_2PdGa_{10}.[32]

Table 3.3. Atomic Positions and Displacement Parameters in Ce_2NiGa_{10} and Pr_2NiGa_{10}

Atom	Wyckoff Position	*x*	*y*	*z*	U_{eq} (Å^2)[a]
Ce	4*e*	0	0	0.35391(4)	0.0067(5)
Ni	*2b*	0	0	1/2	0.0064(8)
Ga1	4*d*	0	1/2	1/4	0.0205(7)
Ga2	8*g*	1/2	0	0.45078(5)	0.0083(5)
Ga3	4*e*	0	0	0.10613(9)	0.0186(7)
Ga4	4*e*	0	0	0.19760(9)	0.0118(6)
Pr	4*e*	0	0	0.35410(6)	0.0060(6)
Ni	*2b*	0	0	1/2	0.0054(11)
Ga1	4*d*	0	1/2	1/4	0.0231(10)
Ga2	8*g*	1/2	0	0.45090(8)	0.0065(7)
Ga3	4*e*	0	0	0.10627(14)	0.0088(8)
Ga4	4*e*	0	0	0.19748(16)	0.0191(10)

[a] U_{eq} is defined as one-third of the trace of the orthogonalized U_{ij} tensor.

The transition metal environment of the Ln_2NiGa_{10} compounds consists of face-sharing $NiGa_{8/2}$ rectangular prisms, where the Ni atoms are connected to Ga2 atoms at distances of 2.4858(7) Å (8x) and 2.4810(11) Å (8x) for Ce_2NiGa_{10} and Pr_2NiGa_{10}, respectively. These Ni-Ga distances are consistent with other Ni-Ga distances in the reported Ce_2NiGa_{10} [2.494(2) Å],[52] and$YNiGa_3Ge$ [2.4632(8) Å][88] compounds.

The *Ln* atoms in the structure of the Ln_2NiGa_{10} compounds are staggered along the *c*-axis and separated by Ga1-Ga4 tetrahedral slab layers, which are similar to the PbO-type Ni_2B_2 and $NiAl_4Ge_2$ slab layers found in the structurally related $LnNi_2B_2C$ (*Ln* = Y, La, Ce, Sm, Tb, Dy, Ho, Er, Tm, Lu)[89] and $Tb_2NiAl_4Ge_2$ compounds, respectively.[53] The Ln-Ln_c contacts across these Ga1-Ga4 tetrahedral slab layers are 6.249(11) Å and 6.252(13) Å for Ce_2NiGa_{10} and Pr_2NiGa_{10}, respectively. The Ln-$Ln_{a\text{-}b}$ contacts are 4.239(3) Å and 4.233(7) Å for Ce_2NiGa_{10} and

Pr_2NiGa_{10}, respectively. These distances are similar to the Ce-Ce_{ab} distance of 4.262(3) Å found in the reported Ce_2NiGa_{10}.[52] Although, these distances are too long to be considered bonding, they are consistent with the Ce-Ce_{ab} distance of 4.323(6) Å and Ce-Ce_c distance of 6.258(5) Å found in Ce_2PdGa_{10}.

Table 3.4. Selected Interatomic Distances (Å) and Bond Angles (°) of Ce_2NiGa_{10} and Pr_2NiGa_{10}

Ce_2NiGa_{10}		Pr_2NiGa_{10}	
Ce-Ga3 layer		*Pr-Ga3 layer*	
Ce-Ga3 (x4)	3.1775(9)	Pr-Ga3 (x4)	3.1703(14)
$NiGa_{8/4}$ segment		*$NiGa_{8/4}$ segment*	
$NiGa_{8/4}$ (x8)	2.4858(7)	$NiGa_{8/4}$ (x8)	2.4810(11)
Ga1-Ga4 slab layer		*Ga1-Ga4 slab layer*	
Ga1-Ga4 (x4)	2.5305(14)	Ga1-Ga4 (x4)	2.529(2)
Ga4-Ga3 (x1)	2.414(4)	Ga4-Ga3 (x1)	2.405(6)
Angles		*Angles*	
Ga3-Ce-Ga3	83.68(3)	Ga3-Pr-Ga3	83.77(4)
Ga2- Ni- Ga2	79.34(4)	Ga2- Ni -Ga2	74.20(4)
	117.00(5)		117.10(8)
	63.00(5)		62.90(8)
Ga1-Ga4-Ga1	72.63(4)	Ga1-Ga4-Ga1	72.56(8)
Ga4-Ga1-Ga4	107.37(5)	Ga4-Ga1-Ga4	107.44(8)
	113.77(9)		113.61(16)

3.3.2. Structure of the Ln_2NiGa_{12} (*Ln* = La, Ce, Pr) Compounds. Figure 3.2 shows the crystal structure of Pr_2NiGa_{12}, which is isostructural to the reported Sm_2NiGa_{12}[87] and Ce_2PdGa_{12}.[32] The Ln_2NiGa_{12} (*Ln* = Ce, Pr) compounds crystallize in a tetragonal space group, *P*4/*nbm* (no. 125 with origin choice 2) with lattice parameters of a = 6.0360(3) Å, c = 15.5060(2) Å, Z = 2, V = 564.93 (15) $Å^3$ and a = 6.0080(7) Å, c = 15.454(3) Å, Z = 2, V = 557.83(13) $Å^3$ for Ce_2NiGa_{12} and Pr_2NiGa_{12}, respectively. The Ln, Ni, Ga1, Ga2, Ga3, and Ga4 atoms occupy the 4*h*, 2*c*, 4*g*,

4*g*, 8*m*, and 8*m* Wyckoff symmetry sites, respectively. The structures of the Ln_2NiGa_{12} (*Ln* = Ce, Pr) compounds consist of the stacking of $NiGa_{8/2}$ rectangular prism layers and *Ln*-Ga layers, where the *Ln* atom is coordinated by 10 Ga atoms. The atomic positions and displacement parameters of the Ln_2NiGa_{12} (*Ln* = Ce, Pr) compounds are provided in Table 3.5. Selected interatomic distances and bond angles in the Ln_2NiGa_{12} (*Ln* = Ce, Pr) compounds are also provided in Table 3.7.

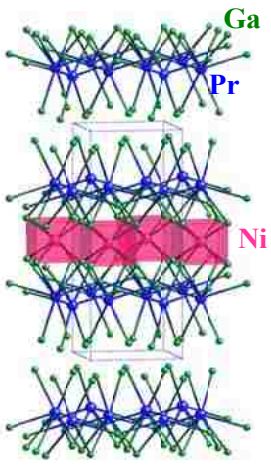

Figure 3.2. The crystal structure of Pr_2NiGa_{12} along the *c*-axis. The Pr atoms are shown in blue, Ni polyhedra are shown in fuschia, and Ga atoms are shown in green.

Table 3.5. Atomic Positions and Displacement Parameters in Ce_2NiGa_{12} and Pr_2NiGa_{12}

Atom	Wyckoff Position	*x*	*y*	*z*	U_{eq} (Å^2)[a]
Ce	4*h*	3/4	1/4	0.24439(4)	0.0074(2)
Ni	2*c*	3/4	1/4	0	0.0079(4)
Ga1	4*g*	3/4	3/4	0.18143(8)	0.0087(3)
Ga2	4*g*	3/4	3/4	0.33955(9)	0.0119(3)
Ga3	8*m*	0.50023(8)	0.00023(8)	−0.08340(5)	0.0093(2)
Ga4	8*m*	0.57027(11)	0.07027(11)	0.42816(7)	0.0212(3)
Pr	4*h*	3/4	1/4	0.24459(1)	0.0065(6)
Ni	2*c*	3/4	1/4	1/2	0.0043(13)
Ga1	4*g*	1/4	1/4	0.3183(2)	0.0085(10)
Ga2	4*g*	1/4	1/4	0.1606(3)	0.0118(10)
Ga3	8*m*	0.50058(3)	0.00058(3)	−0.08399(16)	0.0071(7)
Ga4	8*m*	0.56967(11)	0.06967(11)	0.42809(2)	0.0255(10)

[a] U_{eq} is defined as one-third of the trace of the orthogonalized U_{ij} tensor.

When a bonding cut-off of 3.3 Å is applied, the *Ln* atom is coordinated to 10 Ga atoms: 4 Ga1, 4 Ga3, and 2 Ga4. The Ce-Ga distances [3.1720(5) Å- 3.2855(9) Å] and Pr-Ga distances [3.1575(13) Å- 3.271(3) Å] in these compounds are similar to the expected inter-atomic

distances obtained from the summation of the covalent radii of Ce or Pr (1.65 Å) and Ga (1.25 Å).[65] In particular, the Ce-Ga distances in Ce_2NiGa_{12} [3.1720(5) Å- 3.2855(9) Å] are in good agreement with the Ce-Ga distances in Ce_2CuGa_{12}[41] and Ce_2PdGa_{12}[32] compounds, as shown in Table 3.7.

Table 3.6. Selected Inter-atomic Distances (Å) in Ce_2NiGa_{12} and Pr_2NiGa_{12}

Ce_2NiGa_{12}		**Pr_2NiGa_{12}**	
Ce layer		*Pr layer*	
Ce-Ga1 (x4)	3.1720(5)	Pr-Ga1 (x4)	3.1575(13)
Ce-Ga4 (x2)	3.2361(11)	Pr-Ga4 (x2)	3.220(3)
Ce-Ga3 (x2)	3.2830(9)	Pr-Ga3 (x2)	3.271(3)
Ce-Ga3 (x2)	3.2855(9)	Pr-Ga3 (x2)	3.262(3)
$NiGa_6$ Segment		*$NiGa_6$ Segment*	
Ga1-Ga3 (x4)	2.6201(9)	Ga1-Ga3 (x4)	2.606(3)
Ni-Ga3 (x4)	2.4936(8)	Ni-Ga3 (x4)	2.483(3)
(x4)	2.4969(8)	(x4)	2.496(3)
Ga - only Segment		*Ga - only Segment*	
Ga2-Ga4 (x4)	2.6080(9)	Ga2-Ga4 (x4)	2.599(3)
Ga4-Ga4 (x1)	2.531(2)	Ga4-Ga4 (x1)	2.525(5)

Table 3.7. A Comparison of the Ce-Ga distances (Å) in the Ce_2MGa_{12} Compounds (*M* = Ni, Cu, and Pd) Compounds

Ce_2NiGa_{12}		**Ce_2CuGa_{12}[41]**		**Ce_2PdGa_{12}[32]**	
Ce-Ga1 (×4)	3.1720(5)	Ce-Ga1 (×4)	3.2322(7)	Ce-Ga1 (×4)	3.2033(5)
Ce-Ga4 (×2)	3.2361(11)	Ce-Ga4 (×2)	3.2102(17)	Ce-Ga4 (×2)	3.2286(13)
Ce-Ga3 (×2)	3.2830(9)	Ce-Ga3 (×2)	3.2863(13)	Ce-Ga3 (×2)	3.2772(11)
Ce-Ga3 (×2)	3.2855(9)	Ce-Ga3 (×2)	3.2903(13)	Ce-Ga3 (×2)	3.2808(11)

The transition metal environment of the Ln_2NiGa_{12} compounds consists of face-sharing rectangular prisms, where the Ni atom is coordinated to 8 Ga3 atoms. These Ni-Ga3 distances,

which range from 2.483(3) Å to 2.4969(8)Å, are consistent with the summation of the covalent radii for Ni (1.15 Å) and Ga (1.25 Å).[65]

The Ga-only segment of the Ln_2NiGa_{12} compounds consists of two Ga layers, where one layer is composed of Ga2 atoms and the other of Ga4 atoms. These Ga- only segments separate the *Ln* atoms along the *c*-axis. In the Ln_2NiGa_{12} (*Ln* = Ce, Pr) compounds, there are *Ln*-Ln_{ab} and 2 distinct *Ln*-Ln_c distances. The *Ln*-Ln_{ab} distances, which are 4.268(6) Å and 4.248(4) Å for Ce_2NiGa_{12} and Pr_2NiGa_{12}, respectively, are longer than the summation of the covalent radii of *Ln* and Ga but may exhibit weak bonding interactions. These distances are also in good agreement with the Ce-Ce_{ab} contact distances of 4.316(6) Å[32] and 4.319(7) Å[41] found in Ce_2PdGa_{12} and Ce_2CuGa_{12}, respectively. However, the Ce-Ce_c distances of 7.579(5) Å and 7.927(7) Å found in Ce_2NiGa_{12} and Pr-Pr_c distances of 7.559 (5) Å and 7.895(6) Å in Pr_2NiGa_{12}, are too long to be considered bonding. The distances are also comparable to the Ce-Ce_c distances of 7.669(5) Å and 7.880(6) Å[32] found in Ce_2PdGa_{12} and 7.576(6) Å and 7.799(7)[41] Å found in Ce_2CuGa_{12}.

3.3.3. Transport and Physical Properties of Ln_2NiGa_{10} (*Ln* = Ce, Pr). Figure 3.3 shows the normalized electrical resistivity for Ce_2NiGa_{10} and Pr_2NiGa_{10}. The resistivity data of these samples were measured with the field parallel to the ab-plane of the single crystals. For Pr_2NiGa_{10}, the resistivity from 50 K to 300 K is observed to increase linearly as a function of increasing temperature, which is expected for a

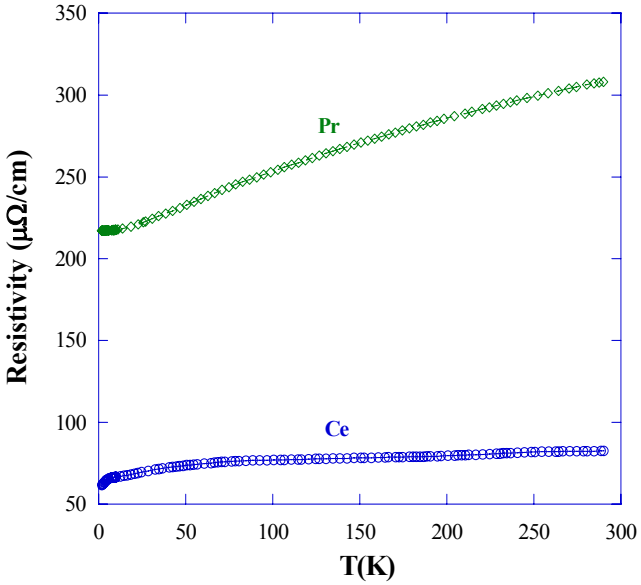

Figure 3.3. The normalized electrical resistivity for the current parallel to the *ab*-plane of single crystals of Ce_2NiGa_{10} (shown in blue) and Pr_2NiGa_{10} (shown in green) as a function of temperature.

typical metal. However, the resistivity of Ce_2NiGa_{10} is smaller in magnitude and shows a linear behavior from 150 K to 300 K. A broad shoulder in the resistivity for the Ce_2NiGa_{10} compound is similar to the broad shoulder observed in Ce_2PdGa_{10}, which indicates the onset of Kondo coherence.

Figure 3.4 shows the magnetic susceptibility of both Ln_2NiGa_{10} with field perpendicular to the *a*-*b* plane. Antiferromagnetic transitions occur at T_N = 2.78 K, with θ = -9, and T_N = 7.3 K, with θ = -5.2, for Ce_2NiGa_{10} and Pr_2NiGa_{10}, respectively. The inset shows the Curie Weiss fit from 10 K to 80 K for the Ce analog. Using this fit, Ce is observed to possess a magnetic moment of 2.58 μ_B, which is consistent with the Ce^{3+}moment of 2.54 μ_B. Using a similar fit for the Pr analog, a magnetic moment of 3.48 μ_B is obtained for Pr, which is consistent with the Pr^{3+} moment of 3.58 μ_B.

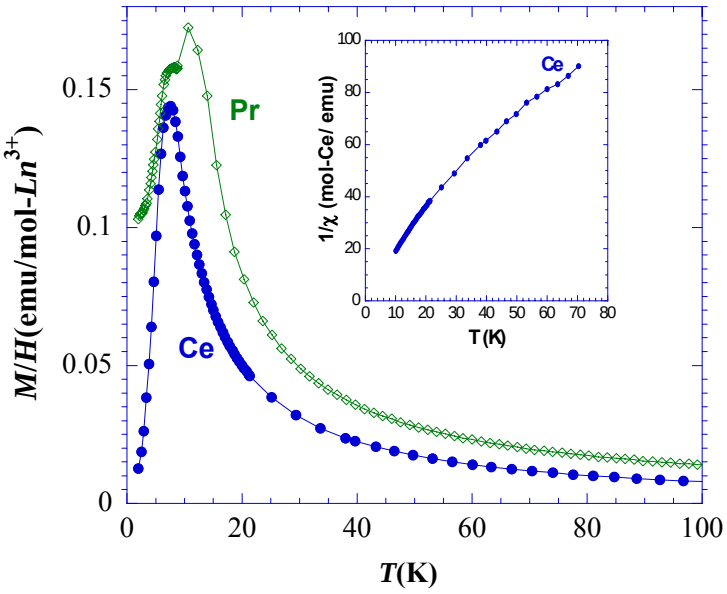

Figure 3.4. The magnetic susceptibility of a single crystals of Ce_2NiGa_{10} (shown in blue) and Pr_2NiGa_{10} (shown in green) as a function of temperature for field perpendicular to the *ab*-plane. The inset shows the inverse susceptibility (*H*/*M*) of Ce_2NiGa_{10} with Curie-Weiss behavior as a function of temperature from 10 K to 80 K. The solid lines in the figures are a fit to the data as described in the text.

Figure 3.5 shows the magnetization data as a function of field for both Ln_2NiGa_{10} (*Ln* = Ce, Pr) compounds. The Ce analogue is observed to saturate at a lower value (~ 1.9 μ_B) than the calculated μ_{sat} of 2.14 μ_B for Ce^{+3}. This may be attributed to spin disorder scattering in this compound, which is indicated by the drop in the resistivity data. Step-like transitions are observed for the Pr_2NiGa_{10} with increasing field. These

transitions are consistent with metamagnetic behavior, where a compound fluctuates from antiferromagnetic to ferromagnetic transitions as magnetic fields are induced.

3.3.4. Transport and Physical Properties of the Ln_2NiGa_{12} (Ln = La, Ce, Pr) Compounds. Figure 3.6 shows the resistivity for the Ln_2NiGa_{12} (Ln = Ce, Pr) and Ce_2CuGa_{12} compounds. The electrical resistivity for Ce_2NiGa_{12} is observed to increase linearly as a function of increasing temperature from T = 100 K- 300 K. However, a broad shoulder is observed in the resistivity at T = 100 K- 0 K, and a kink is observed at 7.5 K, which correlates with the ordering temperature. For Pr_2NiGa_{12}, the resistivity is observed to increase linearly with increasing temperature at T = 10 K- 300 K. The resistivity of

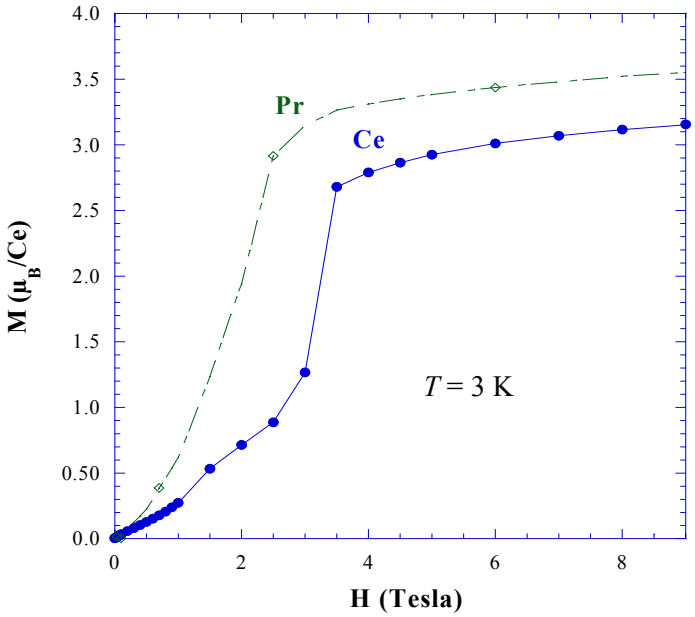

Figure 3.5. Magnetization versus field for single crystals of Ce_2NiGa_{10} and Pr_2NiGa_{10} at 3 K shown in closed blue and open green diamonds, respectively, for the field parallel to the *ab*-plane.

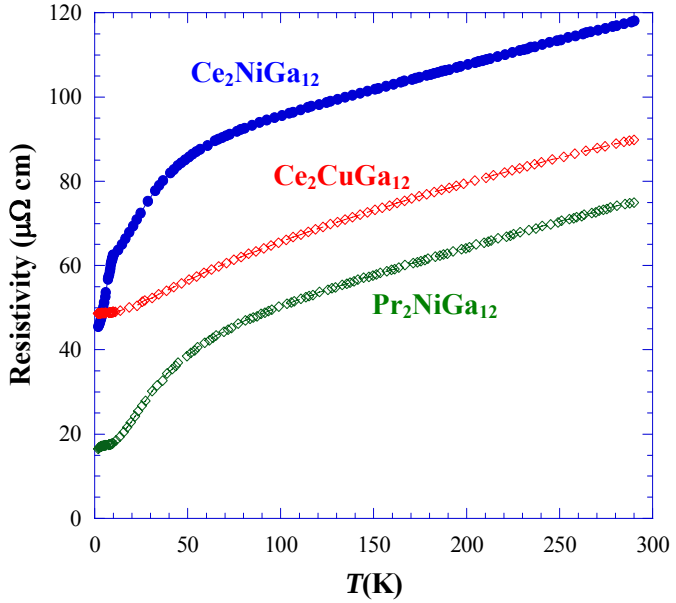

Figure 3.6. The normalized electrical resistivity of a single crystals of Ce_2NiGa_{12}, Ce_2CuGa_{12}, and Pr_2NiGa_{12} are shown in blue closed circles, red open diamonds, and green open diamonds, respectively, as a function of temperature for the current parallel to the *ab*-plane.

Ce_2CuGa_{12}, which is shown for comparison, exhibits a linear behavior from T = 300 K to 100 K. However, below 100 K, there is a large drop in resisitivity accompanied by a broad shoulder, which is also indicative of the onset of Kondo coherence. This signature feature in the resistivity is similar to the one found in that of Ce_2NiGa_{10} and Ce_2PdGa_{10}.[31]

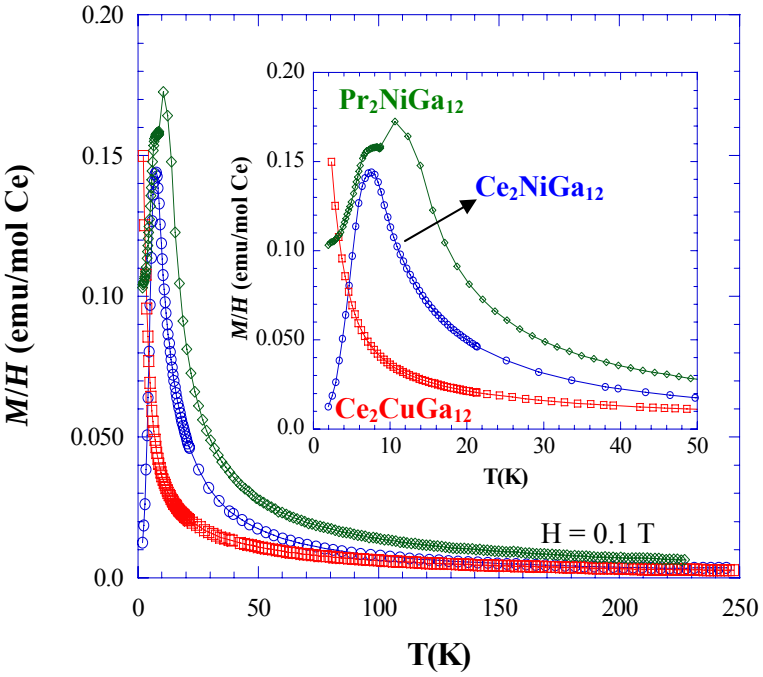

Figure 3.7. The magnetic susceptibilities of single crystals of Ce_2NiGa_{12} (shown in blue), Ce_2CuGa_{12} (shown in red), and Pr_2NiGa_{12} (shown in green) as a function of temperature for field perpendicular to the *ab*-plane. The inset shows a closer view of the magnetic susceptibility from 0 K to 50 K.

Figure 3.7 shows the magnetic susceptibilities of the Ln_2NiGa_{12} (Ln = Ce, Pr) and Ce_2CuGa_{12}[31] compound with field parallel to the *c*-axis. Kinks in the magnetic susceptibility, which suggest antiferromagnetic transitions occur at T_N = 7.5 K and 10.56 K for Ce_2NiGa_{12} and Pr_2NiGa_{12}, respectively. However, paramagnetic behavior is observed for Ce_2CuGa_{12} down to 3 K.

A Curie Weiss fit (not shown) for Ce_2NiGa_{12} from T = 15 K to 120 K is used to obtain an effective magnetic moment of 2.48 μ_B for Ce, which is consistent with a Ce^{3+}moment of 2.54 μ_B Ce^{3+}. Using a similar fit, from T = 10 K to 150 K an effective magnetic moment of 3.38 μ_B was obtained for Pr, which is consistent with the Pr^{3+} moment of 3.58 μ_B. For comparison, an

effective magnetic moment of 2.36 μ_B was obtained for Ce in Ce_2CuGa_{12}, which is slightly smaller than the expected value for Ce^{3+} (2.54 μ_B).

Figure 3.8 shows the magnetization data as a function of field at 3 K for Ln_2NiGa_{12} and Ce_2CuGa_{12}. For Ce_2NiGa_{12}, saturation is observed up to fields of 9 Tesla, which is consistent with the calculated μ_{sat} of 2.14 μ_B for Ce^{3+}. For the Pr_2NiGa_{12}, the onset of saturation is also observed at fields up to 9 Tesla, which is consistent with the calculated μsat of 3.20 μ_B for Pr^{3+}. However, the magnitude of the magnetization of Ce_2CuGa_{12} is lower than the expected μ_{sat} of 2.14 μ_B for Ce^{3+}, which may be attributed to the Kondo shielding effects observed in the resistivity data (Figure 3.6).

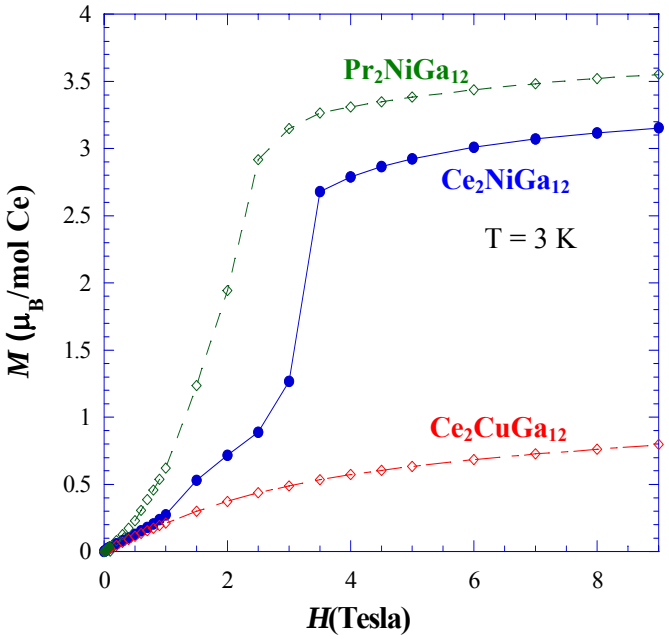

Figure 3.8. Magnetization as a function of magnetic field for single crystals of Ce_2NiGa_{12} (shown in blue), Pr_2NiGa_{12} (shown in green), and Ce_2CuGa_{12} (shown in red) at 3 K.

Figure 3.9 shows the normalized electrical resistivity of single crystals of La_2NiGa_{12} and La_2CuGa_{12} for current parallel to the *a*-*b* plane. The resistivity of La_2NiGa_{12} exhibits linear behavior from 250 K down to 10 K. However, a drop in the resistivity is observed at 2 K, which may be attributed to an impurity phase or Ga flux on the surface of the crystal.

Figure 3.10 shows the in plane magnetoresistance (MR(%) = [(ρ(H) - ρ(0)) / ρ(0)] x 100) of single crystals of La_2NiGa_{12} and La_2CuGa_{12}. While both compounds exhibit large MR, the MR for La_2NiGa_{12} (MR% > 600 at 9 Tesla) is substantially larger than the MR of La_2CuGa_{12}

(MR %. ~ 90 % at 9 Tesla). The recalibrated magnetoresistance of La_2NiGa_{12} (not shown) with the Ga impurity at 0.09 K subtracted is still large (MR% > 200%) and does not saturate.

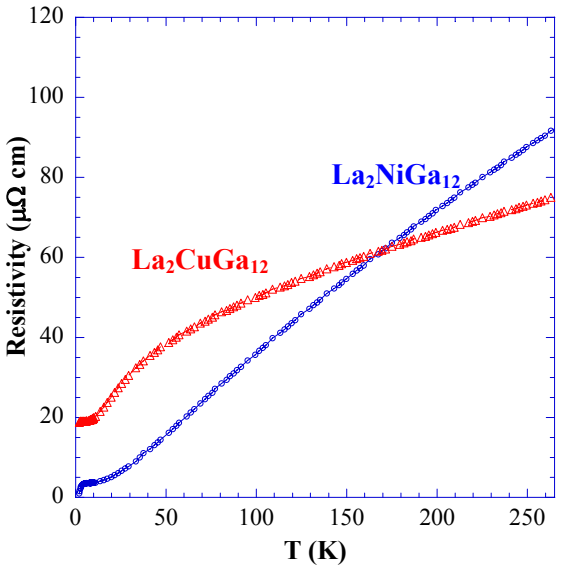

Figure 3.9. The normalized electrical resistivity of single crystals of La_2NiGa_{12} and La_2CuGa_{12} are shown in blue open circles and red open diamonds, respectively, as a function of temperature for the current parallel to the *ab*-plane. The inset shows the kink in the resistivity at $T = 2$ K for La_2NiGa_{12}.

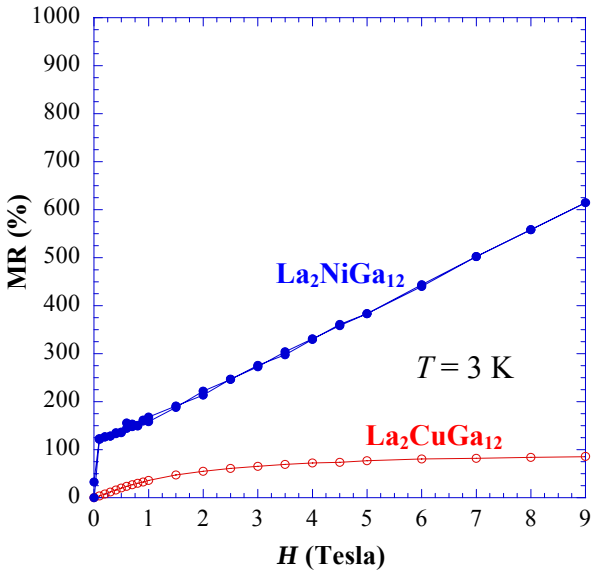

Figure 3.10. The in plane magnetoresistance (MR) of single crystals of La_2NiGa_{12} and La_2CuGa_{12} are shown in blue open circles and red open circles, respectively.

3.4. Discussion

3.41. Ce_2PdGa_{10} with Ni. It has been observed that the Ln_2NiGa_{12} compounds consistently exhibit higher magnetic ordering temperatures than their Ln_2NiGa_{10} counterparts. Table 3.8 shows the magnetic data for Ln_2NiGa_{10} and Ln_2NiGa_{12} (*Ln* = Ce, Pr) in comparison to the reported magnetic data for Ce_2PdGa_{10}[31] and Ce_2PdGa_{12}.[32] While Ce_2NiGa_{12} and Pr_2NiGa_{12} magnetically order at $T_N = 7.6$ K and 10.4 K, respectively, the magnetic order observed for their Ce_2NiGa_{10} ($T_N = 2.78$ K) and Pr_2NiGa_{10} ($T_N = 7.22$ K) counterparts is slightly lower. One explanation is that magnetic ordering can be quenched through Kondo- like interactions, where the conduction electrons "shield" the magnetic ion, thus leading to a lower ordering temperature

in Ln_2NiGa_{10} (*Ln* = Ce, Pr). This suppression of the magnetic order is similar to that observed in Ce_2PdGa_{10} (magnetic transition at 1.86 K) when compared to that of $CePdGa_6$ (T_N = 5.5 K)and Ce_2PdGa_{12} (T_N = 10.5 K).[31]

3.4.2. Ce_2PdGa_{12} with Ni. In other systems, such as the Ln_2NiGa_{12} (*Ln* = Ce, Pr) and Ce_2PdGa_{12},[32] RKKY- like interactions may dominate due to hybridization effects influenced by "close" conduction electron carriers, and magnetic ordering is more pronounced. However, we propose that in the Ce_2CuGa_{12} compound, Kondo- like interactions are more dominant due to the extra conduction electrons in this compound. This is also suggested by the large drop and broad shoulder near 100 K, which is present in the resistivity data for this compound as shown in Figure 3.6.

Table 3.8. Overview of the Physical Properties Data of the Ln_2NiGa_{10} (*Ln* = Ce, Pr) and Ln_2NiGa_{12} (*Ln* = Ce, Pr) Compounds

Compound	Ordering Type	Ordering Temperature (K)	θ_W (K)	μ_{eff} (calc.) (μ_B)	μ_{eff} (exp.) (μ_B)
Ce_2NiGa_{10}	AFM[a]	2.78	−9.0	2.54	2.58
Pr_2NiGa_{10}	AFM[a]	7.22	−5.2	3.58	3.48
Ce_2PdGa_{10}[31]	?	1.86	~ 0	2.54	2.50
Ce_2NiGa_{12}	AFM[a]	7.50	5.20	2.54	2.48
Pr_2NiGa_{12}	AFM[a]	10.56	0.84	3.58	3.34
Ce_2CuGa_{12}	PM[b]	—	−11.14	2.36	2.54
Ce_2PdGa_{12}[32]	AFM[a]	10.5	−14.5	2.54	2.59

[a]Antiferromagnetic
[b]Paramagnetic down to 3 K

Because the number of Ce-Ga contacts is the same for each compound within a given family, comparing the *Ln-Ln* contact distances may offer insight into the physical properties

observed for each particular compound. Tables 3.9 shows the *Ln-Ln* contact distances in the Ln_2NiGa_{10} and Ln_2NiGa_{12} compounds in comparison to those found in Ce_2PdGa_{10}[31] and Ce_2PdGa_{12},[32] respectively. For example, the Ce-Ce_{a-b} contact found in Ce_2NiGa_{10} [4.239(3) Å] are noticeably closer than the Ce-Ce_{a-b} contact [4.323(6) Å] found in Ce_2PdGa_{10}. As a result, a higher magnetic ordering temperature of 2.78 K is observed for Ce_2NiGa_{10} when compared to Ce_2PdGa_{10}, which exhibits a magnetic transition at 1.86 K. In contrast, although the *Ln-Ln*$_{a-b}$ distances of 4.268(6) Å and 4.248(4) Å found in Ce_2NiGa_{12} and Pr_2NiGa_{12}, respectively, are closer than the Ce-Ce_{a-b} contact distance of 4.316(6) Å found in Ce_2PdGa_{12}, lower ordering temperatures are observed for the Ln_2NiGa_{12} compounds. These lower ordering temperatures may be attributed to Kondo-like interactions, which may suppress the magnetic ordering in these materials, as suggested in the resistivity data for these compounds (Figure 3.6).

Table 3.9. Selected *Ln-Ln* distances in Ln_2MGa_{10} and Ln_2MGa_{12} (*Ln* = Ce, Pr; *M* = Ni, Pd)

Distances (Å)	Ce_2NiGa_{10}	Pr_2NiGa_{10}	Ce_2PdGa_{10}
$(Ln\text{-}Ln)_{a-b}$	4.239(3)	4.233(7)	4.323(6)
$(Ln\text{-}Ln)_c^1$	6.249(11)	6.252(13)	6.258(5)
$(Ln\text{-}Ln)_c^2$	7.709(8)	7.693(10)	7.807(7)
Ordering Type	AFM[a]	AFM[a]	PM[b]
Ordering Temp. (K)	2.78	7.3	—
Distances (Å)	Ce_2NiGa_{12}	Pr_2NiGa_{12}	Ce_2PdGa_{12}
$(Ln\text{-}Ln)_{a-b}$	4.268(6)	4.248(4)	4.316(6)
$(Ln\text{-}Ln)_c^1$	7.579(5)	7.559(5)	7.669(5)
$(Ln\text{-}Ln)_c^2$	7.927(7)	7.895(6)	7.880(6)
Ordering Type	AFM[a]	AFM[a]	AFM[a]

(Table Continued)

Ordering Temp. (K)	7.5	10.56	10.5

[a]Antiferromagnetic
[b]Paramagnetic down to 3 K

CHAPTER IV. INVESTIGATING THE STRUCTURE OF Yb_5Pt_9 USING SINGLE CRYSTAL X-RAY DIFFRACTION AND NEUTRON POWDER DIFFRACTION[1]

4.1. Introduction

Studying quantum criticality in HF systems materials may lead to a better understanding of the underlying behavior in these complex systems.[9] Yb-based compounds are of great interest because they can be viewed as the hole-doped analogue to Ce, and the vast majority of heavy fermion compounds are Ce and Yb-based.[50] For example, in the well studied $YbRh_2Si_2$ compound, which lies near a QCP, magnetic field (B_c = 0.66 T) was used as a tuning parameter to suppress the magnetic order (T_N = 70 mK) in this compound.[12-14, 90-92] Another example, YbBiPt, which is a member of the MgAgAs-type compounds where the lattices of Mg and As atoms form the rock salt structure with Ag atoms being encapsulated in every other cube,[93, 94] is the "heaviest" known heavy fermion [Sommerfeld coefficient (γ) of 8000 mJ/ mol K^2] and also exhibits magnetic ordering.[95, 96]

In our interest in investigating the structure-property relationships of highly correlated materials, we have studied various Yb binaries. Mixed valency (Yb^{3+}/Yb^{4+}) has been observed in several Yb-Pt binary phases, such as Yb_2Pt, Yb_5Pt_3, and Yb_5Pt_4.[97, 98] In theory, these valence fluctuations in these materials should diminish magnetic ordering. However, magnetic ordering has been found in several of the Yb-Pt mixed-valent compounds, such as in $YbPt_3$ and Yb_3Pt_5, where antiferromagnetic ordering is observed at T_N = 0.30 K and 0.95 K, respectively.[99]

Recently, a new ferromagnetic Yb-based binary compound, Yb_5Pt_9, has been synthesized using flux growth. Yb_5Pt_9 is a rare example of a ferromagnetic heavy fermion compound with double magnetic transitions at T_C = 0.6 and 0.65 K, and $\gamma \sim$ 12,000 mJ/mol-K^2 below 0.8 K.[100]

[1] Section of this chapter is taken from Phys Rev B., 74, Kim, M. S.; Bennett, M. C.; Sokolov, D. A.; Aronson, M. C.; Millican, J. N.; Chan, J.Y.; Huang, Q.; Chen, Y.; Lynn, J. W., Copyright (2006), with permission from APS

Figure 4.1 shows the location of Yb_5Pt_9 in the Yb-Pt binary phase diagram. Structural information for other Yb-Pt binaries is provided in Table 4.1.

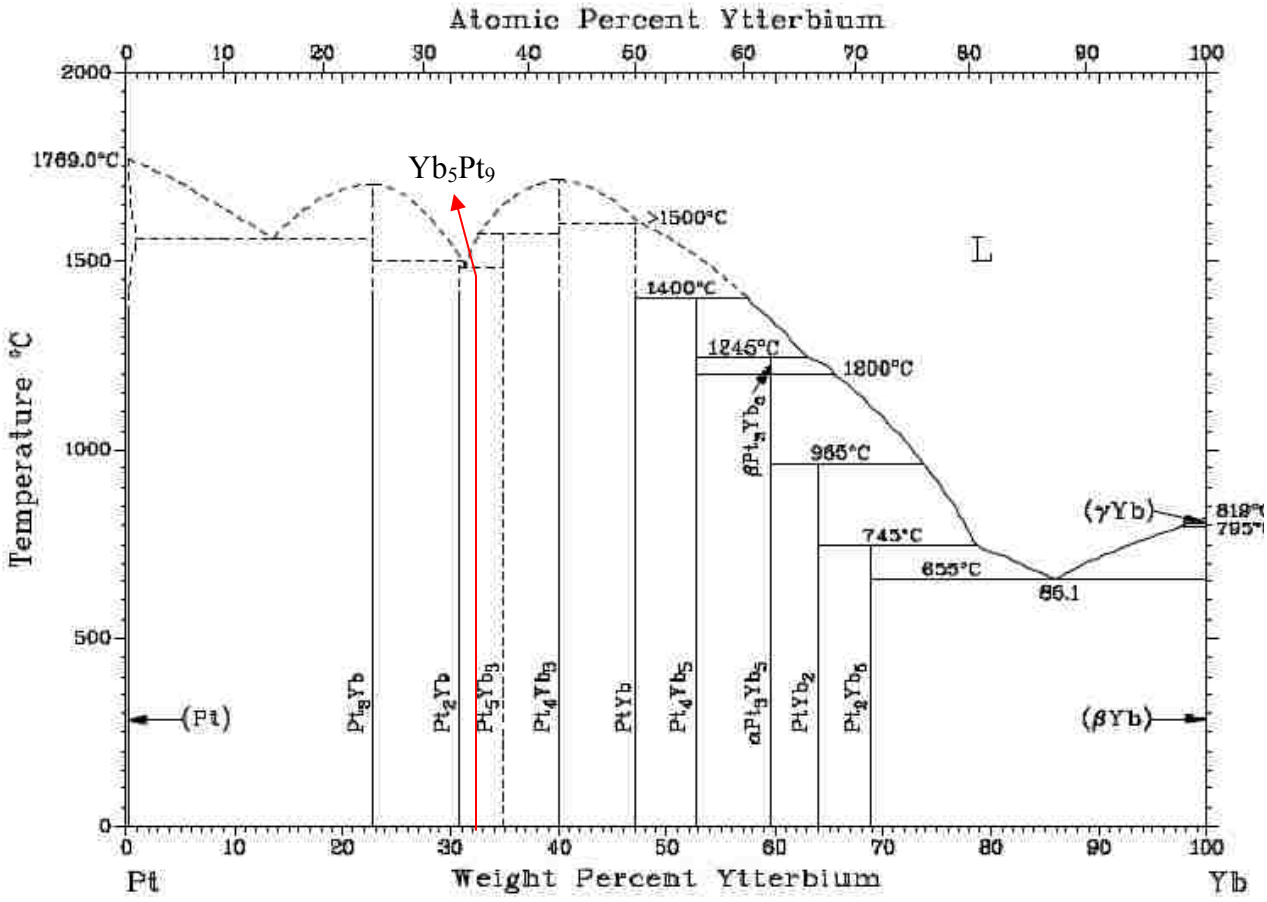

Figure 4.1. The Yb-Pt binary Phase Diagram. The red line shows the position of Yb_5Pt_9 in the Yb-Pt binary phase diagram based on stoichiometry.
Retrieved from: Massalski, T., et al., Binary Alloy Phase Diagrams, Vol. 2, 1986, pp. 1922.

Table 4.1. Structural information for several Yb-Pt binary compounds

Compound	Structure type*	Lattice constants (Å)			Method*
		a	***b***	***c***	
Yb_5Pt_2	Mn_5C_2	15.896	6.476	7.576	sc
Yb_2Pt	$PbCl_2$	7.614	4.400	8.957	sc, p
Yb_5Pt_3	Mn_5Si_3	8.337	—	6.251	sc, p
Yb_5Pt_4	Sm_5Ge_4	7.390	14.319	7.506	sc, p

(Table Continued)

YbPt	FeB	6.8514	4.429	5.480	sc, p
Yb_3Pt_4	Pu_3Pd_4	12.888	—	5.629	p
$YbPt_2$	$MgCu_2$	7.546	—	—	p
$YbPt_3$	$AuCu_3$	4.040	—	—	p

* sc = single crystal, p = powder.
Adapted from: Iandelli, A. and Palenzona, A., J. Less Common Met., Vol. 43, 1975, pp. 207.

4.2.1. Single Crystal X-ray Diffraction. Single crystals of Yb_5Pt_9 were synthesized using excess Pb, as shown in Figure 4.2. A silver colored crystal fragment of dimensions 0.025 x 0.025 x 0.025 mm^3 was mechanically extracted and mounted onto the goniometer of a Nonius Kappa CCD diffractometer equipped with a MoK_α (λ = 0.71073 Å) radiation tube. The structure was solved and refined using the SHELXL97 program.[51] Suggested systematic absences were used in assigning the space group, *Cmmm*. Table 4.2 lists several other possible space group choices, which included the suggested systematic absences, but did not reflect the best possible structural model. Corrections were made for absorption and extinction, and the atomic positions were refined with anisotropic displacement parameters. Due to the large mass absorption coefficients of Yb (80.23 cm^2g^{-1}) and Pt (108.6 cm^2g^{-1}) using a MoK_α (λ = 0.71073 Å) X-ray source, the R-value of 9.3%, was obtained for the best structural model. However, neutron powder diffraction was used as a complementary tool in confirming the orthorhombic structure. In addition, electron microanalysis experiments were also conducted on polished single crystals using a Cameca SX100 microprobe system in order to confirm the lack of Pb impurities. Selected crystallographic parameters for Yb_5Pt_9 are provided in Table 4.3.

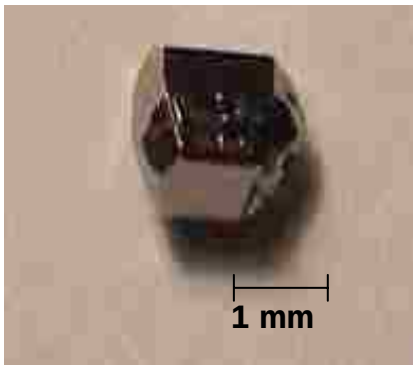

Figure 4.2. Single crystal of Yb_5Pt_9.

Table 4.2. Space group choices for Yb_5Pt_9

Space group	[a]R-value (%)
$C2\bar{c}$	~21
*Cmmm**	9.30
Cc	14.96
$A2\bar{m}$	13.16
$P42\bar{n}$	79.6
$P2_122_1$	24.90

[a] $R_1 = \sum||F_o| - |F_c||/\sum|F_o|$
* Space group applied to construct the best structural model

Table 4.3. Crystallographic Data for Yb_5Pt_9

Formula	**Yb_5Pt_9**
a (Å)	13.5550(5)
b (Å)	13.3720(5)
c (Å)	5.6540(3)
V (Å^3)	1024.83(8)
Z	16
Crystal Dimension (mm^3)	0.025 x 0.025 x 0.025
Crystal System	Orthorhombic
Space Group	*Cmmm*
θ range(°)	0.998 - 30.034
μ (mm^{-1})	155.811
Data Collection	
Measured reflections	2354
Independent reflections	848
Reflections with $I > 4\sigma(I)$	765
R_{int}	0.1051
h	$-18 \rightarrow 18$
k	$-18 \rightarrow 16$
l	$-7 \rightarrow 7$
Refinement	
[a]$R_1[F^2 > 2\sigma(F^2)]$	0.0930
[b]$wR_2(F^2)$	0.2807
Reflections	848
(Table Continued)	
Parameters	50
$\Delta\rho_{max}$ (e Å^{-3})	20.721
$\Delta\rho_{min}$ (e Å^{-3})	−14.005

[a] $R_1 = \sum||F_o| - |F_c||/\sum|F_o|$
[b] $wR_2 = [\sum[w(F_o^2 - F_c^2)^2]/ \sum[w(F_o^2)^2]]^{1/2}$

4.2.2. Neutron Powder Diffraction. Single crystals of Yb_5Pt_9 were crushed into a 4 gram powder sample. Neutron Diffraction measurements were conducted on the polycrystalline sample using the BT-1 powder diffractometer, which is equipped with a Ge 311 vertically focusing monochromater ($\lambda = 2.079$ Å).

4.3. Results and Discusssion

4.3.1. Structure. The crystal structure of Yb_5Pt_9 is shown in Figure 4.3. The atomic positions and displacement parameters of Yb_5Pt_9 are provided in Table 4.4. Yb_5Pt_9 crystallizes in an orthorhombic *Cmmm* (No. 65) space group with lattice parameters of a = 13.5550(5), b = 13.3720(5), c = 5.6540(3) Å, and V = 1024.83(8) Å^3, with Z = 19. The unit cell consists of 4 unique Yb and 6 unique Pt atoms, which reside in the 2*b*, 2*d*, 8*p*, and 8*q* and 2*a*, 2*c*, 8*n*, 8*o*, 8*p*, and 8*q* Wyckoff sites, respectively.

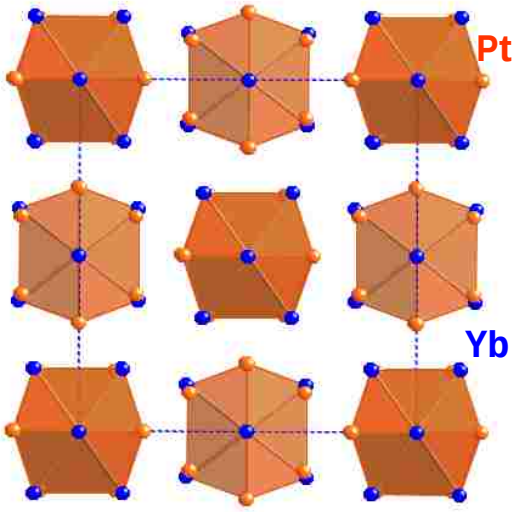

Figure 4.3. The crystal structure of Yb_5Pt_9. Yb atoms are shown in blue, and Pt atoms are shown in orange.

Table 4.4. Atomic Positions and Displacement Parameters for Yb_5Pt_9

Atom	Wyckoff Position	*x*	*y*	*z*	U_{eq} (Å^2)[a]
Yb1	2*b*	1/2	0	0	0.0071(10)
Yb2	2*d*	1/2	1/2	1/2	0.0038(9)
Yb3	8*p*	0.32260(14)	0.63083(19)	0	0.0062(7)
Yb4	8*q*	0.36889(15)	0.82253(15)	1/2	0.0043(7)
Pt1	2*a*	1/2	1/2	0	0.0060(8)
Pt2	2*c*	1/2	0	1/2	0.0071(9)
Pt3	8*n*	1/2	0.69230(16)	0.7502(2)	0.0037(7)
Pt4	8*o*	0.30769(13)	0	0.7499(2)	0.0033(7)

(Table Continued)

Pt5	8*p*	0.38884(12)	0.83037(14)	0	0.0041(6)
Pt6	8*q*	0.33043(11)	0.61154(15)	1/2	0.0046(7)

[a]U_{eq} is defined as one-third of the trace of the orthogonalized U_{ij} tensor.

The structure of Yb_5Pt_9 consists of four unique Yb environments and six unique Pt environments. Selected interatomic distances are provided in Table 4.5. While the Yb1 and Yb2 atoms are coordinated to 10 Pt atoms with distances ranging from 2.700(18) Å to 2.935(2) Å and form snubbed cuboctahedra, the Yb3 and Yb4 atoms are coordinated to 9 Pt atoms with distances ranging from 2.815(3) Å to 2.974(2) Å. Figure 4.4 shows the snubbed cuboctahedral environment for Yb1. These distances are similar to the Yb-Pt distances found in Yb_2Pt_2Pb (~2.844 Å – 2.935 Å)[101] and the summation of the covalent radii for Yb (1.70 Å) and Pt (1.29 Å).[65]

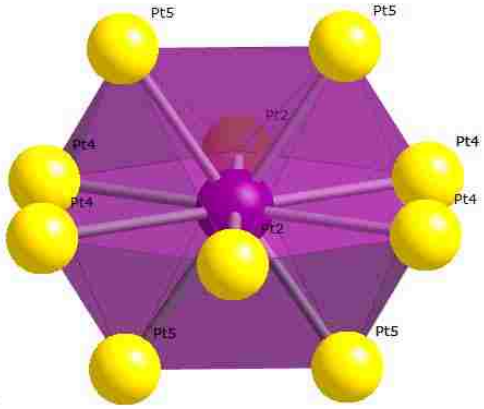

Figure 4.4. Yb1 environment (C.N. = 10) in Yb_5Pt_9. The Yb atom is shown in purple, and the Pt atoms are shown in gold.

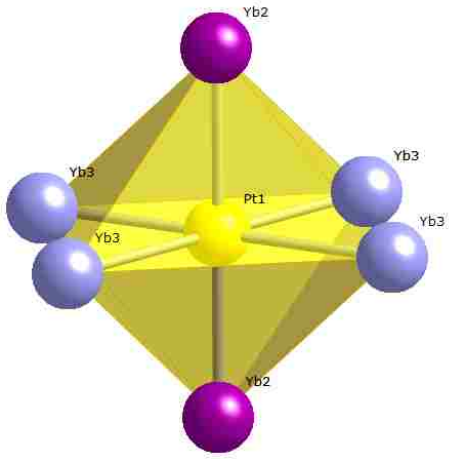

Figure 4.5. The Pt octahedral environment in Yb_5Pt_9. The Pt atom is shown in gold, the Yb2 atoms are shown in purple, and the Yb3 atoms are shown in blue.

The Pt1 and Pt2 atoms form slightly distorted octahedra with Pt-Yb distances ranging from 2.82700(15) Å – 2.974(2) Å and Yb-Pt-Yb angles ranging from 89.230(1)° to

90.769(1)°. However, the Pt3 and Pt4 atoms are coordinated to 7 atoms [Yb (x5) and Pt (x2)]. The distorted Pt1 octahedral environment is shown in Figure 4.5.

Table 4.5. Selected Interatomic Distances (Å) and Angles (°) in Yb_5Pt_9

Distances (Å)	
Yb1-Pt5 (x4)	2.7231(19)
Yb1-Pt2 (x2)	2.8270(15)
Yb1-Pt4 (x4)	2.9450(16)
Yb2-Pt6 (x4)	2.7400(18)
Yb2-Pt1 (x2)	2.8270(15)
Yb2-Pt3 (x4)	2.9350(2)
Yb3-Pt1 (x4)	2.974(2)
Yb3-Pt4 (x2)	2.8450(2)
Yb3-Pt6 (x2)	2.8425(4)
Yb4-Pt2 (x4)	2.965(2)
Pt1-Pt3 (x4)	2.934(2)
Angles (°)	
Yb1-Pt2-Yb4 (x4)	89.431(1)
Yb1-Pt2-Yb4 (x4)	90.569(1)
Yb2-Pt1-Yb3 (x4)	90.768(1)
Yb3-Pt1-Yb2 (x4)	89.232(1)

4.3.2. Neutron Diffraction Experiments for Yb_5Pt_9. Neutron diffraction experiments have been used to investigate the nature of the magnetic order at the 0.6 K and 0.65 K phase transitions in Yb_5Pt_9. Figure 4.6 compares the powder pattern obtained at 1.8 K (a), where the sample is paramagnetic, to the powder pattern at 0.3 K (b), where the sample is magnetically ordered. Figure 4.6 also shows the difference (c) between the neutron diffraction pattern at 1.8 K and 0.3 K. We note that the 1.8 K powder pattern is in full agreement with the orthorhombic structure determined from single crystal X-ray diffraction. While the details of the magnetic structure will be presented elsewhere,[102] the magnetic ordering wave vector was found to be wholly commensurate, adding to the intensities of the nuclear Bragg peaks with reduced temperature. Every peak at 0.3 K can be indexed with the reported orthorhombic structure. There are two possible interpretations of this finding. One possibility is that the ground state is

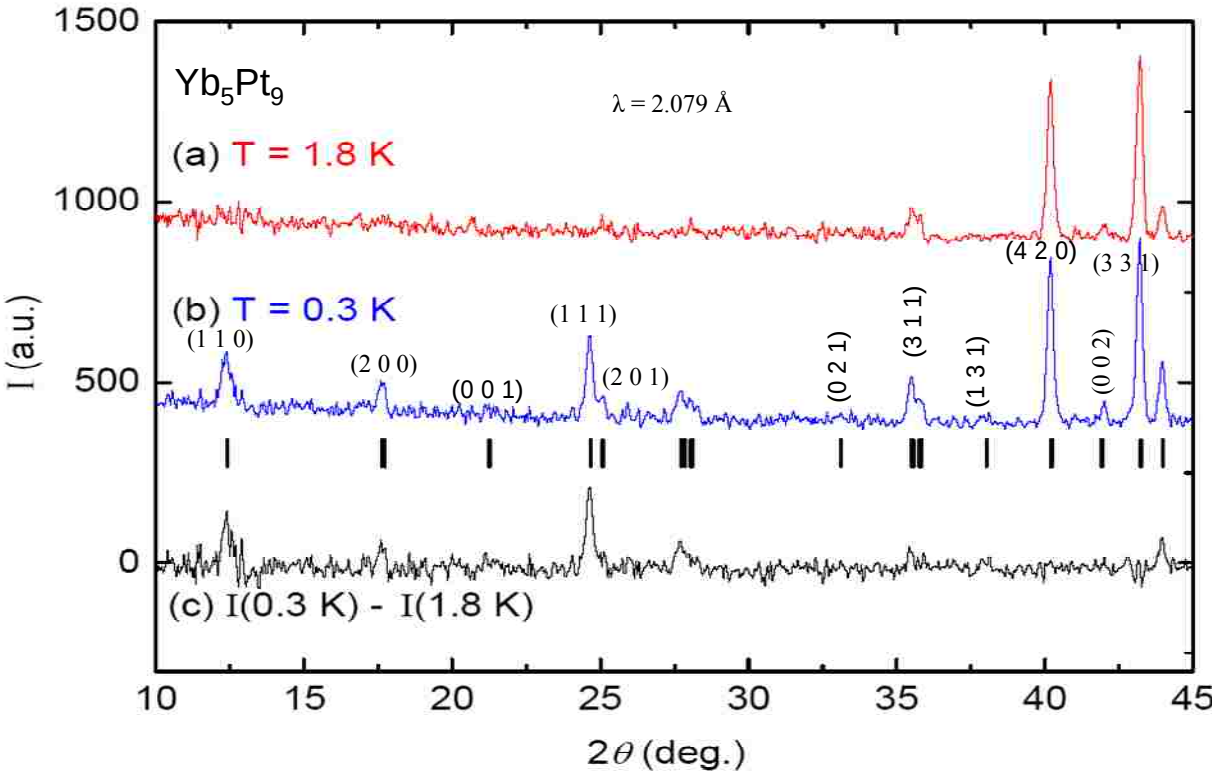

Figure 4.6. A comparison of the neutron powder patterns for Yb_5Pt_9 at (a)1.8 K, (b) 0.3 K, and (c) their difference. All the peaks can be indexed in the crystal unit cell, indicating that the magnetic order is possibly ferromagnetic.

ferromagnetic, or alternatively, given that there are four inequivalent Yb atoms per unit cell, it is possible that the order is antiferromagnetic with a wave vector commensurate with the high temperature reciprocal lattice. While a definitive answer to this question awaits a determination of the magnetic structure,[102] the field dependence of the heat capacity suggests that the magnetic ground state has a ferromagnetic component.

CHAPTER V. CRYSTAL GROWTH AND STRUCTURE OF THE $R_2Ir_2O_7$ (R = Pr, Eu) COMPOUNDS USING MOLTEN KF[1]

5.1. Introduction

Members of the oxide pyrochlore family, with composition $A_2B_2O_7$,[103] are of particular interest for their electronic properties and ionic conductivities.[104-106] The structure of the oxide pyrochlore may be viewed as A_2O anticristobalite networks, which form corner-sharing O2-R_4 tetrahedral sublattices interpenetrating with a vertex-sharing BO_6 octahedral sublattice, where the A^{+3} site is occupied by a trivalent rare-earth and the B^{+4} site is occupied by a transition metal.[103]

The structure of the oxide pyrochlore is of interest because it supports geometric frustration in 2 dimensions.[107] Geometric frustration in materials (GFM), which can result in the suppression of magnetic ordering, is an area that has attracted attention since 1950.[108, 109] GFM occurs when all pair-wise nearest-neighbor interactions of magnetic ions in materials are not satisfied because of constraints in their lattice symmetry, as shown in Figure 5.1. This results in degenerate ground states in temperatures down to almost absolute zero.[107] Triangle-based

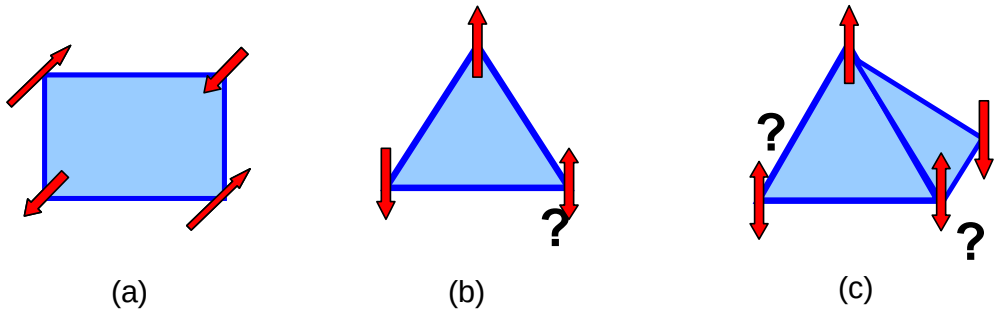

Figure 5.1. Antiferromagnetic nearest neighbor ordering in (a) square- (b) triangle-, and (c) tetrahedral- based lattices.

lattices, such as the pyrochlore, with short-range antiferromagnetic interactions are ideal systems to study the effects of GFM.[107] Experimentally, the signature marker of a geometrically

[1] Reprinted from: Mater. Res. Bull., 42, Millican, J. N.; Macaluso, R. T.; Nakatsujji, S.; Machida, Y.; Maeno, Y.; Chan, J. Y., Copyright (2007), with permission from Elsevier

frustrated antiferromagnetic (AF) system is shown in the inverse susceptibility, χ^{-1}, where the Curie-Weiss Law is obeyed down to temperatures below the mean field ordering transition temperature, Θ_{CW}.[107, 110, 111] However, deviations from linearity occur at some temperature, T_F, indicative of a phase transition. In a frustrated AF system, $T_F << \Theta_{CW}$, and the frustration parameter, T_F/ Θ_{CW}, can be used to quantify the frustration.[107, 110, 111]

In the oxide pyrochlores, it has been established that ferromagnetic nearest-neighbor exchange in combination with strong Ising anisotropy of an *A* site ion leads to the frustrated freezing of spins called "spin ice." This has been realized in systems such as $Dy_2Ti_2O_7$[112-115] and $Ho_2Ti_2O_7$,[116, 117] where spins remain disordered down to low temperatures due to geometrical frustration similar to what is observed for the H-O bonds of common ice.[107, 113, 114, 117]

Because the *A* and *B* sites are on separate sublattices in materials with the pyrochlore structure, the localized spins located at the *A* and/or *B* sites are expected to exhibit highly frustrated magnetism and electrically insulating behavior. It has been theoretically proposed that the pyrochlore oxides with antiferromagnetically-coupled Heisenberg spins may stabilize the spin-liquid ground state.[118] In a spin liquid, spins fluctuate down to low temperatures as a result of antiferromagnetic coupling of the magnetic ions, and magnetic ordering is suppressed.[118, 119] Among a number of extensively studied systems, only a few candidates for the spin-liquid state are known, including $Tb_2Ti_2O_7$.[120, 121] Surprisingly, paramagnetic behavior is observed down to 0.07 K in $Tb_2Ti_2O_7$,[120-124] which is unusual since antiferromagnetic interactions normally lead to either an ordered state or spin glass behavior.[120, 123]

It is of interest to determine whether exotic spin liquid states or spin ice states appear in other materials with different types of moment coupling mechanisms. Thus far, the studies on the highly frustrated states have been mostly limited to the insulators, where the moments are

predominantly coupled through short-range classical dipole-dipole interactions and superexchange coupling.[119, 125] Therefore, it is significant to examine the presence of the itinerant carriers on the geometrical frustration of localized moments. In metallic systems, however, itinerant carriers from the *B* site induce Kondo coupling with *A* site localized moments, and long-range RKKY interactions should be induced among the localized moments.[119, 125] Since the Kondo coupling inherently involves a spin-flipping process that enhances quantum fluctuations, this type of "geometrically frustrated Kondo lattice" might be suitable for the search for another spin liquid system in three-dimensions.

There have been a number of metallic systems reported among the $A_2B_2O_7$ pyrochlore oxides. When pyrochlore compounds are metallic, they exhibit a variety of electronic transport properties. Examples include the anomalous Hall effect in $Nd_2Mo_2O_7$,[126] giant magnetoresistance in $Tl_2Mn_2O_7$,[127-129] and superconductivity in $Cd_2Re_2O_7$.[130] However, none of the metallic pyrochlores are known to remain disordered at low temperatures except the newly developed pyrochlore iridates.[131] Yanagishima and Maeno have shown that polycrystalline samples of $R_2Ir_2O_7$ exhibit a metal-insulator transition where the metallic state was found with *R* = Pr, Nd, Sm, and Eu, and a nonmetallic state was observed for those with a smaller radius.[131] The substitution with a *R* ion of smaller ionic radius decreases the Ir-O-Ir angle and narrows the Ir 5*d* band.

Nakatsuji et al. have succeeded in growing single crystals of $Pr_2Ir_2O_7$ and in characterizing the ground state and magnetic and electrical properties.[125] Despite the well-defined localized moments with the Curie-Weiss temperature of 20 K, $Pr_2Ir_2O_7$ is found to remain paramagnetic down to 0.08 K.[125] This combination of Kondo and spin liquid behavior is a rare observation and places $Pr_2Ir_2O_7$ as a unique material to study the spin liquid behavior in a

geometrically frustrated Kondo lattice. In this paper, we report the crystal growth and structures of two pyrochlore compounds, $Pr_2Ir_2O_7$ and Eu_2IrO_7, at T = 110, 115, and 298 K.

5.2. Experimental

5.2.1. Synthesis. Polycrystalline samples of $Pr_2Ir_2O_7$ and $Eu_2Ir_2O_7$ were prepared by solid state reactions of the rare-earth oxides, Pr_6O_{11} or Eu_2O_3, with IrO_2, respectively. Powders were ground and pelletized at regular intervals and heated at 1273 K for several days. Single crystals were prepared by combining these polycrystalline samples with KF flux in a ratio of 1:200. The samples were heated to 1373 K and annealed for 3-5 h. The temperature was then decreased to 1123 K at a rate of 2 K /h. Figure 5.2 shows a typical black, metallic, octahedral-shaped $Pr_2Ir_2O_7$ single crystal, which has been separated from the KF flux with distilled H_2O as an etchant. The crystal size ranges from 0.20 x 0.20 x 0.20 to 1.0 x 1.0 x 1.0 mm^3. X-ray diffraction was used to confirm the homogeneity of the single crystal and polycrystalline samples of $Pr_2Ir_2O_7$ and $Eu_2Ir_2O_7$. The single crystals were not sensitive to air or moisture.

5.2.2. Single Crystal X-ray Diffraction of $R_2Ir_2O_7$ (R = Pr, Eu). Fragments of single crystals of $Pr_2Ir_2O_7$ (0.050 x 0.050 x 0.130 mm^3) and $Eu_2Ir_2O_7$ (0.050 x 0.080 x 0.080 mm^3) were mechanically extracted and mounted onto a Nonius Kappa CCD diffractometer with Mo K_α, (λ = 0.71073 Å) radiation. Single crystal X-ray diffraction data were collected at 110 K, 115 K, and 298 K for both $Pr_2Ir_2O_7$ and $Eu_2Ir_2O_7$. For the $R_2Ir_2O_7$ (R = Pr, Eu) compounds, the same single crystal fragment was used for each data collection, while the temperature was modified. The structural models were solved and refined using SHELXL97.[51] In the final least squares cycles, the atomic positions of the

Figure 5.2. Single Crystal of $Pr_2Ir_2O_7$.

pyrochlore structure type were used for comparison.[103] The data were corrected for extinction and the displacement parameters for the Pr, Eu, Ir, and O1 atoms were treated as anisotropic while displacement parameters for the O2 atom were refined as isotropic due to its $\bar{4}3m$ site symmetry. The *x* atomic position for O1 at the 48*f* Wyckoff site is the only refinable atomic position. For the $Pr_2Ir_2O_7$ and $Eu_2Ir_2O_7$ compounds, $x = 0.3299(2)$ and $x = 0.3390(3)$, respectively. These values are comparable to the *x* atomic positions obtained from the structural determinations of polycrystalline samples of $Pr_2Ir_2O_7$, [132] where $x = 0.3310(4)$ and $Tb_2Ti_2O_7$, where $x = 0.3285(1)$.[122] Selected crystallographic parameters for $Pr_2Ir_2O_7$ and $Eu_2Ir_2O_7$ are provided in Table 5.1 and Table 5.2, respectively, for comparison.

Table 5.1. Crystallographic Parameters for $Pr_2Ir_2O_7$ at 110 K, 115 K, and 298 K

Crystal Data			
temperature (K)	110	115	298
formula	$Pr_2Ir_2O_7$	$Pr_2Ir_2O_7$	$Pr_2Ir_2O_7$
a (Å)	10.4030(16)	10.400(16)	10.396(15)
V (Å^3)	1125.8(3)	1125.0(3)	1124.0(3)
Z	8	8	8
crystal dimension (mm^3)	0.05 x 0.05 x 0.13	0.05 x 0.05 x 0.13	0.05 x 0.05 x 0.13
crystal system	Cubic	Cubic	Cubic
space group	$Fd\bar{3}m$	$Fd\bar{3}m$	$Fd\bar{3}m$
θ range (°)	5.54-29.83	5.55-29.84	3.39-29.85
μ(mm^{-1})	72.128	64.170	72.274
Data Collection			
measured reflections	203	197	217
independent reflections	89	88	102
reflections with I > 3σ(I)	78	79	93
R_{int}	0.0519	0.0317	0.0667
h	−14 → 14	−14 → 14	−14 → 14
k	−10 → 10	−10 → 10	−10 → 10
l	−9 → 9	−9 → 9	−9 → 9
Refinement			
$R_1[F^2>2\sigma(F^2)]$ [a]	0.0374	0.0388	0.0404
$wR_2(F^2)$ [b]	0.1205	0.1282	0.1507
reflections	203	197	217
parameters	11	11	11

(Table Continued)

$\Delta\rho_{max}$ (e Å^{-3})	1.875	2.085	3.494
$\Delta\rho_{min}$ (e Å^{-3})	-2.893	-3.396	-2.804
extinction coefficient	0.0013(3)	0.0025(6)	0.0026(5)

[a] $R_1 = \sum \| F_o \| - |F_c| \| / \sum |F_o|$

[b] $wR_2 = \left[\sum \left[w(F_o^2 - F_c^2) \right] / \sum \left[w(F_o^2)^2 \right] \right]^{\overline{2}}$

Table 5.2. Crystallographic Parameters for $Eu_2Ir_2O_7$ at 110 K, 115 K, and 298 K

Crystal Data			
temperature (K)	110	115	298
formula	$Eu_2Ir_2O_7$	$Eu_2Ir_2O_7$	$Eu_2Ir_2O_7$
a (Å)	10.243(3)	10.248(3)	10.274(3)
V (Å^3)	1074.7(5)	1076.3(5)	1084.5(6)
Z	8	8	8
crystal dimension (mm^3)	0.05 x 0.08 x 0.08	0.05 x 0.08 x 0.08	0.05 x 0.08 x 0.08
crystal system	Cubic	Cubic	Cubic
space group	$Fd\bar{3}m$	$Fd\bar{3}m$	$Fd\bar{3}m$
θ range (º)	2.55-32.03	2.55-32.03	2.55-32.03
μ(mm^{-1})	72.377	72.271	71.723
Data Collection			
measured reflections	202	142	140
independent reflections	82	68	73
reflections with I > 3σ(I)	73	46	52
R_{int}	0.0813	0.0226	0.0570
h	-13 → 14	-13 → 14	-14 → 14
k	-9 → 10	-10 → 10	-10 → 10
l	-9 → 9	-8 → 9	-9 → 9
Refinement			
$R_1[F^2>2\sigma(F^2)]$ [a]	0.0523	0.0468	0.0589
$wR_2(F^2)$ [b]	0.1496	0.3073	0.1613
reflections	202	142	140
parameters	79	9	
$\Delta\rho_{max}$ (e Å^{-3})	2.0150	1.797	2.780
$\Delta\rho_{min}$ (e Å^{-3})	-2.393	-1.801	-1.757
extinction coefficient	None	0.05(2)	0.018(9)

[a] $R_1 = \sum \| F_o \| - |F_c| \| / \sum |F_o|$

[b] $wR_2 = \left[\sum \left[w(F_o^2 - F_c^2) \right] / \sum \left[w(F_o^2)^2 \right] \right]^{\frac{1}{2}}$.

5.3. Results and Discussion

5.3.1. Structure of $R_2Ir_2O_7$ (R = Pr, Eu). The $R_2Ir_2O_7$ (R = Pr, Eu) compounds crystallize in the cubic space group, $Fd\bar{3}m$ (No. 227, origin choice 2), with the R (R = Pr, Eu), Ir, O1, and O2 atoms occupying the 16*c*, 16d, 48*f*, and 8*b* Wyckoff symmetry sites, respectively. The structure is provided in Figure 6.2. At 298 K, the $Pr_2Ir_2O_7$ and $Eu_2Ir_2O_7$ compounds have lattice parameters of a = 10.3937(4) Å, V = 1122.82(7) Å^3, and a = 10.274(3) Å, V = 1084.5(6) Å^3, respectively. The lattice parameters a = 10.396(15) Å and a = 10.274(3) Å for single crystalline $Pr_2Ir_2O_7$ and $Eu_2Ir_2O_7$, respectively, are similar to previous structure determinations on polycrystalline samples, where a = 10.406(2)[133] and 10.4159(2) Å [132] for $Pr_2Ir_2O_7$ and a = 10.290(1) Å for $Eu_2Ir_2O_7$.[103, 134]

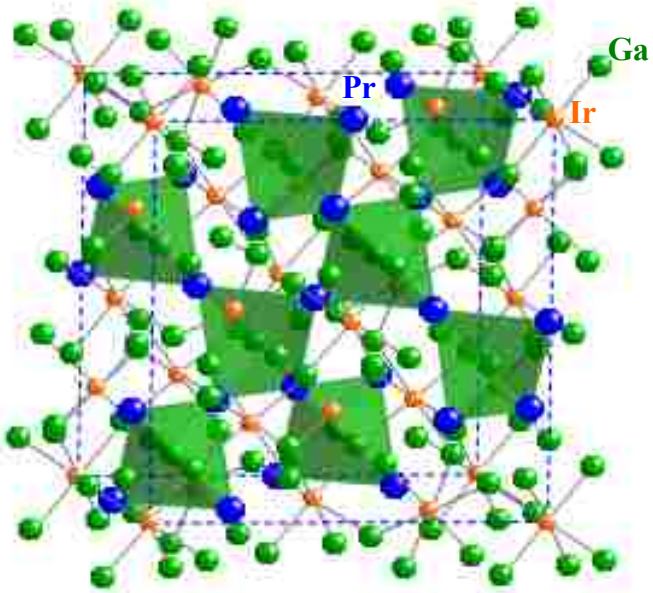

Figure 5.2. The Crystal structure of $Pr_2Ir_2O_7$ at 298 K. The O(2)-Pr_4 tetrahedra are shown in green; the Ir atoms are shown with orange filled spheres; the Pr atoms are shown with blue filled spheres; and the O(1) atoms are shown with green filled spheres.

The crystal structure of $R_2Ir_2O_7$ (R = Pr, Eu), as shown in Figure 5.2, consists of two distinct sublattices: R_2O anticrystobalite networks, where the O2 atoms are connected to 4 R (R = Pr, Eu) atoms and form O2-R_4 vertex sharing tetrahedra (shown in Figure 5.3), and distorted corner-sharing IrO_6 octahedra (shown in Figure 5.4). Atomic positions for $Pr_2Ir_2O_7$ and $Eu_2Ir_2O_7$ are provided in Table 5.3.

Single crystal X-ray diffraction experiments were performed for $Pr_2Ir_2O_7$ at 110, 115, and 298 K with no significant differences observed in the structures. Tables 5.4 lists the interatomic distances and bond angles in the tetrahedra for $Pr_2Ir_2O_7$ at T = 110, 115, and 298 K.

For instance, the Pr-O2 inter-atomic distances of 2.2523(3), 2.2520(3), and 2.2510(3) Å for T = 110, 115, and 298 K, respectively, are comparable and differ by less than 0.5 σ. The Ir-O1 distances of 2.023(8), 2.017(10), and 2.013(8) Å at T = 110, 115, and 298 K, respectively, are also comparable, differing by less than 1σ. Although, the O1-Ir-O1 bond angles of 83.0(7)° and 97.0(7)° at 110 K, 83.4(8)° and 96.6(8)° at 115 K, and 83.7(7)° and 96.3(7)° at 298 K differ from that of an ideal octahedron, these values are comparable to those of other known pyrochlores.[103]

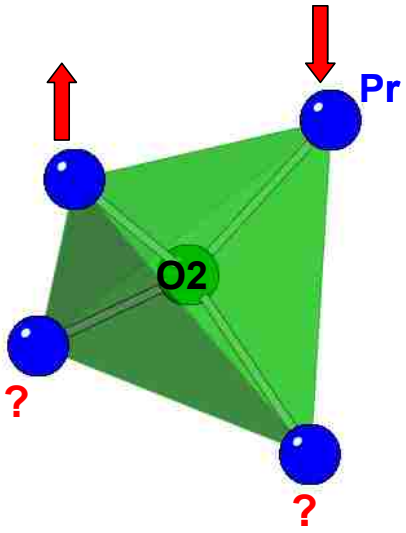

Figure 5.3. Corner sharing O2-Pr_4 tetrahedra in $Pr_2Ir_2O_7$ at 298 K. The O2 polyhedra are shown in green, and the Pr atoms are shown in blue.

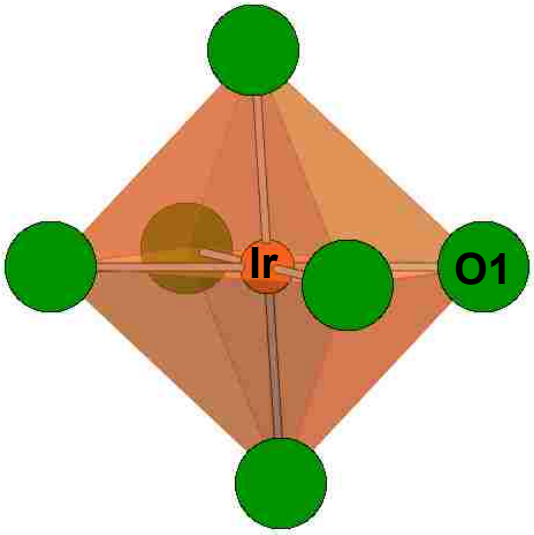

Figure 5.4. The distorted IrO_6 octahedron of $Pr_2Ir_2O_7$ at 298 K. The Ir atom is shown in orange, and the O1 atom is shown in green.

Table 5.3. Atomic Positions for $Pr_2Ir_2O_7$ and $Eu_2Ir_2O_7$ (298 K)

Atom	Wyckoff site	*x*	*y*	*z*	$U_{eq}(Å^2)^a$ *or* $U_{iso}(Å^2)^b$
Pr	16*c*	½	½	½	0.01075(1)[a]
Ir	16*d*	0	0	0	0.00781(1)[a]
O1	48*f*	0.3290(18)	1/8	1/8	0.014(4)[a]
O2	8*b*	3/8	3/8	3/8	0.022(11)[b]
Eu	16*c*	½	½	½	0.02680(2)[a]
Ir	16*d*	0	0	0	0.02827(2)[a]
O1	48*f*	0.339(3)	1/8	1/8	0.043(8)[a]
O2	8*b*	3/8	3/8	3/8	0.025(11)[b]

[a] U_{eq} is defined as one-third of the trace of the orthogonalized U_{ij} tensor.

Table 5.4. Selected Inter-atomic Distances (Å) and bond angles (°) of $Pr_2Ir_2O_7$

		110 K	**115 K**	**298 K**
Distances				
Pr-O2	(x4)	2.2523(3)	2.252(3)	2.251(3)
Ir-O1	(x6)	2.023(8)	2.017(10)	2.013(8)
Angles				
Pr-O2-Pr	(x4)	109.47(5)	109.47(3)	109.47(5)
O1-Ir-O1	(x3)	83.0(7)	83.4(8)	83.7(7)
	(x3)	97.0(7)	96.6(8)	96.3(7)
Ir-O1-Ir	(x4)	130.7(10)	131.4(12)	131.8(10)

Single crystal X-ray diffraction experiments were also performed at T = 110, 115, and 298 K for $Eu_2Ir_2O_7$. Table 5.5 lists the interatomic distances and bond angles in $Eu_2Ir_2O_7$ at T = 110, 115, and 298 K. The Eu-O2 distances of 2.2177(6), 2.2187(6), and 2.2244(7) Å are observed at T = 110, 115, and 298 K, respectively. Notably, an unexpected difference of over 6σ and 7σ are observed between T = 115 K and 298 K and T = 110 K and 298 K, respectively.

Table 5.5. Selected Inter-atomic Distances (Å) and bond angles (°) of $Eu_2Ir_2O_7$

		110 K	115 K	298 K
Distances				
Eu-O2	(x4)	2.2177(6)	2.2187(6)	2.2244(7)
Ir-O1	(x6)	2.002(12)	2.044(9)	2.033(12)
Angles				
Eu-O2-Eu	(x4)	109.5(5)	109.5(3)	109.5(5)
O1-Ir-O1	(x3)	82.2(9)	79.2(6)	80.3(9)
	(x3)	97.8(9)	100.8(6)	99.7(9)
Ir-O1-Ir	(x4)	129.5(14)	124.8(9)	126.7(14)

In the IrO_6 octahedral sublattice of $Eu_2Ir_2O_7$, the Ir-O1 interatomic distances of 2.044(9) and 2.033(12) Å at T = 115 and 298 K, respectively, only differ by less than ~ 0.7 σ. However, the Ir-Ol interatomic distance of 2.002(12) Å at T = 110 K differs by 2.8 σ and 1.8 σ, when compared to the Ir-O1 distances at T = 115 K and 298 K, respectively. The O1-Ir-O1 bond angles of 97.8(9)° at T = 110 K, 100.8(6)° at 115 K, and 99.7(9)° at 298 K, are shown in Table 4. These O1-Ir-O1 bond angles are more distorted than the O1-Ir-O1 bond angles observed for the Pr analogue.

In structural investigations of the ruthenate pyrochlores ($R_2Ru_2O_7$; R = La, Pr, Nd, and Sm-Lu), it has been suggested that smaller Ru-O distances and larger Ru-O1-Ru bond angles enhance the overlap of Ru (4*d*) and O1(2*p*) orbitals, leading to metallic behavior. Through neutron diffraction studies, it has also been suggested that $R_2Ru_2O_7$ compounds, in which the overlap of the Ru (4*d*) and O1 (2*p*) orbitals is enhanced and with Ru-O1-Ru bond angles ranging from 135° to 140°, metallic behavior is observed.[132, 135] Whereas, in $R_2Ru_2O_7$ compounds, in which Ru-Ol-Ru bond angles range from 129° to 134°, semiconducting behavior is exhibited. [132, 135] We note that although the Ir-O1 distances and O1-Ir-O1 bond angles for the $Eu_2Ir_2O_7$ are not statistically different for the data at 110 K, 115 K, and 298 K, respectively, these distances differ

when compared to the Ir-O1 distances and O1-Ir-O1 bond angles for the $Pr_2Ir_2O_7$ at T = 110 K, 115 K, and 298 K. It may be worthwhile to correlate the structure, measure the physical properties, and perform neutron scattering measurements.

CHAPTER VI. CONCLUSIONS AND FUTURE OUTLOOK

The goal of this dissertation is to provide an explanation of complex physical behavior, using one of nature's most fundamental elements- structure. Although at first glance, the concepts presented within may seem unrelated, the common tie that binds is that many of these materials are in the vicinity of the quantum critical region of the phase diagram, where unexplained phenomena exist. The architectures of these materials with unconventional behavior serve as platforms to investigate or prove the existence of structure- property relationships in advanced materials. In turn, structure-property correlations can be used to better understand and/or predict complex phenomena in the vicinity of instability, where theoretical models often fail. By proactively probing along this fringe of instability, it may be possible to determine the forces that drive the quantum behavior in these materials, which may ultimately lead to the discovery of novel materials and behavior.

As a result of carefully analyzing and comparing the crystal structures of the Ce-Pd-Ga phases, which exhibit intriguing properties ranging from heavy fermion behavior to large magnetoresistance, it has been determined that the study of structural aspects, such as lanthanide environment, dimensionality, and layering effects in these materials may reveal what factors trigger differences in their intricate physical property behavior. In addition, by substituting Ni and Cu, which have smaller atomic radii in comparison to Pd, into the Ce_2PdGa_{10} and Ce_2PdGa_{12} structures, it has been discovered that intra-layer interactions and hybridization effects still dominate the physical property behavior of these materials.

Another system that allows for the study of a three-dimensional system in the vicinity of a quantum critical point is the triangle-based structure of the geometrically frustrated $R_2Ir_2O_7$ (R = Pr, Eu) compounds. The structures of the $R_2Ir_2O_7$ (R = Pr, Eu) compounds consists of corner-

sharing tetrahedral and octahedral sub-lattices, which are the most prevalent basic structural motifs found in inorganic compounds. In these compounds, there is a direct correlation between its structure and properties, where frustration, which occurs due to geometric constraints in the tetrahedral sub-lattice, results in a signature deviation from linear behavior in the inverse susceptibility data (χ^{-1}). This frustration is another parameter that can be used to suppress magnetic ordering in materials- introducing exotic phenomena, such as spin liquids, where spins remain disordered down to low temperatures. In addition, observable structural distortions of the interatomic distances and bond angles in the IrO_6 octahedra found in $Eu_2Ir_2O_7$ at 110 K, may suggest the enhanced super-exchange overlap of the Ir (5*d*) and O1(2*p*) orbitals, which corresponds to a metal- insulating transition at 110 K confirmed by the physical property measurements.

In our continued interest in systems near quantum critical regions of the magnetic phase diagram, we will fully investigate the structure- property relationships of the low dimensional quantum S = ½ system, $Cs_4Cu_3(MoO_4)_3$. S = ½ quantum spin liquid systems have attracted recent interest because these unique systems allow for the study of the real systems, which exhibit the co-existence of frustration and quantum effects.[136] It has been suggested that in S =1/2 quantum spin liquid systems, where the spins fluctuate down to absolute zero, quantum effects may dominate- resulting in new exotic behavior.[136] In particular, low dimensional Cu^{2+} containing S = ½ quantum systems, such as $Cu_2Te_2O_5X_4$ (X = Br, Cl)[137], $CaCu_2O_3$,[138] and $Cu_3(CO_3)_2(OH)_2$,[139] offer experimental realizations of spin liquid systems with high degrees of frustration and quantum fluctuations. We have studied the crystal structure of a new S = 1/2 quantum spin liquid system, $Cs_4Cu_3(MoO_4)_3$.[140, 141] Preliminary single crystal data is provided in Appendix A.

REFERENCES

(1) Fisk, Z.; Hess, D. W.; Pethick, C. J.; Pines, D.; Smith, J. L.; Thompson, J. D.; Willis, J. O., *Science* **1988**, *239*, 33.

(2) Fisk, Z.; Ott, H. R.; Rice, T. M.; Smith, J. L., *Nature* **1986**, *320*, 124.

(3) Fisk, Z.; Sarrao, J. L.; Smith, J. L.; Thompson, J. D., *Proc. Natl. Acad. Sci. USA* **1995**, *92*, 6663.

(4) Stewart, G. R., *Reviews of Modern Physics* **1984**, *56*, 755.

(5) Stewart, G. R., *Rev. Mod. Phys.* **1984**, *56*, 755.

(6) Fisk, Z., *Physica B* **2006**, *378-380*, 13.

(7) Mathur, N. D.; Grosche, F. M.; Julian, S. R.; Walker, I. R.; Freye, D. M.; Haselwimmer, R. K. W.; Lonzarich, G. G., *Nature* **1998**, *394*, 39.

(8) Hegger, H.; Petrovic, C.; Moshopoulou, E. G.; Hundley, M. F.; Sarrao, J. L.; Fisk, Z.; Thompson, J. D., *Phys. Rev. Lett.* **2000**, *84*, 4986.

(9) Laughlin, R. B.; Lonzarich, G. G.; Monthoux, P.; Pines, D., *Adv. Phys.* **2001**, *50*, 361.

(10) Coleman, P.; Schofield, A. J., *Nature* **2005**, *433*, 226.

(11) Continentino, M. A., *Braz. J. Phys.* **2005**, *35*, 197.

(12) Gegenwart, P.; Custers, J.; Geibel, C.; Neumaier, K.; Tayama, T.; Tenya, K.; Trovarelli, O.; Steglich, F., *Phys. Rev. Lett.* **2002**, *89*.

(13) Custers, J.; Gegenwart, P.; Neumaier, K.; Wilhelm, H.; Oeschler, N.; Ishida, K.; Kitaoka, Y.; Geibel, C.; Steglich, F., *J. Phys.: Condens. Matter* **2003**, *15*, S2047.

(14) Gegenwart, P.; Tokiwa, Y.; Westerkamp, T.; Weickert, F.; Custers, J.; Ferstl, J.; Krellner, C.; Geibel, C.; Kerschl, P.; Muller, K. H.; Steglich, F., *New J. Phys.* **2006**, *8*, 1.

(15) Marezio, M.; Licci, F.; Gauzzi, A., *Physica C* **2000**, *337*, 195.

(16) Cieplak, M.; Xiao, G.; Chien, C. L.; Bakhshai, A.; Artymowicz, D.; Bryden, W.; Stalick, J. K.; Rhyne, J. J., *Phys. Rev. B* **1990**, *42*, 6200.

(17) Jaccard, D.; Wilhelm, H.; Alami-Yadri, K.; Vargoz, E., *Physica B* **1999**, *261*, 1.

(18) Bao, W.; Pagliuso, P. G.; Sarrao, J. L.; Thompson, J. D.; Fisk, Z.; Lynn, J. W., *Phys. Rev. B* **2001**, *64*, 0204011.

(19) Bao, W.; Trevino, S. F.; Lynn, J. W.; Pagliuso, P. G.; Sarrao, J. L.; Thompson, J. D.; Fisk, Z., *Appl. Phys. A* **2002**, *74*, S557.

(20) Bianchi, A.; Movshovich, R.; Oeschler, N.; Gegenwart, P.; Steglich, F.; Thompson, J. D.; Pagliuso, P. G.; Sarrao, J. L., *Phys. Rev. Lett.* **2002**, *89*, 1370021.

(21) Küchler, R.; Gegenwart, P.; Custers, J.; Stockert, O.; Caroca-Canales, N.; Geibel, C.; Sereni, J. G.; Steglich, F., *Phys. Rev. Lett.* **2006**, *96*, 2564031.

(22) Moshopoulou, E. G.; Ibberson, R. M.; Sarrao, J. L.; Thompson, J. D.; Fisk, Z., *Acta Cryst.* **2006**, *B62*, 173.

(23) Pham, L. D.; Park, T.; Maquilon, S.; Thompson, J. D.; Fisk, Z., *Phys. Rev. Lett.* **2006**, *97*, 0564041.

(24) Petrovic, C.; Pagliuso, P. G.; Hundley, M. F.; Movshovich, R.; Sarrao, J. L.; Thompson, J. D.; Fisk, Z.; Monthoux, P., *J. Phys.: Condens. Matter* **2001**, *13*, L337.

(25) Movshovich, R.; Jaime, M.; Thompson, J. D.; Petrovic, C.; Fisk, Z.; Pagliuso, P. G.; Sarrao, J. L., *Phys. Rev. Lett.* **2001**, *86*, 5152.

(26) Petrovic, C.; Movshovich, R.; Jaime, M.; Pagliuso, P. G.; Hundley, M. F.; Sarrao, J. L.; Fisk, Z.; Thompson, J. D., *Europhys. Lett.* **2001**, *53*, 354.

(27) Nicklas, M.; Sidorov, V. A.; Borges, H. A.; Pagliuso, P. G.; Petrovic, C.; Fisk, Z.; Sarrao, J. L.; Thompson, J. D., *Phys. Rev. B* **2003**, *67*, 0205061.

(28) Bauer, E. D.; Frederick, N. A.; Ho, P. C.; Zapf, V. S.; Maple, M. B., *Phys. Rev. B* **2002**, *65*, 1005061.

(29) Maple, M. B.; Ho, P. C.; Frederick, N. A.; Zapf, V. S.; Yuhasz, W. M.; Bauer, E. D.; Christianson, A. D.; Lacerda, A. H., *J. Phys.: Condens. Matter* **2003**, *15*, S2071.

(30) Macaluso, R. T.; Nakatsuji, S.; Lee, H.; Fisk, Z.; Moldovan, M.; Young, D. P.; Chan, J. Y., *J. Solid State Chem.* **2003**, *174*, 296.

(31) Millican, J. N.; Macaluso, R. T.; Young, D. P.; Moldovan, M.; Chan, J. Y., *J. Solid State Chem.* **2004**, *177*, 4695.

(32) Macaluso, R. T.; Millican, J. N.; Nakatsuji, S.; Lee, H. O.; Carter, B.; Moreno, N. O.; Fisk, Z.; Chan, J. Y., *J. Solid State Chem.* **2005**, *178*, 3547.

(33) Ruderman, M. A.; Kittel, C., *Phys. Rev.* **1954**, *96*, 99.

(34) Kasuya, T., *Prog. Theoret. Phys. (Kyoto)* **1956**, *16*, 45.

(35) Yosida, K., *Phys. Rev.* **1957**, *106*, 893.

(36) Kittel, C., *Introduction to Solid State Physics*. 4th ed.; John Wiley & Sons: New York, **1971**.

(37) Kondo, J., *Prog. Theoret. Phys. (Kyoto)* **1964**, *32*, 37.

(38) Glusker, J. P.; Trueblood, K. N., *Crystal Structure Analysis: A Primer*. ed.; Oxford University Press: New York, **1972**.

(39) West, A. R., *Basic Solid State Chemistry*. ed.; John Wiley & Sons: Chichester, **2002**.

(40) Warren, B. E., *X-ray Diffraction*. ed.; Dover Publications: New York, **1990**.

(41) Cho, J. Y.; Millican, J. N.; Sokolov, D. A.; Aronson, M. C.; Moldovan, M.; Young, D. P.; Chan, J. Y., *In Preparation* **2007**.

(42) Stewart, G. R.; Fisk, Z.; Willis, J. O.; Smith, J. L., *Phys. B* **1984**, *127*, 448.

(43) Fisk, Z.; Aeppli, G., *Science* **1993**, *260*, 38.

(44) Petrovic, C.; Pagliuso, P. G.; Hundley, M. F.; Movschovich, R.; Sarrao, J. L.; Thompson, J. D.; Fisk, Z.; Monthoux, P., *J. Phys. Condens. Matter* **2001**, *13*, L337.

(45) Petrovic, C.; Movshovich, R.; Jaime, M.; Pagliuso, P. G.; Hundley, M. F.; J.L.Sarrao; Fisk, Z.; Thompson, J. D., *Europhys. Lett.* **2001**, *53*, 354.

(46) Hegger, H.; Moshopoulou, E. G.; Hundley, M. F.; Sarrao, J. L.; Fisk, Z.; J.D.Thompson, *Phys. Rev. Lett* **2000**, *84*, 4986.

(47) Cornelius, A. L.; Arko, A. J.; Sarrao, J. L.; Hundley, M. F.; Fisk, Z., *Phys. Rev. B* **2000**, *62*, 14 182.

(48) Thompson, J. D.; Movshovich, R.; Fisk, Z.; Bouquet, F.; Curro, N. J.; Fisher, R. A.; Hammel, P. C.; Hegger, H.; Hundley, M. F.; Jaime, M.; Pagliuso, P. G.; Petrovic, C.; Phillips, N. E.; Sarrao, J. L., *J. Magn. Magn. Mater* **2001**, *226*, 5.

(49) Macaluso, R. T.; Sarrao, J. L.; Moreno, N. O.; Pagliuso, P. G.; Thompson, J. D.; Fronczek, F. R.; Hundley, M. F.; Malinowski, A.; Chan, J. Y., *Chem. Mater.* **2003**, *15*, 1394.

(50) Thomas, E. L.; Okudzeto, E.; Millican, J. N.; Chan, J. Y., *Comments Inorg. Chem. (Review Article)* **2006**, *27*, 1.

(51) Sheldrick, G. M., *SHELXL97*. ed.; University of Gottingen: Germany, **1997**.

(52) Yarmolyuk, Y.; Grin, Y.; Rozhdestvenskaya, I.; Usov, O.; Kuz'min, A.; Bruskov, V.; Gladyshevskii, E., *Sov. Phys. Crystallogr.* **1982**, *27*, 599.

(53) Sieve, B.; Trikalitis, P.; Kanatzidis, M., *Z. anorg.allg.Chem.* **2002**, *628*, 1568.

(54) Muller, U., *Inorganic Structural Chemistry*. ed.; John Wiley & Sons: New York, **1993**.

(55) Pelleg, J.; Kimmel, G.; Dayan, D., *J. Less-Common Metals* **1981**, *81*, 33.

(56) Kimmel, G.; Dayan, D.; Grill, A.; Pelleg, J., *J. Less-Common Metals 75*, 133.

(57) Welter, R.; Venturini, G.; Malaman, B., *J. Less-Common Metals* **2001**, *329*, 69.

(58) Donohue, J., *The Structures of the Elements*. ed.; John Wiley & Sons: New York, **1974**.

(59) Chen, X. Z.; Small, P.; Sportouch, S.; Zhuravleva, M.; Brazis, P.; Kannewurf, C. R.; Kanatzidis, M. G., *Chem. Mater.* **2000**, *12*, 2520.

(60) Bhan, S.; Kudielka, H., *Z Metallkd.* **1978**, *69*, 333.

(61) Schubert, K.; Lukas, H. L.; -G., M. H.; Bhan, S., *Z. Metallkd.* **1959**, *50*, 534.

(62) Macaluso, R. T.; Nakatsuji, S.; Lee, H.; Moldovan, M.; Fisk, Z.; Chan, J. Y., *J. Solid State Chem.* **2003**, *174*, 296.

(63) Sutton, L., *Tables of Interatomic Distances and Configurations in Molecules and Ions*. ed.; The Chemical Society: London, **1965**.

(64) Kimmel, G.; Dayan, D.; Grill, A.; Pelleg, J., *J. Less-Common Met.* **1980**, *75*, 133.

(65) Emsley, J., *The Elements*. 2 ed.; Oxford University Press: New York, **1991**.

(66) Macaluso, R. T.; Wells, D.; Sykora, R. E.; Albrecht-Schmitt, T. E.; Mar, A.; Nakatsuji, S.; Lee, H.; Fisk, Z.; Chan, J. Y., *J. Solid State Chem.* **2004**, *177*, 293.

(67) Ferguson, M. J.; Ellenwood, R. E.; Mar, A., *Inorg. Chem.* **1999**, *38*, 4503.

(68) Brylak, M.; Jeitschko, W., *Z. Naturforsch. B: Chem. Sci* **1995**, *50*, 899.

(69) Wang, R.; Steinfink, H., *Inorg. Chem.* **1967**, *6*, 1685.

(70) Eatough, N. L.; Hall, H. T., *Inorg. Chem.* **1969**, *8*, 1439.

(71) Macaluso, R. T.; Sarrao, J. L.; Moreno, N. O.; Pagliuso, P. G.; Thompson, J. D.; Fronczek, F. R.; Hundley, M. F.; Movshovich, R.; Chan, J. Y., *Chem. Mater.* **2003**, *15*, 1394.

(72) Moshopoulou, E. G.; Prokes, K.; Garcia-Matres, E.; Pagliuso, P. G.; Sarrao, J. L.; Thompson, J. D. In *Neutron-diffraction study of field-induced transitions in the heavy-fermion compound Ce_2RhIn_8*, ICNS, 2002; 'Ed.'^'Eds.' Physica B: 2002; p^pp.

(73) Moldovan, M.; R.G. Goodrich, L. L. H., R.T. Macaluso, J.Y. Chan, P.W. Adams, and D.P.Young, *(In Preparation)* **2004**.

(74) Deakin, L.; Mar, A., *Chem. Mater.* **2003**, *15*, 3343.

(75) Williams, W. M.; Macaluso, R. T.; Moldovan, M.; Young, D. P.; Chan, J. Y., *Inorg. Chem.* **2003**, *42*, 7315.

(76) Branford, W. R.; Clowes, S. K.; Syed, M. H.; Bugoslavsky, Y. V.; Grigorescu, C. E. A.; Berenov, A. V.; Roy, S. B.; Cohen, L. F., *Appl. Phys. Lett.* **2004**, *84*, 2358.

(77) Sechovsky, V.; Havela, L.; Prokes, K.; Nakotte, H.; de Boer, F. R.; Bruck, E., *J. Appl. Phys.* **1994**, *76*, 6913.

(78) Fukuhara, T.; Maezawa, K.; Ohkuni, H.; Sakurai, J.; Sato, H.; Azuma, H.; Sugiyama, K.; Ōnuki, Y.; Kindo, K., *J. Phys. Soc. Japan* **1996**, *65*, 1559.

(79) Grosche, F. M.; Lister, S. J. S.; Carter, F. V.; Saxena, S. S.; Haselwimmer, R. K. W.; Mathur, N. D.; Julian, S. R.; Lonzarich, G. G., *Physica B.* **1997**, *239*, 62.

(80) Knopp, G.; Loidl, A.; Caspary, R.; Gottwick, U.; Bredl, C. D.; Spille, H.; Steglich, F.; Murani, A. P., *J. Magn. Magn. Mater* **1988**, *74*, 341.

(81) Lister, S. J. S.; Grosche, F. M.; Carter, F. V.; Haselwimmer, R. K. W.; Saxena, S. S.; Mathur, N. D.; Julian, S. R.; Lonzarich, G. G., *Z. Phys. B Condens. Mater.* **1997**, *103*, 263.

(82) Zheng, C.; Hoffmann, R., *J. Solid State Chem.* **1988**, *72*, 58.

(83) Beyermann, W. P.; Hundley, M. F.; Canfield, P. C.; Thompson, J. D.; Latroche, M.; Godart, C.; Selsane, M.; Fisk, Z.; Smith, J. L., *Phys. Rev. B* **1991**, *43*, 13130.

(84) Liang, G.; Jisrawi, N.; Croft, M., *Physica B.* **1990**, *163*, 134.

(85) Selsane, M.; Lebail, M.; Hamdaoui, N.; Kappler, J. P.; Noel, H.; Achard, J. C.; Godart, C., *Physica B.* **1990**, *163*, 134.

(86) Takabatake, T.; Teshima, F.; Fujii, H.; Nishigori, S.; Suzuki, T.; Fujita, T.; Yamaguchi, Y.; Sakurai, J., *J. Magn. Magn. Mater* **1990**, *90-1*, 474.

(87) Chen, X. Z.; Small, P.; Sportouch, S.; Zhuravleva, M.; Brazis, P.; Kannewurf, R.; Kanatzidis, M., *Chem. Mater.* **2000**, *12*, 2520.

(88) Zhuravleva, M. A.; Pcionek, R. J.; Wang, X.; Schultz, A. J.; Kanatzidis, M. G., *Inorg. Chem.* **2003**, *42*, 6412.

(89) Halet, J. F., *Inorg. Chem.* **1994**, *33*, 4173.

(90) Trovarelli, O.; Geibel, C.; Mederle, S.; Langhammer, C.; Grosche, F. M.; Gegenwart, P.; Lang, M.; Sparn, G.; Steglich, F., *Phys. Rev. Lett.* **2000**, *85*, 626.

(91) Plessel, J.; Abd-Elmeguid, M. M.; Sanchez, J. P.; Knebel, G.; Geibel, C.; Trovarelli, O.; Steglich, F., *Phys. Rev. B* **2003**, *67*.

(92) Tokiwa, Y.; Gegenwart, P.; Hossain, Z.; Ferstl, J.; Sparn, G.; Geibel, C.; Steglich, F., *Phys. B-Condens. Mat.* **2006**, *378-80*, 746.

(93) Evers, C. B. H.; Richter, C. G.; Hartjes, K.; Jeitschko, W., *J. Alloys Compd.* **1997**, *252*, 93.

(94) Hohl, H.; Ramirez, A. P.; Goldmann, C.; Ernst, G.; Wolfing, B.; Bucher, E., *J. Phys.: Condens. Matter* **1998**, *10*, 7843.

(95) Canfield, P. C.; Thompson, J. D.; Beyermann, W. P.; Lacerda, A.; Hundley, M. F.; Peterson, E.; Fisk, Z.; Ott, H. R., *J. Appl. Phys.* **1991**, *70*, 5800.

(96) Fisk, Z.; Canfield, P. C.; Beyermann, W. P.; Thompson, J. D.; Hundley, M. F.; Ott, H. R.; Felder, E.; Maple, M. B.; Delatorre, M. A. L.; Visani, P.; Seaman, C. L., *Phys. Rev. Lett.* **1991**, *67*, 3310.

(97) Iandelli, A.; Palenzona, A., *J. Less-Common Metals* **1975**, *43*, 205.

(98) Iandelli, A.; Palenzona, A., *J. Less Comm. Met.* **1981**, *80*, 71.

(99) Oster, F.; Politt, B.; Braun, E.; Schmidt, H.; Langen, J.; Lossau, N., *J. Magn. Magn. Mat.* **1987**, *63-64*, 629.

(100) Kim, M. S.; Bennett, M. C.; Sokolov, D. A.; Aronson, M. C.; Millican, J. N.; Chan, J. Y.; Huang, F. Q.; Chen, Y.; Lynn, J. W., *Phys. Rev. B* **2006**, *74*, 2244311.

(101) Pöttgen, R.; Arpe, P. E.; Felser, C.; Kuβmann, D.; Müllmann, R.; Mosel, B. D.; Künnen, B.; Kotzyba, G., *J. Solid State Chem.* **1999**, *145*, 668.

(102) Kim, M. S.; Sokolov, D. A.; Bennett, M. C.; Aronson, M. C.; Huang, Q.; Chen, Y.; Lynn, J. W., *In Preparation* **2007**.

(103) Subramanian, M. A.; Aravamudan, G.; Subba Rao, G. V., *Prog. Solid St. Chem.* **1983**, *15*, 55.

(104) Adachi, G.; Imanaka, N.; Tamura, S., *Chem. Rev.* **2002**, *102*, 2405.

(105) Minervini, L.; Grimes, R. W., *J. Am. Ceram. Soc.* **2000**, *83*, 873.

(106) Shimura, T.; Komori, M.; Iwahara, H., *Solid State Ionics* **1996**, *86-8*, 685.

(107) Ramirez, A. P., *Annu. Rev. Mater. Sci.* **1994**, *24*, 453.

(108) Houtappel, R. M. F., *Physica* **1950**, *16*, 425.

(109) Wannier, G. H., *Phys. Rev.* **1950**, *79*, 357.

(110) Moessner, R., *Can. J. Phys.* **2001**, *79*, 1283.

(111) Moessner, R.; Chalker, J. T., *Phys. Rev. Lett.* **1998**, *80*, 2929.

(112) Harris, M. J.; Bramwell, S. T.; Holdsworth, P. C. W.; Champion, J. D. M., *Phys. Rev. Lett.* **1998**, *81*, 4496.

(113) Harris, M., *Nature* **1999**, *399*, 311.

(114) Ramirez, A. P.; Hayahi, A.; Cava, R. J.; Siddharthan, R.; Shastry, B. S., *Nature* **1999**, *399*, 333.

(115) Higashinaka, R.; Fukazawa, H.; Deguchi, K.; Maeno, Y., *J. Phys. Condens. Matter* **2004**, *16*, S679.

(116) Harris, M. J.; Bramwell, S. T.; McMorrow, D. F.; Zeiske, T.; Godfrey, K. W., *Phys. Rev. Lett.* **1997**, *79*, 2554.

(117) Bramwell, S. T.; Gingras, M. J. P., *Science* **2001**, *294*, 1495.

(118) Canals, B.; Lacroix, C., *Phys. Rev. Lett.* **1998**, *80*, 2933.

(119) Burdin, S.; Grempel, D. R.; Georges, A., *Phys. Rev. B* **2002**, *66*, 0451111.

(120) Gardner, J. S.; Dunsiger, S. R.; Gaulin, B. D.; Gingras, M. J. P.; Greedan, J. E.; Kiefl, R. F.; Lumsden, M. D.; MacFarlane, W. A.; Raju, N. P.; Sonier, J. E.; Swainson, I.; Tun, Z., *Phys. Rev. Lett.* **1999**, *82*, 1012.

(121) Enjalran, M.; Gingras, M. J. P.; Kao, Y.; Maestro, A.; Molavian, H. R., *J. Phys. Condens. Matter* **2004**, *16*, S673.

(122) Han, S. W.; Gardner, J. S.; Booth, C. H., *Phys. Rev. B* **2004**, *69*, 0244161.

(123) Mirebeau, I.; Goncharenko, I., *J. Phys. Condens. Matter* **2004**, *16*, S653.

(124) Keren, A.; Gardner, J. S.; Ehlers, G.; Fukaya, A.; Segal, E.; Uemura, Y. J., *Phys. Rev. Lett.* **2004**, *92*, 1072041.

(125) Nakatsuji, S.; Machida, Y.; Maeno, Y.; Tayama, T.; Sakakibara, T.; Duijn, J. v.; Balicas, L.; Millican, J. N.; Macaluso, R. T.; Chan, J. Y., *Phys. Rev. Lett* **2006**, *96*, 0872041.

(126) Taguchi, Y.; Oohara, Y.; Yoshizawa, H.; Nagaosa, N.; Tokura, Y., *Science* **2001**, *291*, 2573.

(127) Subramanian, M. A.; Toby, B. H.; Ramirez, A. P.; Marshall, W. J.; Sleight, A. W.; Kwei, G. H., *Science* **1996**, *273*, 81.

(128) Subramanian, M. A.; Greedan, J. E.; Raju, N. P., *J. Phys. IV* **1997**, *7*, C1625.

(129) Ramirez, A. P.; Subramanian, M. A., *Science* **1997**, *277*, 546.

(130) Hanawa, M.; Muraoka, Y.; Tayama, T.; Sakakibara, T.; Yamamura, J.; Hiroi, Z., *Phys. Rev. Lett.* **2001**, *87*, 1870011.

(131) Yanagishima, D.; Maeno, Y., *J. Phys. Soc. Jpn.* **2001**, *70*, 2880.

(132) Kennedy, B. J., *Physica B* **1998**, *241-243*, 303.

(133) Lazarev, V. B.; Shaplygin, I. S.; Russ, J., *J. Inorg. Chem.* **1978**, *23*, 163.

(134) Blacklock, K.; White, H. W., *J. Chem. Phys.* **1980**, *72*, 2191.

(135) Kennedy, B. J.; Vogt, T., *J. Solid State Chem.* **1996**, *126*, 261.

(136) Levi, B. G., *Phys. Today* **2007**, *60*, 16.

(137) Rahaman, B.; Jeschke, H. O.; Valenti, R.; Saha-Dasgupta, T., *Phys. Rev. B* **2007**, *75*.

(138) Kiryukhin, V.; Kim, Y. J.; Thomas, K. J.; Chou, F. C.; Erwin, R. W.; Huang, Q.; Kastner, M. A.; Birgeneau, R. J., *Phys. Rev. B* **2001**, *6314*.

(139) Kikuchi, H.; Fujii, Y.; Chiba, M.; Mitsudo, S.; Idehara, T., *Phys. B-Condens. Mater.* **2003**, *329*, 967.

(140) Klevtsov, P. V.; Kim, V. G.; Kruglik, A. I.; Klevtsova, R. F., *Sov. Phys. Crystallogr.* **1989**, *34*, 1475.

(141) Solodovnikov, S. F.; Klevtsova, R. F.; Glinskaya, L. A.; Klevtsov, P. V., *Sov. Phys. Crystallogr.* **1988**, *33*, 1380.

APPENDIX A: INVESTIGATING THE STRUCTURE OF $Cs_4Cu(MoO_4)_3$

A.1. Overview. Single crystals of $Cs_4Cu(MoO_4)_3$ samples have been synthesized using high temperature methods. As shown in Figure A.1.1, the crystal structure of $Cs_4Cu_3(MoO_4)_3$ consists of layers of disordered MoO_4 tetrahdra and CuO_5 trigonal bipyramids.[1, 2] Three structural phase transitions have been observed in this material. However, the hexagonal phase is reportedly stable above 413 K (140° C).[1] Previous reports suggest that the single crystals of $Cs_4Cu(MoO_4)_3$ crystallize in a hexagonal space group ($P6_3/mmc$) with lattice parameters a = 6.286(1) Å and c = 23.669(5) Å.

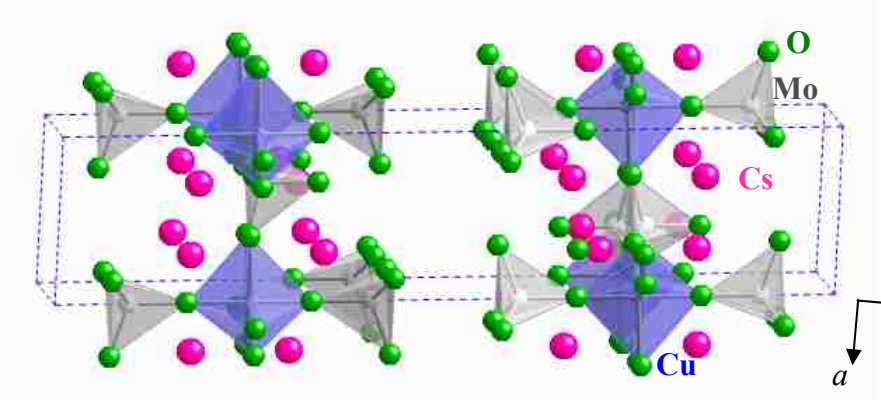

Figure A.1. The crystal structure of $Cs_4Cu(MoO_4)_3$ at 298 K. The Cs atoms are shown in pink, Cu polyhedra are shown in blue, Mo tetrahedral are shown in gray, and O atoms are shown in green.

A.2. Single crystal X-ray Diffraction. The crystallographic information obtained from single crystal X-ray diffraction is provided in Table A.1. Single crystal X-ray diffraction data were measured on the same single crystal fragment at different temperatures (T = 100, 260, 265, 270, 275, and 298 K). The R_{factor} or "Reliability factor" obtained for each structural model at different temperature are also provided in Table A.1. For some compounds, which I may suspect with this system, it may be possible to refine the structural models to acceptable R-values using several different symmetry, space groups, or crystallographic positions. Some orthorhombic systems may appear to have hexagonal symmetry (pseudohexagonality), where $a_o \sim a_h = \sqrt{3}$, $b_o \sim c_h$, and $c_o \sim a_h$.[1]

It has also been observed that the mosaicity, which can be used to describe the crystal quality, becomes very large (1.39) at 270 K, where we expect a phase transition to occur. However, for these crystals, this change in mosaicity is reversible upon heating the sample from 100 K to 275 K.

Table A.1. Summary of Temperature dependent Single Crystal X-ray Diffraction Data Collections for $Cs_4Cu(MoO_4)_3$

T (K)	R_{factor}[a]	Stoichiometry[b]	Mosaicity	Lattice Parameters (Å)	
298	2.56	$Cs_4Cu(MoO_{4.02})_{2.97}$	0.449	a = 6.2910(2)	c = 23.6940(8)
275	3.28	$Cs_4Cu(MoO_{4.07})_{3.01}$	0.45	a = 6.2860(7)	c = 23.6910(17)
270	3.66	$Cs_4Cu(MoO_{4.30})_{2.95}$	1.390	a = 6.1510(11)	c = 23.1680(4)
265	2.83	$Cs_4Cu(MoO_{4.04})_{2.96}$	1.034	a = 6.2340(5)	c = 23.6960(22)
260	2.84	$Cs_4Cu(MoO_{3.96})_{2.96}$	1.018	a = 6.2410(5)	c = 23.6290(14)
100	8.81	$Cs_4Cu(MoO_{3.96})_{2.96}$	1.5	a = 6.2010(6)	c = 23.5210(26)

[a] $R_{factor} = \sum \| F_o \| - |F_c| \| / \sum |F_o|$

[b] Stoichiometry calculated using the partial occupancies from the refined data

A.3. Structure of $Cs_4Cu(MoO_4)_3$. Single crystals of $Cs_4Cu(MoO_4)_3$ crystallize in a hexagonal space group $P6_3/mmc$ (no. 194) with lattice parameters of a = 6.2910(2) and c = 23.6940(8) Å at 298 K. Atomic positions are provided in Table A.2 for $Cs_4Cu(MoO_{4.02})_{2.97}$ at 298 K. The crystal structure of $Cs_4Cu(MoO_4)_3$ consists of layers of disordered MoO_4 tetrahdra and CuO_5 trigonal bipyramids. In the distorted MoO4 tetrahedra, Mo2 atoms are connected to O1 (1x) and O2 (3x) atoms at distances of 1.739 and 1.785 Å, respectively, at 298 K. These MoO4 tetrahedra are vertex-sharing with the CuO_5 trigonal bipyramids, which consists of Cu atoms connected to O1 (2x) and O4 (6x) atoms at interatomic distances of 2.104(8) and 1.887(5) Å, respectively, at 298 K.

Table A.2. Atomic Positions and Displacement Parameters of $Cs_4Cu(MoO_{4.02})_{2.97}$ at 298 K

Atom	Wyckoff Position	*x*	*y*	*z*	U_{eq} [a]
Cs1	4*f*	0.3333	-0.3333	0.16469(2)	0.0315(2)
Cs2	4*f*	-0.3333	0.3333	0.031288(19)	0.02279(19)
Mo1	4*e*	0	0	0.09507(2)	0.01706(19)
Mo2	4*f*	0.6667	0.3333	0.23254(6)	0.0206(5)
Cu1	2*b*	0	0	0.2500	0.0232(3)
O2	12*k*	0.1500(3)	0.3000(7)	0.06984(14)	0.0314(9)
O1	4*e*	0	0	0.1704(2)	0.048(2)
O4	12*j*	0.3750(15)	0.2674(15)	0.25	0.054(3)
O3	4f	0.6667	0.3333	0.1599(5)	0.038(5)

[a] U_{eq} is defined as one-third trace of the orthogonalized of the U_{ij} tensor

The lattice parameters (*a* and *c*) are shown in Figure A.2 as a function of temperature. It is observed that at different temperatures, there is a noticeable decrease in the lattice parameters at 270 K, which may be indicative of a phase transition as shown in Figure A.2. However, the structural model can still be refined using the same hexagonal symmetry and space group ($P6_3mmc$).

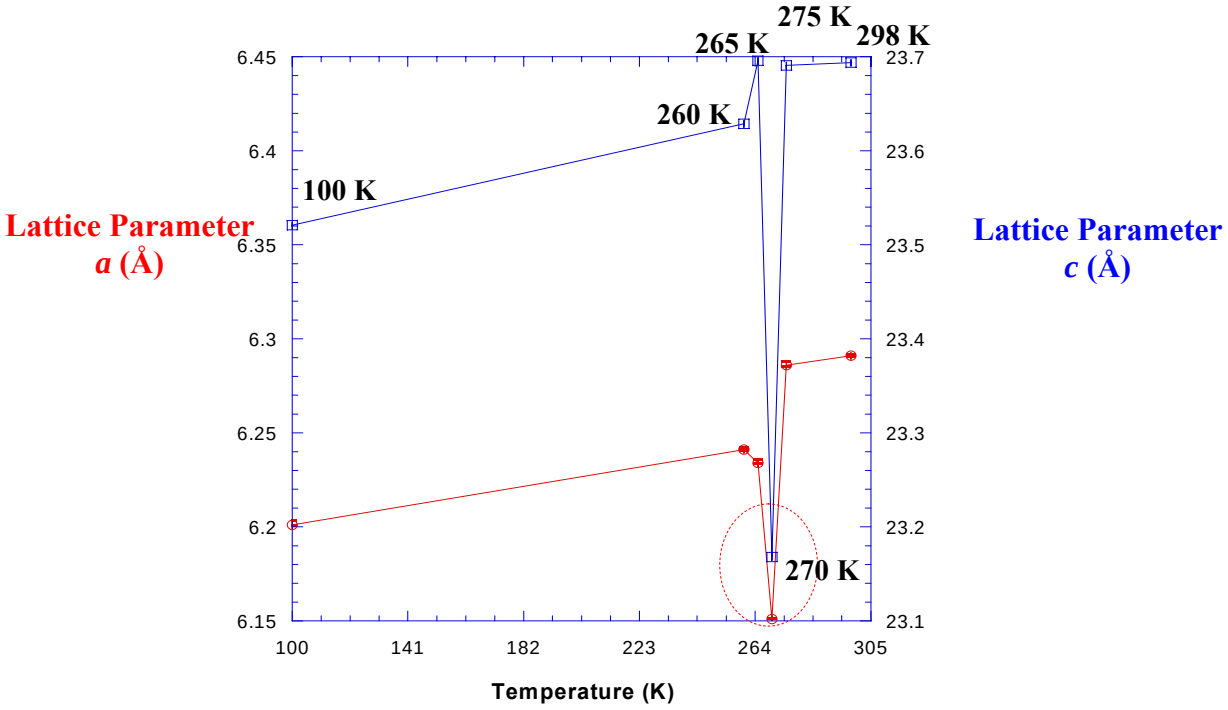

Figure A.2. Lattice parameters vs. Temperature for the $Cs_4Cu(MoO_4)_3$ Compounds.

Appendix A. References

(1) Solodovnikov, S. F.; Klevtsova, R. F.; Glinskaya, L. A.; Klevtsov, P. V. *Sov. Phys. Crystallogr.* **1988**, *33*, 1380.

(2) Klevtsov, P. V.; Kim, V. G.; Kruglik, A. I.; Klevtsova, R. F. *Sov. Phys. Crystallogr.* **1989**, *34*, 1475.

APPENDIX B: SYNTHESIS, STRUCTURE AND CHARACTERIZATION OF $PrNi_2Ga_2$

B.1. Introduction. Pr-based compounds are of recent fascination due to their mixed valence behavior. These compounds can occur as Pr^{3+} or Pr^{4+}, which can lead to valence fluctuations in these compounds.[1] Recently, $PrOs_4Sb_{12}$ has been found to exhibit heavy fermion behavior and superconductivity.[2] The heavy fermion behavior in these compounds can be attributed to the interaction of the moments of the Pr^{3+} ground state with the conduction electrons.[2]

In our exploration of ternary Pr-based heavy fermion compounds, a new ternary compound, $PrNi_2Ga_2$ has been synthesized using excess Ga and characterized by single-crystal X-ray diffraction. $PrNi_2Ga_2$ adopts a tetragonal structure in the *I4/mmm* space group and is related to the $ThCr_2Si_2$ structure type.[3] $PrNi_2Ga_2$ crystallizes in a tetragonal, space group I4/*mmm*, $Z = 2$, with the lattice parameters: $a = 4.2600(4)$ Å and $c = 10.2830(14)$ Å. The compound is metallic ($d\rho/dT > 0$), with the resistance decreasing roughly linearly with temperature from 300 K down to 100 K.

B.2. Synthesis. The starting materials, Pr ingot (Alfa Aesar Laboratory), Ni powder (5N, Alfa Aesar), and Ga shot (5N, Alfa Aesar) were placed in a 2-mL alumina crucible in a 1:1:20 stoichiometric ratio. The constituents were heated to a temperature of 1423 K for 48 hours and slowly cooled to 993 K, at a rate of 278 K/ hr, at which point the hot flux was removed by centrifugation. Metallic single crystals on the order of 1 mm were obtained. X-ray powder diffraction was performed to determine the structure of these samples.

Several modified temperature profiles were used in the attempt to make larger single crystals of $PrNi_2Ga_2$ for neutron diffraction experiments. However, two new phases, Pr_2NiGa_{10} and Pr_2NiGa_{12}, which have been discussed in detail (Chapter 3) were synthesized.

B.3. Single Crystal X-ray Diffraction. A fragment of a single crystal of $PrNi_2Ga_2$ (0.025 x 0.04 x 0.05 mm) was mechanically extracted and mounted on a Nonius KappaCCD diffractometer with Mo Kα, (λ = 0.71073 Å) radiation. Data were collected at 298 K. The atomic positions from the $ThCr_2Si_2$ structure type[3] were used as an initial structural model in determining the atomic positions of $PrNi_2Ga_2$. Corrections were made for extinction, and the data were refined with anisotropic displacement parameters. The structural model was refined using SHELXL97 to a final R_{factor} of 4.89%. The highest peak difference and deepest hole values were 6.275 and -1.700 e/Å^3, respectively. Atomic positions and related structural information are provided in Table B.1. Selected crystallographic information is presented in Table B.2. Selected interatomic distances are provided in Table B.3.

Table B.1. Atomic Positions and Displacement Parameters of $PrNi_2Ga_2$

Atom	Wyckoff Position	*x*	*y*	*z*	U_{eq} [a]
Pr	2*a*	0	0	0	0.01707(11)
Ni	4*e*	1/2	1/2	0.1171(5)	0.0262(13)
Ga	4*d*	0	1/2	1/4	0.0248(12)

[a] U_{eq} is defined as one-third trace of the orthogonalized of the U_{ij} tensor

B.4. Structure of $PrNi_2Ga_2$. $PrNi_2Ga_2$ crystallizes in a tetragonal space group, I4/*mmm* (no. 139), with the Pr, Ni, and Ga atoms occupying the 2*a*, 4*e*, and 4*d* Wyckoff symmetry sites, respectively. The compound has lattice parameters of a = 4.2600(4) Å and c = 10.2830(14) Å, Z = 2 and V = 186.61(4) Å^3.

Table B.2. Selected Crystallographic Parameters for $PrNi_2Ga_2$

Crystal Data	
Formula	$PrNi_2Ga_2$
a (Å)	4.2600(4)
c (Å)	10.2830(14)
V (Å^3)	186.61(4)
Z	2
Crystal Dimension (mm^3)	0.025 x 0.04 x 0.05
Crystal System	Tetragonal
Space Group	*I*4/*mmm*
θ range (º)	2.55-32.03
μ(mm^{-1})	37.329
Data Collection	
Measured Reflections	843
Independent Reflections	117
Reflections with I > 3σ(I)	82
R_{int}	0.041
h	-5 → 5
k	-3 → 3
l	-13 → 9
Refinement	
[a]R[F^2>2σ(F^2)]	0.0489
[b]wR(F^2)	0.1556
Reflections	82
Parameters	19
$\Delta\rho_{max}$ (e Å^{-3})	6.275
$\Delta\rho_{min}$ (e Å^{-3})	-1.700
Extinction coefficient	0.001492(5)

[a] $R_1 = \sum \| F_o \| - |F_c| \| / \sum |F_o|$

[b] $wR_2 = \left[\sum \left[w(F_0^2 - F_c^2) \right] / \sum \left[w(F_0^2)^2 \right] \right]^{\frac{1}{2}}$

Table B.3. Selected Interatomic Distances (Å) and Bond Angles (º) of $PrNi_2Ga_2$

$NiGa_4$ tetrahedra	(Å)
Ni – Ga1 (x4)	2.531 (3)
Ni – Ni (x2)	2.408 (3)
Angle	(º)
Ga1 – Ni – Ga1	114.62 (18)

The crystal structure of $PrNi_2Ga_2$ consists of layers of edge sharing $NiGa_4$ tetrahedra, forming a cage-like linkage, which encapsulates isolated Pr atoms along the *c*-axis as shown in Figure B.1. Each Ni atom in these $NiGa_4$ tetrahedra is coordinate to 4 Ga atoms by an interatomic distance of 2.531(3) Å, which is consistent with the summation of the covalent radii of Ni (1.15Å) and Ga (1.35 Å).[142] Each layer of $NiGa_4$ tetrahedra are linked to the next layer of $NiGa_4$ tetrahedra by a Ni-Ni interatomic distance of 2.408(3) Å. This is consistent with the sum of the covalent radii of Ni (1.15 Å).[4] The Ga-Ni-Ga bond angles in these $NiGa_4$ tetrahedra are 114.62(18)°, which is slightly distorted. In the Pr layer, the Pr-Pr interatomic distance of 4.260 (3) Å is too long to be considered bonding.

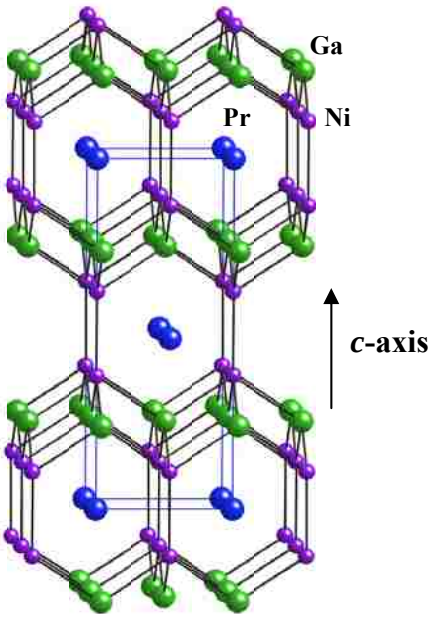

Figure B.1. The crystal structure of $PrNi_2Ga_2$ is shown along the *c*-axis. Pr atoms are shown in blue, the Ni atoms are represented in purple, and the Ga atoms are shown as green circles.

Appendix B References

(1) Luo, K.-q.; Li, J.; De Gong, C. *Phys. Rev. B* **1995**, *52*, 3769.

(2) Bauer, E. D.; Frederick, N. A.; Ho, P. C.; Zapf, V. S.; Maple, M. B. *Phys. Rev. B* **2002**, *65*, 100506.

(3) Zheng, C.; Hoffmann, R. *J. Solid State Chem.* **1988**, *72*, 58.

(4) Müller, U. *Inorganic Structural Chemistry*; John Wiley & Sons: New York, **1993**; 2nd Edition.

APPENDIX C: ADDITIONAL DATA ANALYSIS FOR NEUTRON DIFFRACTION EXPERIMENTS OF $CePdGa_6$

Powder neutron diffraction experiments were conducted for $CePdGa_6$ on B-T1 and B-T9 at NCNR at the National Institute of Standards and Technology (NIST). The magnetic peak at 33.15°, which is observed in the neutron powder diffraction pattern for $CePdGa_6$, may be attributed to either $CePdGa_6$ (T_N = 5.5 K) or a Ce_2PdGa_{12} (T_N = 10.5 K) impurity. Although there are no general conditions for $CePdGa_6$'s space group, $P4/mmm$, there are 3 General conditions for Ce_2PdGa_{12}'s spacegroup, $P4/nbm$:

$h\ k\ 0 : h + k = 2n$
$0\ k\ l: k = 2n$
$h\ 0\ 0: h = 2n$

The spin propagation wave vector (q) was calculated using Formula C.1. Then peaks for $CePdGa_6$ and Ce_2PdGa_{12} were generated using Formula C.2. Tables C.1. and C.2 display the spin propagation wave vector worksheet, where q is calculated using different combinations of miller indices to determine which phase is responsible for the magnetic peak at 33.15°.

$$q = \frac{4\pi \sin\theta}{\lambda},\ \theta = 16.575°, \lambda = 2.3590\ \text{Å} \qquad \text{(C.1.)}$$

$$q = 2\pi\sqrt{\frac{h^2}{a^2} + \frac{k^2}{b^2} + \frac{l^2}{c^2}} \qquad \text{(C.2.)}$$

Table C.1. Spin propagation worksheet for $CePdGa_6$

$$q = 2\pi\sqrt{\frac{h^2}{a^2}+\frac{k^2}{b^2}+\frac{l^2}{c^2}}, \quad q_{\exp} = 1.519631612$$

h^2	k^2	l^2	q_{calc} ($CePdGa_6$)	*a*	b	*c*	*h*	*k*	*l*
0	0	0.25	0.561476744	4.33732	4.33732	7.912853	0	0	0.5
0	0	1	0.794048026	4.33732	4.33732	7.912853	0	0	1
0	0	2.25	0.972506248	4.33732	4.33732	7.912853	0	0	1.5
0	0	4	1.122953488	4.33732	4.33732	7.912853	0	0	2
0	0	6.25	1.255500167	4.33732	4.33732	7.912853	0	0	2.5
1	0	0	1.448633098	4.33732	4.33732	7.912853	1	0	0 *
1	0.25	0	1.774205957	4.33732	4.33732	7.912853	1	0.5	0
1	1	0	2.048676574	4.33732	4.33732	7.912853	1	1	0
1	4	0	2.509106127	4.33732	4.33732	7.912853	1	2	0
1	9	0	2.897266195	4.33732	4.33732	7.912853	1	3	0
1	0	1	1.651983692	4.33732	4.33732	7.912853	1	0	1
1	0	4	1.832910906	4.33732	4.33732	7.912853	1	0	2
1	0	9	1.997517123	4.33732	4.33732	7.912853	1	0	3
1	1	1	2.197177274	4.33732	4.33732	7.912853	1	1	1
1	1	4	2.336257743	4.33732	4.33732	7.912853	1	1	2
1	1	9	2.4675114	4.33732	4.33732	7.912853	1	1	3
1	0	0.25	1.55363895	4.33732	4.33732	7.912853	1	0	0.5*
4	0	1	3.0041078	4.33732	4.33732	7.912853	2	0	1
1	0	4	1.832910906	4.33732	4.33732	7.912853	1	0	2
1	0	1	1.651983692	4.33732	4.33732	7.912853	1	0	1
0.25	0	1	1.074777526	4.33732	4.33732	7.912853	0.5	0	1
0.25	1	0	1.61962104	4.33732	4.33732	7.912853	0.5	1	0
1	0	0	1.448633098	4.33732	4.33732	7.912853	1	0	0 *
0	1	1	1.651983692	4.33732	4.33732	7.912853	0	1	1*

* Possible h k l combinations, where q_{calc} is similar to q_{exp}

Table C.2. Spin propagation worksheet for Ce_2PdGa_{12}

$$q = 2\pi\sqrt{\frac{h^2}{a^2}+\frac{k^2}{b^2}+\frac{l^2}{c^2}}, \quad q_{\exp} = 1.519631612$$

h^2	k^2	l^2	q_{calc} (Ce_2PdGa_{12})	a	b	c	h	k	l
0	0	0.25	0.286498297	6.084353	6.084353	15.507537	0	0	0.5
0	0	1	0.405169777	6.084353	6.084353	15.507537	0	0	1
0	0	2.25	0.496229606	6.084353	6.084353	15.507537	0	0	1.5
0	0	4	0.572996594	6.084353	6.084353	15.507537	0	0	2
0	0	6.25	0.640629667	6.084353	6.084353	15.507537	0	0	2.5
1	0	0	1.032679285	6.084353	6.084353	15.507537	1	0	0
1	0.25	0	1.264768658	6.084353	6.084353	15.507537	1	0.5	0
1	1	0	1.460429051	6.084353	6.084353	15.507537	1	1	0 *
1	4	0	1.78865299	6.084353	6.084353	15.507537	1	2	0
1	9	0	2.06535857	6.084353	6.084353	15.507537	1	3	0
1	0	1	1.109319185	6.084353	6.084353	15.507537	1	0	1
1	0	4	1.180996021	6.084353	6.084353	15.507537	1	0	2
1	0	9	1.248564836	6.084353	6.084353	15.507537	1	0	3
1	1	1	1.515590829	6.084353	6.084353	15.507537	1	1	1 *
1	1	4	1.568814236	6.084353	6.084353	15.507537	1	1	2 *
1	1	9	1.6202903	6.084353	6.084353	15.507537	1	1	3
1	0	0.25	1.071684553	6.084353	6.084353	15.507537	1	0	0.5
4	0	1	2.104725296	6.084353	6.084353	15.507537	2	0	1
1	0	4	1.180996021	6.084353	6.084353	15.507537	1	0	2
1	0	1	1.109319185	6.084353	6.084353	15.507537	1	0	1
0.25	0	1	0.656330081	6.084353	6.084353	15.507537	0.5	0	1
0.25	1	0	1.15457054	6.084353	6.084353	15.507537	0.5	1	0
1	0	0	1.032679285	6.084353	6.084353	15.507537	1	0	0
0	4	0	1.460429051	6.084353	6.084353	15.507537	0	2	0 *
0	1	1	1.109319185	6.084353	6.084353	15.507537	0	1	1
1	0	1	1.109319185	6.084353	6.084353	15.507537	1	0	1

* Possible h k l combinations, where q_{calc} is similar to q_{exp}

The (1 0 ½) and (1 1 1) peaks for $CePdGa_6$ and Ce_2PdGa_{12}, respectively, are both similar to q_{calc}. However the (111) peak for Ce_2PdGa_{12} is much more accurate than the (1 0 ½) peak of $CePdGa_6$ Both peaks have been used to determine the structure factor (F_{hkl}^2) assuming each model is correct. The calculated structure factor squared (F_{111}^2) = 16 f_{Ce} or 216, where f_{Ce} = 13.5, should be proportional to intensity for Ce_2PdGa_{12}.

APPENDIX D: SUPPLEMENTAL INFORMATION: CRYSTALLOGRAPHIC INFORMATION FILES (CIF) FOR UNPUBLISHED WORK

D.1. Ce_2NiGa_{10}

X-ray Filename: Jasmine27

data_Ce_2NiGa_{10}

```
_audit_creation_method           SHELXL-97
_chemical_name_systematic
;
 ?
;
_chemical_name_common             ?
_chemical_melting_point           ?
_chemical_formula_moiety          ?
_chemical_formula_sum
 'Ce Ga20 Ni'
_chemical_formula_weight          1593.23

loop_
 _atom_type_symbol
 _atom_type_description
 _atom_type_scat_dispersion_real
 _atom_type_scat_dispersion_imag
 _atom_type_scat_source
 'Ce'  'Ce'  -0.2486   2.6331
 'International Tables Vol C Tables 4.2.6.8 and 6.1.1.4'
 'Ni'  'Ni'   0.3393   1.1124
 'International Tables Vol C Tables 4.2.6.8 and 6.1.1.4'
 'Ga'  'Ga'   0.2307   1.6083
 'International Tables Vol C Tables 4.2.6.8 and 6.1.1.4'

_symmetry_cell_setting            tetragonal
_symmetry_space_group_name_H-M    I4/mmm

loop_
 _symmetry_equiv_pos_as_xyz
 'x, y, z'
 '-x, -y, z'
 'x, -y, -z'
 '-x, y, -z'
 '-y, -x, -z'
 'y, x, -z'
 'y, -x, z'
 '-y, x, z'
 'x+1/2, y+1/2, z+1/2'
 '-x+1/2, -y+1/2, z+1/2'
 'x+1/2, -y+1/2, -z+1/2'
 '-x+1/2, y+1/2, -z+1/2'
 '-y+1/2, -x+1/2, -z+1/2'
 'y+1/2, x+1/2, -z+1/2'
 'y+1/2, -x+1/2, z+1/2'
 '-y+1/2, x+1/2, z+1/2'
```

'-x, -y, -z'
'x, y, -z'
'-x, y, z'
'x, -y, z'
'y, x, z'
'-y, -x, z'
'-y, x, -z'
'y, -x, -z'
'-x+1/2, -y+1/2, -z+1/2'
'x+1/2, y+1/2, -z+1/2'
'-x+1/2, y+1/2, z+1/2'
'x+1/2, -y+1/2, z+1/2'
'y+1/2, x+1/2, z+1/2'
'-y+1/2, -x+1/2, z+1/2'
'-y+1/2, x+1/2, -z+1/2'
'y+1/2, -x+1/2, -z+1/2'

_cell_length_a 4.2390(5)
_cell_length_b 4.2390(5)
_cell_length_c 26.386(4)
_cell_angle_alpha 90.00
_cell_angle_beta 90.00
_cell_angle_gamma 90.00
_cell_volume 474.13(10)
_cell_formula_units_Z 2
_cell_measurement_temperature 293(2)
_cell_measurement_reflns_used ?
_cell_measurement_theta_min ?
_cell_measurement_theta_max ?

_exptl_crystal_description ?
_exptl_crystal_colour ?
_exptl_crystal_size_max ?
_exptl_crystal_size_mid ?
_exptl_crystal_size_min ?
_exptl_crystal_density_meas ?
_exptl_crystal_density_diffrn 11.160
_exptl_crystal_density_method 'not measured'
_exptl_crystal_F_000 1412
_exptl_absorpt_coefficient_mu 62.291
_exptl_absorpt_correction_type ?
_exptl_absorpt_correction_T_min ?
_exptl_absorpt_correction_T_max ?
_exptl_absorpt_process_details ?

_exptl_special_details
;
?
;

_diffrn_ambient_temperature 293(2)
_diffrn_radiation_wavelength 0.71073
_diffrn_radiation_type MoK\a
_diffrn_radiation_source 'fine-focus sealed tube'
_diffrn_radiation_monochromator graphite
_diffrn_measurement_device_type ?

```
_diffrn_measurement_method       ?
_diffrn_detector_area_resol_mean  ?
_diffrn_standards_number         ?
_diffrn_standards_interval_count  ?
_diffrn_standards_interval_time   ?
_diffrn_standards_decay_%        ?
_diffrn_reflns_number            472
_diffrn_reflns_av_R_equivalents   0.0445
_diffrn_reflns_av_sigmaI/netI     0.0551
_diffrn_reflns_limit_h_min       -5
_diffrn_reflns_limit_h_max       5
_diffrn_reflns_limit_k_min       -4
_diffrn_reflns_limit_k_max       4
_diffrn_reflns_limit_l_min       -24
_diffrn_reflns_limit_l_max       35
_diffrn_reflns_theta_min         3.09
_diffrn_reflns_theta_max         29.70
_reflns_number_total             239
_reflns_number_gt                225
_reflns_threshold_expression     >2sigma(I)

_computing_data_collection       ?
_computing_cell_refinement       ?
_computing_data_reduction        ?
_computing_structure_solution    'SHELXS-97 (Sheldrick, 1990)'
_computing_structure_refinement   'SHELXL-97 (Sheldrick, 1997)'
_computing_molecular_graphics    ?
_computing_publication_material   ?

_refine_special_details
;
 Refinement of F^2^ against ALL reflections.  The weighted R-factor wR and
 goodness of fit S are based on F^2^, conventional R-factors R are based
 on F, with F set to zero for negative F^2^. The threshold expression of
 F^2^ > 2sigma(F^2^) is used only for calculating R-factors(gt) etc. and is
 not relevant to the choice of reflections for refinement.  R-factors based
 on F^2^ are statistically about twice as large as those based on F, and R-
 factors based on ALL data will be even larger.
;

_refine_ls_structure_factor_coef  Fsqd
_refine_ls_matrix_type           full
_refine_ls_weighting_scheme      calc
_refine_ls_weighting_details
 'calc w=1/[\s^2^(Fo^2^)+(0.0390P)^2^+24.4399P] where P=(Fo^2^+2Fc^2^)/3'
_atom_sites_solution_primary     direct
_atom_sites_solution_secondary    difmap
_atom_sites_solution_hydrogens    geom
_refine_ls_hydrogen_treatment    mixed
_refine_ls_extinction_method     SHELXL
_refine_ls_extinction_coef       0.0076(10)
_refine_ls_extinction_expression
 'Fc^*^=kFc[1+0.001xFc^2^\l^3^/sin(2\q)]^-1/4^'
_refine_ls_number_reflns         239
_refine_ls_number_parameters     19
_refine_ls_number_restraints     0
```

```
_refine_ls_R_factor_all          0.0440
_refine_ls_R_factor_gt           0.0409
_refine_ls_wR_factor_ref         0.1086
_refine_ls_wR_factor_gt          0.1057
_refine_ls_goodness_of_fit_ref   1.132
_refine_ls_restrained_S_all      1.132
_refine_ls_shift/su_max          0.000
_refine_ls_shift/su_mean         0.000

loop_
 _atom_site_label
 _atom_site_type_symbol
 _atom_site_fract_x
 _atom_site_fract_y
 _atom_site_fract_z
 _atom_site_U_iso_or_equiv
 _atom_site_adp_type
 _atom_site_occupancy
 _atom_site_symmetry_multiplicity
 _atom_site_calc_flag
 _atom_site_refinement_flags
 _atom_site_disorder_assembly
 _atom_site_disorder_group
Ce1 Ce 0.0000 0.0000 0.35391(4) 0.0067(5) Uani 1 8 d S . .
Ni2 Ni 0.0000 0.0000 0.5000 0.0064(8) Uani 1 16 d S . .
Ga3 Ga 0.0000 0.0000 0.10613(9) 0.0118(6) Uani 1 8 d S . .
Ga1 Ga 0.0000 0.5000 0.2500 0.0205(7) Uani 1 8 d S . .
Ga4 Ga 0.0000 0.0000 0.19760(9) 0.0186(7) Uani 1 8 d S . .
Ga2 Ga 0.5000 0.0000 0.45078(5) 0.0083(5) Uani 1 4 d S . .

loop_
 _atom_site_aniso_label
 _atom_site_aniso_U_11
 _atom_site_aniso_U_22
 _atom_site_aniso_U_33
 _atom_site_aniso_U_23
 _atom_site_aniso_U_13
 _atom_site_aniso_U_12
Ce1 0.0047(5) 0.0047(5) 0.0107(6) 0.000 0.000 0.000
Ni2 0.0051(10) 0.0051(10) 0.0091(15) 0.000 0.000 0.000
Ga3 0.0083(8) 0.0083(8) 0.0188(12) 0.000 0.000 0.000
Ga1 0.0192(9) 0.0192(9) 0.0233(13) 0.000 0.000 0.000
Ga4 0.0197(9) 0.0197(9) 0.0163(12) 0.000 0.000 0.000
Ga2 0.0066(8) 0.0107(9) 0.0076(7) 0.000 0.000 0.000

_geom_special_details
;
 All esds (except the esd in the dihedral angle between two l.s. planes)
 are estimated using the full covariance matrix.  The cell esds are taken
 into account individually in the estimation of esds in distances, angles
 and torsion angles; correlations between esds in cell parameters are only
 used when they are defined by crystal symmetry.  An approximate (isotropic)
 treatment of cell esds is used for estimating esds involving l.s. planes.
;

loop_
```

```
 _geom_bond_atom_site_label_1
 _geom_bond_atom_site_label_2
 _geom_bond_distance
 _geom_bond_site_symmetry_2
 _geom_bond_publ_flag
Ce1 Ga3 3.1775(9) 25 ?
Ce1 Ga3 3.1775(9) 25_445 ?
Ce1 Ga3 3.1775(9) 25_455 ?
Ce1 Ga3 3.1775(9) 25_545 ?
Ce1 Ga4 3.2913(11) 25_445 ?
Ce1 Ga4 3.2913(11) 25 ?
Ce1 Ga4 3.2913(11) 25_455 ?
Ce1 Ga4 3.2913(11) 25_545 ?
Ce1 Ga2 3.3203(13) . ?
Ce1 Ga2 3.3204(13) 21 ?
Ce1 Ga2 3.3204(13) 21_545 ?
Ce1 Ga2 3.3204(13) 1_455 ?
Ni2 Ga2 2.4858(7) 5_566 ?
Ni2 Ga2 2.4858(7) 17_656 ?
Ni2 Ga2 2.4858(7) 5_556 ?
Ni2 Ga2 2.4858(7) 17_556 ?
Ni2 Ga2 2.4858(7) 21_545 ?
Ni2 Ga2 2.4858(7) 1_455 ?
Ni2 Ga2 2.4858(7) 21 ?
Ni2 Ga2 2.4858(7) . ?
Ga3 Ga4 2.414(4) . ?
Ga3 Ga2 2.5975(15) 13_455 ?
Ga3 Ga2 2.5975(15) 25_545 ?
Ga3 Ga2 2.5975(15) 13 ?
Ga3 Ga2 2.5975(15) 25 ?
Ga3 Ce1 3.1775(9) 25 ?
Ga3 Ce1 3.1775(9) 25_445 ?
Ga3 Ce1 3.1775(9) 25_455 ?
Ga3 Ce1 3.1775(9) 25_545 ?
Ga1 Ga4 2.5305(14) 25 ?
Ga1 Ga4 2.5305(14) 25_455 ?
Ga1 Ga4 2.5305(14) 1_565 ?
Ga1 Ga4 2.5306(14) . ?
Ga1 Ga1 2.9974(4) 25_565 ?
Ga1 Ga1 2.9974(4) 25_455 ?
Ga1 Ga1 2.9974(4) 25_465 ?
Ga1 Ga1 2.9974(4) 25 ?
Ga1 Ce1 3.4655(9) 25_455 ?
Ga1 Ce1 3.4655(9) 25 ?
Ga1 Ce1 3.4656(9) 1_565 ?
Ga4 Ga1 2.5306(14) 25 ?
Ga4 Ga1 2.5306(14) 25_455 ?
Ga4 Ga1 2.5306(14) 1_545 ?
Ga4 Ce1 3.2912(11) 25_445 ?
Ga4 Ce1 3.2912(11) 25 ?
Ga4 Ce1 3.2912(11) 25_455 ?
Ga4 Ce1 3.2912(11) 25_545 ?
Ga2 Ni2 2.4858(7) 1_655 ?
Ga2 Ga3 2.5975(15) 25_545 ?
Ga2 Ga3 2.5975(15) 25 ?
Ga2 Ga2 2.598(3) 17_656 ?
```

Ga2 Ga2 2.9974(4) 21_655 ?
Ga2 Ga2 2.9974(4) 21_545 ?
Ga2 Ga2 2.9974(4) 21 ?
Ga2 Ga2 2.9974(4) 21_645 ?
Ga2 Ce1 3.3203(13) 1_655 ?

loop_
 _geom_angle_atom_site_label_1
 _geom_angle_atom_site_label_2
 _geom_angle_atom_site_label_3
 _geom_angle
 _geom_angle_site_symmetry_1
 _geom_angle_site_symmetry_3
 _geom_angle_publ_flag
Ga3 Ce1 Ga3 141.24(9) 25 25_445 ?
Ga3 Ce1 Ga3 83.68(3) 25 25_455 ?
Ga3 Ce1 Ga3 83.68(3) 25_445 25_455 ?
Ga3 Ce1 Ga3 83.68(3) 25 25_545 ?
Ga3 Ce1 Ga3 83.68(3) 25_445 25_545 ?
Ga3 Ce1 Ga3 141.24(9) 25_455 25_545 ?
Ga3 Ce1 Ga4 174.98(6) 25 25_445 ?
Ga3 Ce1 Ga4 43.77(6) 25_445 25_445 ?
Ga3 Ce1 Ga4 97.88(2) 25_455 25_445 ?
Ga3 Ce1 Ga4 97.88(2) 25_545 25_445 ?
Ga3 Ce1 Ga4 43.77(6) 25 25 ?
Ga3 Ce1 Ga4 174.98(6) 25_445 25 ?
Ga3 Ce1 Ga4 97.88(2) 25_455 25 ?
Ga3 Ce1 Ga4 97.88(2) 25_545 25 ?
Ga4 Ce1 Ga4 131.21(8) 25_445 25 ?
Ga3 Ce1 Ga4 97.88(2) 25 25_455 ?
Ga3 Ce1 Ga4 97.88(2) 25_445 25_455 ?
Ga3 Ce1 Ga4 43.77(6) 25_455 25_455 ?
Ga3 Ce1 Ga4 174.98(6) 25_545 25_455 ?
Ga4 Ce1 Ga4 80.18(3) 25_445 25_455 ?
Ga4 Ce1 Ga4 80.18(3) 25 25_455 ?
Ga3 Ce1 Ga4 97.88(2) 25 25_545 ?
Ga3 Ce1 Ga4 97.88(2) 25_445 25_545 ?
Ga3 Ce1 Ga4 174.98(6) 25_455 25_545 ?
Ga3 Ce1 Ga4 43.77(6) 25_545 25_545 ?
Ga4 Ce1 Ga4 80.18(3) 25_445 25_545 ?
Ga4 Ce1 Ga4 80.18(3) 25 25_545 ?
Ga4 Ce1 Ga4 131.21(8) 25_455 25_545 ?
Ga3 Ce1 Ga2 47.06(3) 25 . ?
Ga3 Ce1 Ga2 99.81(5) 25_445 . ?
Ga3 Ce1 Ga2 99.81(5) 25_455 . ?
Ga3 Ce1 Ga2 47.06(3) 25_545 . ?
Ga4 Ce1 Ga2 136.80(3) 25_445 . ?
Ga4 Ce1 Ga2 84.65(4) 25 . ?
Ga4 Ce1 Ga2 136.80(3) 25_455 . ?
Ga4 Ce1 Ga2 84.65(4) 25_545 . ?
Ga3 Ce1 Ga2 47.06(3) 25 21 ?
Ga3 Ce1 Ga2 99.81(5) 25_445 21 ?
Ga3 Ce1 Ga2 47.06(3) 25_455 21 ?
Ga3 Ce1 Ga2 99.81(5) 25_545 21 ?
Ga4 Ce1 Ga2 136.80(3) 25_445 21 ?
Ga4 Ce1 Ga2 84.66(4) 25 21 ?

Ga4 Ce1 Ga2 84.66(4) 25_455 21 ?
Ga4 Ce1 Ga2 136.80(3) 25_545 21 ?
Ga2 Ce1 Ga2 53.66(2) . 21 ?
Ga3 Ce1 Ga2 99.81(5) 25 21_545 ?
Ga3 Ce1 Ga2 47.06(3) 25_445 21_545 ?
Ga3 Ce1 Ga2 99.81(5) 25_455 21_545 ?
Ga3 Ce1 Ga2 47.06(3) 25_545 21_545 ?
Ga4 Ce1 Ga2 84.66(4) 25_445 21_545 ?
Ga4 Ce1 Ga2 136.80(3) 25 21_545 ?
Ga4 Ce1 Ga2 136.80(3) 25_455 21_545 ?
Ga4 Ce1 Ga2 84.66(4) 25_545 21_545 ?
Ga2 Ce1 Ga2 53.66(2) . 21_545 ?
Ga2 Ce1 Ga2 79.33(4) 21 21_545 ?
Ga3 Ce1 Ga2 99.81(5) 25 1_455 ?
Ga3 Ce1 Ga2 47.06(3) 25_445 1_455 ?
Ga3 Ce1 Ga2 47.06(3) 25_455 1_455 ?
Ga3 Ce1 Ga2 99.81(5) 25_545 1_455 ?
Ga4 Ce1 Ga2 84.66(4) 25_445 1_455 ?
Ga4 Ce1 Ga2 136.80(3) 25 1_455 ?
Ga4 Ce1 Ga2 84.66(4) 25_455 1_455 ?
Ga4 Ce1 Ga2 136.80(3) 25_545 1_455 ?
Ga2 Ce1 Ga2 79.34(4) . 1_455 ?
Ga2 Ce1 Ga2 53.66(2) 21 1_455 ?
Ga2 Ce1 Ga2 53.66(2) 21_545 1_455 ?
Ga2 Ni2 Ga2 74.16(2) 5_566 17_656 ?
Ga2 Ni2 Ga2 117.00(5) 5_566 5_556 ?
Ga2 Ni2 Ga2 74.16(2) 17_656 5_556 ?
Ga2 Ni2 Ga2 74.16(2) 5_566 17_556 ?
Ga2 Ni2 Ga2 117.00(5) 17_656 17_556 ?
Ga2 Ni2 Ga2 74.16(2) 5_556 17_556 ?
Ga2 Ni2 Ga2 180.0 5_566 21_545 ?
Ga2 Ni2 Ga2 105.84(2) 17_656 21_545 ?
Ga2 Ni2 Ga2 63.00(5) 5_556 21_545 ?
Ga2 Ni2 Ga2 105.84(2) 17_556 21_545 ?
Ga2 Ni2 Ga2 105.84(2) 5_566 1_455 ?
Ga2 Ni2 Ga2 180.0 17_656 1_455 ?
Ga2 Ni2 Ga2 105.84(2) 5_556 1_455 ?
Ga2 Ni2 Ga2 63.00(5) 17_556 1_455 ?
Ga2 Ni2 Ga2 74.16(2) 21_545 1_455 ?
Ga2 Ni2 Ga2 63.00(5) 5_566 21 ?
Ga2 Ni2 Ga2 105.84(2) 17_656 21 ?
Ga2 Ni2 Ga2 180.0 5_556 21 ?
Ga2 Ni2 Ga2 105.84(2) 17_556 21 ?
Ga2 Ni2 Ga2 117.00(5) 21_545 21 ?
Ga2 Ni2 Ga2 74.16(2) 1_455 21 ?
Ga2 Ni2 Ga2 105.84(2) 5_566 . ?
Ga2 Ni2 Ga2 63.00(5) 17_656 . ?
Ga2 Ni2 Ga2 105.84(2) 5_556 . ?
Ga2 Ni2 Ga2 180.0 17_556 . ?
Ga2 Ni2 Ga2 74.16(2) 21_545 . ?
Ga2 Ni2 Ga2 117.00(5) 1_455 . ?
Ga2 Ni2 Ga2 74.16(2) 21 . ?
Ga4 Ga3 Ga2 125.32(5) . 13_455 ?
Ga4 Ga3 Ga2 125.32(5) . 25_545 ?
Ga2 Ga3 Ga2 70.48(5) 13_455 25_545 ?
Ga4 Ga3 Ga2 125.32(5) . 13 ?

Ga2 Ga3 Ga2 109.37(10) 13_455 13 ?
Ga2 Ga3 Ga2 70.48(5) 25_545 13 ?
Ga4 Ga3 Ga2 125.32(5) . 25 ?
Ga2 Ga3 Ga2 70.48(5) 13_455 25 ?
Ga2 Ga3 Ga2 109.37(10) 25_545 25 ?
Ga2 Ga3 Ga2 70.48(5) 13 25 ?
Ga4 Ga3 Ce1 70.62(5) . 25 ?
Ga2 Ga3 Ce1 137.40(3) 13_455 25 ?
Ga2 Ga3 Ce1 137.40(3) 25_545 25 ?
Ga2 Ga3 Ce1 69.36(2) 13 25 ?
Ga2 Ga3 Ce1 69.36(2) 25 25 ?
Ga4 Ga3 Ce1 70.62(5) . 25_445 ?
Ga2 Ga3 Ce1 69.36(2) 13_455 25_445 ?
Ga2 Ga3 Ce1 69.36(2) 25_545 25_445 ?
Ga2 Ga3 Ce1 137.40(3) 13 25_445 ?
Ga2 Ga3 Ce1 137.40(3) 25 25_445 ?
Ce1 Ga3 Ce1 141.24(9) 25 25_445 ?
Ga4 Ga3 Ce1 70.62(5) . 25_455 ?
Ga2 Ga3 Ce1 69.36(2) 13_455 25_455 ?
Ga2 Ga3 Ce1 137.40(3) 25_545 25_455 ?
Ga2 Ga3 Ce1 137.40(3) 13 25_455 ?
Ga2 Ga3 Ce1 69.36(2) 25 25_455 ?
Ce1 Ga3 Ce1 83.68(3) 25 25_455 ?
Ce1 Ga3 Ce1 83.68(3) 25_445 25_455 ?
Ga4 Ga3 Ce1 70.62(5) . 25_545 ?
Ga2 Ga3 Ce1 137.40(3) 13_455 25_545 ?
Ga2 Ga3 Ce1 69.36(2) 25_545 25_545 ?
Ga2 Ga3 Ce1 69.36(2) 13 25_545 ?
Ga2 Ga3 Ce1 137.40(3) 25 25_545 ?
Ce1 Ga3 Ce1 83.68(3) 25 25_545 ?
Ce1 Ga3 Ce1 83.68(3) 25_445 25_545 ?
Ce1 Ga3 Ce1 141.24(9) 25_455 25_545 ?
Ga4 Ga1 Ga4 113.77(9) 25 25_455 ?
Ga4 Ga1 Ga4 107.37(5) 25 1_565 ?
Ga4 Ga1 Ga4 107.37(5) 25_455 1_565 ?
Ga4 Ga1 Ga4 107.37(5) 25 . ?
Ga4 Ga1 Ga4 107.37(5) 25_455 . ?
Ga4 Ga1 Ga4 113.77(9) 1_565 . ?
Ga4 Ga1 Ga1 53.68(2) 25 25_565 ?
Ga4 Ga1 Ga1 126.32(2) 25_455 25_565 ?
Ga4 Ga1 Ga1 53.68(2) 1_565 25_565 ?
Ga4 Ga1 Ga1 126.32(2) . 25_565 ?
Ga4 Ga1 Ga1 126.32(2) 25 25_455 ?
Ga4 Ga1 Ga1 53.68(2) 25_455 25_455 ?
Ga4 Ga1 Ga1 126.32(2) 1_565 25_455 ?
Ga4 Ga1 Ga1 53.68(2) . 25_455 ?
Ga1 Ga1 Ga1 180.0 25_565 25_455 ?
Ga4 Ga1 Ga1 126.32(2) 25 25_465 ?
Ga4 Ga1 Ga1 53.68(2) 25_455 25_465 ?
Ga4 Ga1 Ga1 53.68(2) 1_565 25_465 ?
Ga4 Ga1 Ga1 126.32(2) . 25_465 ?
Ga1 Ga1 Ga1 90.0 25_565 25_465 ?
Ga1 Ga1 Ga1 90.0 25_455 25_465 ?
Ga4 Ga1 Ga1 53.68(2) 25 25 ?
Ga4 Ga1 Ga1 126.32(2) 25_455 25 ?
Ga4 Ga1 Ga1 126.32(2) 1_565 25 ?

Ga4 Ga1 Ga1 53.68(2) . 25 ?
Ga1 Ga1 Ga1 90.0 25_565 25 ?
Ga1 Ga1 Ga1 90.0 25_455 25 ?
Ga1 Ga1 Ga1 180.0 25_465 25 ?
Ga4 Ga1 Ce1 160.82(5) 25 25_455 ?
Ga4 Ga1 Ce1 85.41(5) 25_455 25_455 ?
Ga4 Ga1 Ce1 64.39(4) 1_565 25_455 ?
Ga4 Ga1 Ce1 64.39(4) . 25_455 ?
Ga1 Ga1 Ce1 115.626(7) 25_565 25_455 ?
Ga1 Ga1 Ce1 64.377(7) 25_455 25_455 ?
Ga1 Ga1 Ce1 64.377(7) 25_465 25_455 ?
Ga1 Ga1 Ce1 115.626(7) 25 25_455 ?
Ga4 Ga1 Ce1 85.41(5) 25 25 ?
Ga4 Ga1 Ce1 160.82(5) 25_455 25 ?
Ga4 Ga1 Ce1 64.39(4) 1_565 25 ?
Ga4 Ga1 Ce1 64.39(4) . 25 ?
Ga1 Ga1 Ce1 64.377(7) 25_565 25 ?
Ga1 Ga1 Ce1 115.626(7) 25_455 25 ?
Ga1 Ga1 Ce1 115.626(7) 25_465 25 ?
Ga1 Ga1 Ce1 64.377(7) 25 25 ?
Ce1 Ga1 Ce1 75.41(2) 25_455 25 ?
Ga4 Ga1 Ce1 64.39(4) 25 . ?
Ga4 Ga1 Ce1 64.39(4) 25_455 . ?
Ga4 Ga1 Ce1 160.82(5) 1_565 . ?
Ga4 Ga1 Ce1 85.41(5) . . ?
Ga1 Ga1 Ce1 115.622(7) 25_565 . ?
Ga1 Ga1 Ce1 64.375(7) 25_455 . ?
Ga1 Ga1 Ce1 115.622(7) 25_465 . ?
Ga1 Ga1 Ce1 64.375(7) 25 . ?
Ce1 Ga1 Ce1 128.752(14) 25_455 . ?
Ce1 Ga1 Ce1 128.752(14) 25 . ?
Ga4 Ga1 Ce1 64.39(4) 25 1_565 ?
Ga4 Ga1 Ce1 64.39(4) 25_455 1_565 ?
Ga4 Ga1 Ce1 85.41(5) 1_565 1_565 ?
Ga4 Ga1 Ce1 160.82(5) . 1_565 ?
Ga1 Ga1 Ce1 64.375(7) 25_565 1_565 ?
Ga1 Ga1 Ce1 115.622(7) 25_455 1_565 ?
Ga1 Ga1 Ce1 64.375(7) 25_465 1_565 ?
Ga1 Ga1 Ce1 115.622(7) 25 1_565 ?
Ce1 Ga1 Ce1 128.752(14) 25_455 1_565 ?
Ce1 Ga1 Ce1 128.752(14) 25 1_565 ?
Ce1 Ga1 Ce1 75.41(2) . 1_565 ?
Ga3 Ga4 Ga1 123.12(5) . . ?
Ga3 Ga4 Ga1 123.12(5) . 25 ?
Ga1 Ga4 Ga1 72.63(4) . 25 ?
Ga3 Ga4 Ga1 123.12(5) . 25_455 ?
Ga1 Ga4 Ga1 72.63(5) . 25_455 ?
Ga1 Ga4 Ga1 113.76(9) 25 25_455 ?
Ga3 Ga4 Ga1 123.12(5) . 1_545 ?
Ga1 Ga4 Ga1 113.77(9) . 1_545 ?
Ga1 Ga4 Ga1 72.63(5) 25 1_545 ?
Ga1 Ga4 Ga1 72.63(5) 25_455 1_545 ?
Ga3 Ga4 Ce1 65.61(4) . 25_445 ?
Ga1 Ga4 Ce1 139.908(17) . 25_445 ?
Ga1 Ga4 Ce1 139.908(17) 25 25_445 ?
Ga1 Ga4 Ce1 71.716(15) 25_455 25_445 ?

Ga1 Ga4 Ce1 71.716(15) 1_545 25_445 ?
Ga3 Ga4 Ce1 65.61(4) . 25 ?
Ga1 Ga4 Ce1 71.714(15) . 25 ?
Ga1 Ga4 Ce1 71.716(15) 25 25 ?
Ga1 Ga4 Ce1 139.908(17) 25_455 25 ?
Ga1 Ga4 Ce1 139.908(17) 1_545 25 ?
Ce1 Ga4 Ce1 131.22(8) 25_445 25 ?
Ga3 Ga4 Ce1 65.61(4) . 25_455 ?
Ga1 Ga4 Ce1 71.714(15) . 25_455 ?
Ga1 Ga4 Ce1 139.908(17) 25 25_455 ?
Ga1 Ga4 Ce1 71.716(15) 25_455 25_455 ?
Ga1 Ga4 Ce1 139.908(17) 1_545 25_455 ?
Ce1 Ga4 Ce1 80.18(3) 25_445 25_455 ?
Ce1 Ga4 Ce1 80.18(3) 25 25_455 ?
Ga3 Ga4 Ce1 65.61(4) . 25_545 ?
Ga1 Ga4 Ce1 139.908(17) . 25_545 ?
Ga1 Ga4 Ce1 71.716(15) 25 25_545 ?
Ga1 Ga4 Ce1 139.908(17) 25_455 25_545 ?
Ga1 Ga4 Ce1 71.716(15) 1_545 25_545 ?
Ce1 Ga4 Ce1 80.18(3) 25_445 25_545 ?
Ce1 Ga4 Ce1 80.18(3) 25 25_545 ?
Ce1 Ga4 Ce1 131.22(8) 25_455 25_545 ?
Ni2 Ga2 Ni2 117.00(5) . 1_655 ?
Ni2 Ga2 Ga3 107.58(2) . 25_545 ?
Ni2 Ga2 Ga3 107.58(2) 1_655 25_545 ?
Ni2 Ga2 Ga3 107.58(2) . 25 ?
Ni2 Ga2 Ga3 107.58(2) 1_655 25 ?
Ga3 Ga2 Ga3 109.37(10) 25_545 25 ?
Ni2 Ga2 Ga2 58.50(3) . 17_656 ?
Ni2 Ga2 Ga2 58.50(3) 1_655 17_656 ?
Ga3 Ga2 Ga2 125.31(5) 25_545 17_656 ?
Ga3 Ga2 Ga2 125.31(5) 25 17_656 ?
Ni2 Ga2 Ga2 127.078(12) . 21_655 ?
Ni2 Ga2 Ga2 52.921(12) 1_655 21_655 ?
Ga3 Ga2 Ga2 125.24(2) 25_545 21_655 ?
Ga3 Ga2 Ga2 54.76(2) 25 21_655 ?
Ga2 Ga2 Ga2 90.0 17_656 21_655 ?
Ni2 Ga2 Ga2 52.921(12) . 21_545 ?
Ni2 Ga2 Ga2 127.077(12) 1_655 21_545 ?
Ga3 Ga2 Ga2 54.76(2) 25_545 21_545 ?
Ga3 Ga2 Ga2 125.24(2) 25 21_545 ?
Ga2 Ga2 Ga2 90.0 17_656 21_545 ?
Ga2 Ga2 Ga2 180.0 21_655 21_545 ?
Ni2 Ga2 Ga2 52.921(12) . 21 ?
Ni2 Ga2 Ga2 127.077(12) 1_655 21 ?
Ga3 Ga2 Ga2 125.24(2) 25_545 21 ?
Ga3 Ga2 Ga2 54.76(2) 25 21 ?
Ga2 Ga2 Ga2 90.0 17_656 21 ?
Ga2 Ga2 Ga2 90.0 21_655 21 ?
Ga2 Ga2 Ga2 90.0 21_545 21 ?
Ni2 Ga2 Ga2 127.078(12) . 21_645 ?
Ni2 Ga2 Ga2 52.921(12) 1_655 21_645 ?
Ga3 Ga2 Ga2 54.76(2) 25_545 21_645 ?
Ga3 Ga2 Ga2 125.24(2) 25 21_645 ?
Ga2 Ga2 Ga2 90.0 17_656 21_645 ?
Ga2 Ga2 Ga2 90.0 21_655 21_645 ?

Ga2 Ga2 Ga2 90.0 21_545 21_645 ?
Ga2 Ga2 Ga2 180.0 21 21_645 ?
Ni2 Ga2 Ce1 161.17(4) . 1_655 ?
Ni2 Ga2 Ce1 81.832(19) 1_655 1_655 ?
Ga3 Ga2 Ce1 63.58(4) 25_545 1_655 ?
Ga3 Ga2 Ce1 63.58(4) 25 1_655 ?
Ga2 Ga2 Ce1 140.331(19) 17_656 1_655 ?
Ga2 Ga2 Ce1 63.169(11) 21_655 1_655 ?
Ga2 Ga2 Ce1 116.833(11) 21_545 1_655 ?
Ga2 Ga2 Ce1 116.833(11) 21 1_655 ?
Ga2 Ga2 Ce1 63.169(11) 21_645 1_655 ?
Ni2 Ga2 Ce1 81.832(19) . . ?
Ni2 Ga2 Ce1 161.17(4) 1_655 . ?
Ga3 Ga2 Ce1 63.58(4) 25_545 . ?
Ga3 Ga2 Ce1 63.58(4) 25 . ?
Ga2 Ga2 Ce1 140.332(19) 17_656 . ?
Ga2 Ga2 Ce1 116.833(11) 21_655 . ?
Ga2 Ga2 Ce1 63.169(11) 21_545 . ?
Ga2 Ga2 Ce1 63.169(11) 21 . ?
Ga2 Ga2 Ce1 116.833(11) 21_645 . ?
Ce1 Ga2 Ce1 79.34(4) 1_655 . ?

_diffrn_measured_fraction_theta_max 0.941
_diffrn_reflns_theta_full 29.70
_diffrn_measured_fraction_theta_full 0.941
_refine_diff_density_max 2.591
_refine_diff_density_min -2.564
_refine_diff_density_rms 0.558

D.2. CIF for Pr_2NiGa_{10}

X-ray Filename: Jasmine18
data_Pr_2NiGa_{10}

_audit_creation_method SHELXL-97
_chemical_name_systematic
;
?
;
_chemical_name_common ?
_chemical_melting_point ?
_chemical_formula_moiety ?
_chemical_formula_sum
'Ga20 Ni Pr'
_chemical_formula_weight 1594.02

loop_
_atom_type_symbol
_atom_type_description
_atom_type_scat_dispersion_real
_atom_type_scat_dispersion_imag
_atom_type_scat_source
'Pr' 'Pr' -0.2180 2.8214
'International Tables Vol C Tables 4.2.6.8 and 6.1.1.4'
'Ni' 'Ni' 0.3393 1.1124

'International Tables Vol C Tables 4.2.6.8 and 6.1.1.4'
'Ga' 'Ga' 0.2307 1.6083
'International Tables Vol C Tables 4.2.6.8 and 6.1.1.4'

_symmetry_cell_setting Tetragonal
_symmetry_space_group_name_H-M *I*4/*mmm*

loop_
_symmetry_equiv_pos_as_xyz
'x, y, z'
'-x, -y, z'
'x, -y, -z'
'-x, y, -z'
'-y, -x, -z'
'y, x, -z'
'y, -x, z'
'-y, x, z'
'x+1/2, y+1/2, z+1/2'
'-x+1/2, -y+1/2, z+1/2'
'x+1/2, -y+1/2, -z+1/2'
'-x+1/2, y+1/2, -z+1/2'
'-y+1/2, -x+1/2, -z+1/2'
'y+1/2, x+1/2, -z+1/2'
'y+1/2, -x+1/2, z+1/2'
'-y+1/2, x+1/2, z+1/2'
'-x, -y, -z'
'x, y, -z'
'-x, y, z'
'x, -y, z'
'y, x, z'
'-y, -x, z'
'-y, x, -z'
'y, -x, -z'
'-x+1/2, -y+1/2, -z+1/2'
'x+1/2, y+1/2, -z+1/2'
'-x+1/2, y+1/2, z+1/2'
'x+1/2, -y+1/2, z+1/2'
'y+1/2, x+1/2, z+1/2'
'-y+1/2, -x+1/2, z+1/2'
'-y+1/2, x+1/2, -z+1/2'
'y+1/2, -x+1/2, -z+1/2'

_cell_length_a 4.2330(4)
_cell_length_b 4.2330(4)
_cell_length_c 26.364(3)
_cell_angle_alpha 90.00
_cell_angle_beta 90.00
_cell_angle_gamma 90.00
_cell_volume 472.40(8)
_cell_formula_units_Z 2
_cell_measurement_temperature 293(2)
_cell_measurement_reflns_used ?
_cell_measurement_theta_min ?
_cell_measurement_theta_max ?

_exptl_crystal_description ?

```
_exptl_crystal_colour            ?
_exptl_crystal_size_max          ?
_exptl_crystal_size_mid          ?
_exptl_crystal_size_min          ?
_exptl_crystal_density_meas      ?
_exptl_crystal_density_diffrn    11.206
_exptl_crystal_density_method    'not measured'
_exptl_crystal_F_000             1414
_exptl_absorpt_coefficient_mu    62.858
_exptl_absorpt_correction_type   ?
_exptl_absorpt_correction_T_min  ?
_exptl_absorpt_correction_T_max  ?
_exptl_absorpt_process_details   ?

_exptl_special_details
;
 ?
;

_diffrn_ambient_temperature      293(2)
_diffrn_radiation_wavelength     0.71073
_diffrn_radiation_type           MoK\a
_diffrn_radiation_source         'fine-focus sealed tube'
_diffrn_radiation_monochromator  graphite
_diffrn_measurement_device_type  ?
_diffrn_measurement_method       ?
_diffrn_detector_area_resol_mean ?
_diffrn_standards_number         ?
_diffrn_standards_interval_count ?
_diffrn_standards_interval_time  ?
_diffrn_standards_decay_%        ?
_diffrn_reflns_number            573
_diffrn_reflns_av_R_equivalents  0.0385
_diffrn_reflns_av_sigmaI/netI    0.0444
_diffrn_reflns_limit_h_min       -5
_diffrn_reflns_limit_h_max       5
_diffrn_reflns_limit_k_min       -4
_diffrn_reflns_limit_k_max       4
_diffrn_reflns_limit_l_min       -25
_diffrn_reflns_limit_l_max       36
_diffrn_reflns_theta_min         3.09
_diffrn_reflns_theta_max         29.98
_reflns_number_total             254
_reflns_number_gt                244
_reflns_threshold_expression     >2sigma(I)

_computing_data_collection       ?
_computing_cell_refinement       ?
_computing_data_reduction        ?
_computing_structure_solution    'SHELXS-97 (Sheldrick, 1990)'
_computing_structure_refinement  'SHELXL-97 (Sheldrick, 1997)'
_computing_molecular_graphics    ?
_computing_publication_material  ?

_refine_special_details
;
```

```
 Refinement of F^2^ against ALL reflections.  The weighted R-factor wR and
 goodness of fit S are based on F^2^, conventional R-factors R are based
 on F, with F set to zero for negative F^2^. The threshold expression of
 F^2^ > 2sigma(F^2^) is used only for calculating R-factors(gt) etc. and is
 not relevant to the choice of reflections for refinement.  R-factors based
 on F^2^ are statistically about twice as large as those based on F, and R-
 factors based on ALL data will be even larger.
;

_refine_ls_structure_factor_coef  Fsqd
_refine_ls_matrix_type           full
_refine_ls_weighting_scheme       calc
_refine_ls_weighting_details
 'calc w=1/[\s^2^(Fo^2^)+(0.0596P)^2^+79.6220P] where P=(Fo^2^+2Fc^2^)/3'
_atom_sites_solution_primary      direct
_atom_sites_solution_secondary    difmap
_atom_sites_solution_hydrogens    geom
_refine_ls_hydrogen_treatment     mixed
_refine_ls_extinction_method      SHELXL
_refine_ls_extinction_coef        0.0015(8)
_refine_ls_extinction_expression
 'Fc^*^=kFc[1+0.001xFc^2^\l^3^/sin(2\q)]^-1/4^'
_refine_ls_number_reflns          254
_refine_ls_number_parameters      19
_refine_ls_number_restraints      0
_refine_ls_R_factor_all           0.0605
_refine_ls_R_factor_gt            0.0585
_refine_ls_wR_factor_ref          0.1577
_refine_ls_wR_factor_gt           0.1556
_refine_ls_goodness_of_fit_ref    1.242
_refine_ls_restrained_S_all       1.242
_refine_ls_shift/su_max           0.000
_refine_ls_shift/su_mean          0.000

loop_
 _atom_site_label
 _atom_site_type_symbol
 _atom_site_fract_x
 _atom_site_fract_y
 _atom_site_fract_z
 _atom_site_U_iso_or_equiv
 _atom_site_adp_type
 _atom_site_occupancy
 _atom_site_symmetry_multiplicity
 _atom_site_calc_flag
 _atom_site_refinement_flags
 _atom_site_disorder_assembly
 _atom_site_disorder_group
Pr1 Pr 0.0000 0.0000 0.35410(6) 0.0060(6) Uani 1 8 d S . .
Ga1 Ga 0.0000 0.5000 0.2500 0.0231(10) Uani 1 8 d S . .
Ga2 Ga 0.5000 0.0000 0.45090(8) 0.0065(7) Uani 1 4 d S . .
Ni1 Ni 0.0000 0.0000 0.5000 0.0054(11) Uani 1 16 d S . .
Ga4 Ga 0.0000 0.0000 0.19748(16) 0.0191(10) Uani 1 8 d S . .
Ga3 Ga 0.0000 0.0000 0.10627(14) 0.0088(8) Uani 1 8 d S . .

loop_
```

```
 _atom_site_aniso_label
 _atom_site_aniso_U_11
 _atom_site_aniso_U_22
 _atom_site_aniso_U_33
 _atom_site_aniso_U_23
 _atom_site_aniso_U_13
 _atom_site_aniso_U_12
Pr1 0.0037(7) 0.0037(7) 0.0106(9) 0.000 0.000 0.000
Ga1 0.0259(15) 0.0259(15) 0.0173(18) 0.000 0.000 0.000
Ga2 0.0049(11) 0.0089(12) 0.0058(10) 0.000 0.000 0.000
Ni1 0.0019(14) 0.0019(14) 0.013(2) 0.000 0.000 0.000
Ga4 0.0219(14) 0.0219(14) 0.0135(17) 0.000 0.000 0.000
Ga3 0.0064(10) 0.0064(10) 0.0138(17) 0.000 0.000 0.000

_geom_special_details
;
 All esds (except the esd in the dihedral angle between two l.s. planes)
 are estimated using the full covariance matrix.  The cell esds are taken
 into account individually in the estimation of esds in distances, angles
 and torsion angles; correlations between esds in cell parameters are only
 used when they are defined by crystal symmetry.  An approximate (isotropic)
 treatment of cell esds is used for estimating esds involving l.s. planes.
;

loop_
 _geom_bond_atom_site_label_1
 _geom_bond_atom_site_label_2
 _geom_bond_distance
 _geom_bond_site_symmetry_2
 _geom_bond_publ_flag
Pr1 Ga3 3.1703(14) 25 ?
Pr1 Ga3 3.1703(14) 25_445 ?
Pr1 Ga3 3.1703(14) 25_455 ?
Pr1 Ga3 3.1703(14) 25_545 ?
Pr1 Ga4 3.2875(18) 25_445 ?
Pr1 Ga4 3.2875(18) 25 ?
Pr1 Ga4 3.2875(18) 25_455 ?
Pr1 Ga4 3.2875(18) 25_545 ?
Pr1 Ga2 3.316(2) 21 ?
Pr1 Ga2 3.316(2) 1_455 ?
Pr1 Ga2 3.316(2) 21_545 ?
Pr1 Ga2 3.316(2) . ?
Ga1 Ga4 2.529(2) . ?
Ga1 Ga4 2.529(2) 25 ?
Ga1 Ga4 2.529(2) 25_455 ?
Ga1 Ga4 2.529(2) 1_565 ?
Ga1 Ga1 2.9932(3) 25_565 ?
Ga1 Ga1 2.9932(3) 25_455 ?
Ga1 Ga1 2.9932(3) 25_465 ?
Ga1 Ga1 2.9932(3) 25 ?
Ga1 Pr1 3.4658(13) 1_565 ?
Ga1 Pr1 3.4658(13) 25_455 ?
Ga1 Pr1 3.4658(13) 25 ?
Ga2 Ni1 2.4810(11) . ?
Ga2 Ni1 2.4810(11) 1_655 ?
Ga2 Ga2 2.589(4) 17_656 ?
```

Ga2 Ga3 2.598(2) 25_545 ?
Ga2 Ga3 2.598(2) 25 ?
Ga2 Ga2 2.9932(3) 21_545 ?
Ga2 Ga2 2.9932(3) 21_655 ?
Ga2 Ga2 2.9932(3) 21_645 ?
Ga2 Ga2 2.9932(3) 21 ?
Ga2 Pr1 3.316(2) 1_655 ?
Ni1 Ga2 2.4809(11) 5_566 ?
Ni1 Ga2 2.4809(11) 17_656 ?
Ni1 Ga2 2.4809(11) 5_556 ?
Ni1 Ga2 2.4809(11) 17_556 ?
Ni1 Ga2 2.4810(11) 21_545 ?
Ni1 Ga2 2.4810(11) 1_455 ?
Ni1 Ga2 2.4810(11) 21 ?
Ga4 Ga3 2.405(6) . ?
Ga4 Ga1 2.529(2) 25 ?
Ga4 Ga1 2.529(2) 25_455 ?
Ga4 Ga1 2.529(2) 1_545 ?
Ga4 Pr1 3.2876(18) 25_445 ?
Ga4 Pr1 3.2876(18) 25 ?
Ga4 Pr1 3.2876(18) 25_455 ?
Ga4 Pr1 3.2876(18) 25_545 ?
Ga3 Ga2 2.598(2) 13_455 ?
Ga3 Ga2 2.598(2) 25_545 ?
Ga3 Ga2 2.598(2) 13 ?
Ga3 Ga2 2.598(2) 25 ?
Ga3 Pr1 3.1703(14) 25 ?
Ga3 Pr1 3.1703(14) 25_445 ?
Ga3 Pr1 3.1703(14) 25_455 ?
Ga3 Pr1 3.1703(14) 25_545 ?

loop_
 _geom_angle_atom_site_label_1
 _geom_angle_atom_site_label_2
 _geom_angle_atom_site_label_3
 _geom_angle
 _geom_angle_site_symmetry_1
 _geom_angle_site_symmetry_3
 _geom_angle_publ_flag
Ga3 Pr1 Ga3 141.52(14) 25 25_445 ?
Ga3 Pr1 Ga3 83.77(4) 25 25_455 ?
Ga3 Pr1 Ga3 83.77(4) 25_445 25_455 ?
Ga3 Pr1 Ga3 83.77(4) 25 25_545 ?
Ga3 Pr1 Ga3 83.77(4) 25_445 25_545 ?
Ga3 Pr1 Ga3 141.52(14) 25_455 25_545 ?
Ga3 Pr1 Ga4 174.81(10) 25 25_445 ?
Ga3 Pr1 Ga4 43.67(9) 25_445 25_445 ?
Ga3 Pr1 Ga4 97.83(3) 25_455 25_445 ?
Ga3 Pr1 Ga4 97.83(3) 25_545 25_445 ?
Ga3 Pr1 Ga4 43.67(9) 25 25 ?
Ga3 Pr1 Ga4 174.81(10) 25_445 25 ?
Ga3 Pr1 Ga4 97.83(3) 25_455 25 ?
Ga3 Pr1 Ga4 97.83(3) 25_545 25 ?
Ga4 Pr1 Ga4 131.14(14) 25_445 25 ?
Ga3 Pr1 Ga4 97.83(3) 25 25_455 ?
Ga3 Pr1 Ga4 97.83(3) 25_445 25_455 ?

Ga3 Pr1 Ga4 43.67(9) 25_455 25_455 ?
Ga3 Pr1 Ga4 174.81(10) 25_545 25_455 ?
Ga4 Pr1 Ga4 80.15(5) 25_445 25_455 ?
Ga4 Pr1 Ga4 80.15(5) 25 25_455 ?
Ga3 Pr1 Ga4 97.83(3) 25 25_545 ?
Ga3 Pr1 Ga4 97.83(3) 25_445 25_545 ?
Ga3 Pr1 Ga4 174.81(10) 25_455 25_545 ?
Ga3 Pr1 Ga4 43.67(9) 25_545 25_545 ?
Ga4 Pr1 Ga4 80.15(5) 25_445 25_545 ?
Ga4 Pr1 Ga4 80.15(5) 25 25_545 ?
Ga4 Pr1 Ga4 131.14(14) 25_455 25_545 ?
Ga3 Pr1 Ga2 47.17(5) 25 21 ?
Ga3 Pr1 Ga2 99.93(7) 25_445 21 ?
Ga3 Pr1 Ga2 47.17(5) 25_455 21 ?
Ga3 Pr1 Ga2 99.93(7) 25_545 21 ?
Ga4 Pr1 Ga2 136.83(6) 25_445 21 ?
Ga4 Pr1 Ga2 84.69(6) 25 21 ?
Ga4 Pr1 Ga2 84.69(6) 25_455 21 ?
Ga4 Pr1 Ga2 136.83(6) 25_545 21 ?
Ga3 Pr1 Ga2 99.93(7) 25 1_455 ?
Ga3 Pr1 Ga2 47.17(5) 25_445 1_455 ?
Ga3 Pr1 Ga2 47.17(5) 25_455 1_455 ?
Ga3 Pr1 Ga2 99.93(7) 25_545 1_455 ?
Ga4 Pr1 Ga2 84.69(6) 25_445 1_455 ?
Ga4 Pr1 Ga2 136.83(6) 25 1_455 ?
Ga4 Pr1 Ga2 84.69(6) 25_455 1_455 ?
Ga4 Pr1 Ga2 136.83(6) 25_545 1_455 ?
Ga2 Pr1 Ga2 53.66(4) 21 1_455 ?
Ga3 Pr1 Ga2 99.93(7) 25 21_545 ?
Ga3 Pr1 Ga2 47.17(5) 25_445 21_545 ?
Ga3 Pr1 Ga2 99.93(7) 25_455 21_545 ?
Ga3 Pr1 Ga2 47.17(5) 25_545 21_545 ?
Ga4 Pr1 Ga2 84.69(6) 25_445 21_545 ?
Ga4 Pr1 Ga2 136.83(6) 25 21_545 ?
Ga4 Pr1 Ga2 136.83(6) 25_455 21_545 ?
Ga4 Pr1 Ga2 84.69(6) 25_545 21_545 ?
Ga2 Pr1 Ga2 79.34(6) 21 21_545 ?
Ga2 Pr1 Ga2 53.66(4) 1_455 21_545 ?
Ga3 Pr1 Ga2 47.17(5) 25 . ?
Ga3 Pr1 Ga2 99.93(7) 25_445 . ?
Ga3 Pr1 Ga2 99.93(7) 25_455 . ?
Ga3 Pr1 Ga2 47.17(5) 25_545 . ?
Ga4 Pr1 Ga2 136.83(6) 25_445 . ?
Ga4 Pr1 Ga2 84.69(6) 25 . ?
Ga4 Pr1 Ga2 136.83(6) 25_455 . ?
Ga4 Pr1 Ga2 84.69(6) 25_545 . ?
Ga2 Pr1 Ga2 53.66(4) 21 . ?
Ga2 Pr1 Ga2 79.34(6) 1_455 . ?
Ga2 Pr1 Ga2 53.66(4) 21_545 . ?
Ga4 Ga1 Ga4 107.44(8) . 25 ?
Ga4 Ga1 Ga4 107.44(8) . 25_455 ?
Ga4 Ga1 Ga4 113.61(16) 25 25_455 ?
Ga4 Ga1 Ga4 113.61(16) . 1_565 ?
Ga4 Ga1 Ga4 107.44(8) 25 1_565 ?
Ga4 Ga1 Ga4 107.44(8) 25_455 1_565 ?
Ga4 Ga1 Ga1 126.28(4) . 25_565 ?

Ga4 Ga1 Ga1 53.72(4) 25 25_565 ?
Ga4 Ga1 Ga1 126.28(4) 25_455 25_565 ?
Ga4 Ga1 Ga1 53.72(4) 1_565 25_565 ?
Ga4 Ga1 Ga1 53.72(4) . 25_455 ?
Ga4 Ga1 Ga1 126.28(4) 25 25_455 ?
Ga4 Ga1 Ga1 53.72(4) 25_455 25_455 ?
Ga4 Ga1 Ga1 126.28(4) 1_565 25_455 ?
Ga1 Ga1 Ga1 180.0 25_565 25_455 ?
Ga4 Ga1 Ga1 126.28(4) . 25_465 ?
Ga4 Ga1 Ga1 126.28(4) 25 25_465 ?
Ga4 Ga1 Ga1 53.72(4) 25_455 25_465 ?
Ga4 Ga1 Ga1 53.72(4) 1_565 25_465 ?
Ga1 Ga1 Ga1 90.0 25_565 25_465 ?
Ga1 Ga1 Ga1 90.0 25_455 25_465 ?
Ga4 Ga1 Ga1 53.72(4) . 25 ?
Ga4 Ga1 Ga1 53.72(4) 25 25 ?
Ga4 Ga1 Ga1 126.28(4) 25_455 25 ?
Ga4 Ga1 Ga1 126.28(4) 1_565 25 ?
Ga1 Ga1 Ga1 90.0 25_565 25 ?
Ga1 Ga1 Ga1 90.0 25_455 25 ?
Ga1 Ga1 Ga1 180.0 25_465 25 ?
Ga4 Ga1 Pr1 85.56(8) . . ?
Ga4 Ga1 Pr1 64.31(6) 25 . ?
Ga4 Ga1 Pr1 64.31(6) 25_455 . ?
Ga4 Ga1 Pr1 160.84(8) 1_565 . ?
Ga1 Ga1 Pr1 115.582(10) 25_565 . ?
Ga1 Ga1 Pr1 64.415(11) 25_455 . ?
Ga1 Ga1 Pr1 115.582(11) 25_465 . ?
Ga1 Ga1 Pr1 64.415(11) 25 . ?
Ga4 Ga1 Pr1 160.83(8) . 1_565 ?
Ga4 Ga1 Pr1 64.31(6) 25 1_565 ?
Ga4 Ga1 Pr1 64.31(6) 25_455 1_565 ?
Ga4 Ga1 Pr1 85.56(8) 1_565 1_565 ?
Ga1 Ga1 Pr1 64.415(11) 25_565 1_565 ?
Ga1 Ga1 Pr1 115.582(11) 25_455 1_565 ?
Ga1 Ga1 Pr1 64.415(11) 25_465 1_565 ?
Ga1 Ga1 Pr1 115.582(10) 25 1_565 ?
Pr1 Ga1 Pr1 75.28(3) . 1_565 ?
Ga4 Ga1 Pr1 64.31(6) . 25_455 ?
Ga4 Ga1 Pr1 160.83(8) 25 25_455 ?
Ga4 Ga1 Pr1 85.56(8) 25_455 25_455 ?
Ga4 Ga1 Pr1 64.31(6) 1_565 25_455 ?
Ga1 Ga1 Pr1 115.584(10) 25_565 25_455 ?
Ga1 Ga1 Pr1 64.419(11) 25_455 25_455 ?
Ga1 Ga1 Pr1 64.419(10) 25_465 25_455 ?
Ga1 Ga1 Pr1 115.584(11) 25 25_455 ?
Pr1 Ga1 Pr1 128.83(2) . 25_455 ?
Pr1 Ga1 Pr1 128.83(2) 1_565 25_455 ?
Ga4 Ga1 Pr1 64.31(6) . 25 ?
Ga4 Ga1 Pr1 85.56(8) 25 25 ?
Ga4 Ga1 Pr1 160.83(8) 25_455 25 ?
Ga4 Ga1 Pr1 64.31(6) 1_565 25 ?
Ga1 Ga1 Pr1 64.419(11) 25_565 25 ?
Ga1 Ga1 Pr1 115.584(11) 25_455 25 ?
Ga1 Ga1 Pr1 115.584(10) 25_465 25 ?
Ga1 Ga1 Pr1 64.419(11) 25 25 ?

Pr1 Ga1 Pr1 128.83(2) . 25 ?
Pr1 Ga1 Pr1 128.83(2) 1_565 25 ?
Pr1 Ga1 Pr1 75.28(3) 25_455 25 ?
Ni1 Ga2 Ni1 117.10(8) . 1_655 ?
Ni1 Ga2 Ga2 58.55(4) . 17_656 ?
Ni1 Ga2 Ga2 58.55(4) 1_655 17_656 ?
Ni1 Ga2 Ga3 107.62(3) . 25_545 ?
Ni1 Ga2 Ga3 107.62(3) 1_655 25_545 ?
Ga2 Ga2 Ga3 125.46(7) 17_656 25_545 ?
Ni1 Ga2 Ga3 107.62(3) . 25 ?
Ni1 Ga2 Ga3 107.62(3) 1_655 25 ?
Ga2 Ga2 Ga3 125.46(7) 17_656 25 ?
Ga3 Ga2 Ga3 109.08(15) 25_545 25 ?
Ni1 Ga2 Ga2 52.898(19) . 21_545 ?
Ni1 Ga2 Ga2 127.101(19) 1_655 21_545 ?
Ga2 Ga2 Ga2 90.0 17_656 21_545 ?
Ga3 Ga2 Ga2 54.83(4) 25_545 21_545 ?
Ga3 Ga2 Ga2 125.17(4) 25 21_545 ?
Ni1 Ga2 Ga2 127.102(19) . 21_655 ?
Ni1 Ga2 Ga2 52.899(19) 1_655 21_655 ?
Ga2 Ga2 Ga2 90.0 17_656 21_655 ?
Ga3 Ga2 Ga2 125.17(4) 25_545 21_655 ?
Ga3 Ga2 Ga2 54.83(4) 25 21_655 ?
Ga2 Ga2 Ga2 180.0 21_545 21_655 ?
Ni1 Ga2 Ga2 127.102(19) . 21_645 ?
Ni1 Ga2 Ga2 52.899(19) 1_655 21_645 ?
Ga2 Ga2 Ga2 90.0 17_656 21_645 ?
Ga3 Ga2 Ga2 54.83(4) 25_545 21_645 ?
Ga3 Ga2 Ga2 125.17(4) 25 21_645 ?
Ga2 Ga2 Ga2 90.0 21_545 21_645 ?
Ga2 Ga2 Ga2 90.0 21_655 21_645 ?
Ni1 Ga2 Ga2 52.898(19) . 21 ?
Ni1 Ga2 Ga2 127.101(19) 1_655 21 ?
Ga2 Ga2 Ga2 90.0 17_656 21 ?
Ga3 Ga2 Ga2 125.17(4) 25_545 21 ?
Ga3 Ga2 Ga2 54.83(4) 25 21 ?
Ga2 Ga2 Ga2 90.0 21_545 21 ?
Ga2 Ga2 Ga2 90.0 21_655 21 ?
Ga2 Ga2 Ga2 180.0 21_645 21 ?
Ni1 Ga2 Pr1 161.12(7) . 1_655 ?
Ni1 Ga2 Pr1 81.78(3) 1_655 1_655 ?
Ga2 Ga2 Pr1 140.33(3) 17_656 1_655 ?
Ga3 Ga2 Pr1 63.48(6) 25_545 1_655 ?
Ga3 Ga2 Pr1 63.48(6) 25 1_655 ?
Ga2 Ga2 Pr1 116.832(18) 21_545 1_655 ?
Ga2 Ga2 Pr1 63.167(18) 21_655 1_655 ?
Ga2 Ga2 Pr1 63.167(18) 21_645 1_655 ?
Ga2 Ga2 Pr1 116.833(18) 21 1_655 ?
Ni1 Ga2 Pr1 81.78(3) . . ?
Ni1 Ga2 Pr1 161.12(7) 1_655 . ?
Ga2 Ga2 Pr1 140.33(3) 17_656 . ?
Ga3 Ga2 Pr1 63.48(6) 25_545 . ?
Ga3 Ga2 Pr1 63.48(6) 25 . ?
Ga2 Ga2 Pr1 63.167(18) 21_545 . ?
Ga2 Ga2 Pr1 116.832(18) 21_655 . ?
Ga2 Ga2 Pr1 116.832(18) 21_645 . ?

Ga2 Ga2 Pr1 63.167(18) 21 . ?
Pr1 Ga2 Pr1 79.34(6) 1_655 . ?
Ga2 Ni1 Ga2 74.20(4) 5_566 17_656 ?
Ga2 Ni1 Ga2 117.10(8) 5_566 5_556 ?
Ga2 Ni1 Ga2 74.20(4) 17_656 5_556 ?
Ga2 Ni1 Ga2 74.20(4) 5_566 17_556 ?
Ga2 Ni1 Ga2 117.10(8) 17_656 17_556 ?
Ga2 Ni1 Ga2 74.20(4) 5_556 17_556 ?
Ga2 Ni1 Ga2 105.80(4) 5_566 . ?
Ga2 Ni1 Ga2 62.90(8) 17_656 . ?
Ga2 Ni1 Ga2 105.80(4) 5_556 . ?
Ga2 Ni1 Ga2 180.00(8) 17_556 . ?
Ga2 Ni1 Ga2 180.0 5_566 21_545 ?
Ga2 Ni1 Ga2 105.80(4) 17_656 21_545 ?
Ga2 Ni1 Ga2 62.90(8) 5_556 21_545 ?
Ga2 Ni1 Ga2 105.80(4) 17_556 21_545 ?
Ga2 Ni1 Ga2 74.20(4) . 21_545 ?
Ga2 Ni1 Ga2 105.80(4) 5_566 1_455 ?
Ga2 Ni1 Ga2 180.0 17_656 1_455 ?
Ga2 Ni1 Ga2 105.80(4) 5_556 1_455 ?
Ga2 Ni1 Ga2 62.90(8) 17_556 1_455 ?
Ga2 Ni1 Ga2 117.10(8) . 1_455 ?
Ga2 Ni1 Ga2 74.20(4) 21_545 1_455 ?
Ga2 Ni1 Ga2 62.90(8) 5_566 21 ?
Ga2 Ni1 Ga2 105.80(4) 17_656 21 ?
Ga2 Ni1 Ga2 180.0 5_556 21 ?
Ga2 Ni1 Ga2 105.80(4) 17_556 21 ?
Ga2 Ni1 Ga2 74.20(4) . 21 ?
Ga2 Ni1 Ga2 117.10(8) 21_545 21 ?
Ga2 Ni1 Ga2 74.20(4) 1_455 21 ?
Ga3 Ga4 Ga1 123.19(8) . . ?
Ga3 Ga4 Ga1 123.20(8) . 25 ?
Ga1 Ga4 Ga1 72.56(8) . 25 ?
Ga3 Ga4 Ga1 123.20(8) . 25_455 ?
Ga1 Ga4 Ga1 72.56(8) . 25_455 ?
Ga1 Ga4 Ga1 113.61(16) 25 25_455 ?
Ga3 Ga4 Ga1 123.20(8) . 1_545 ?
Ga1 Ga4 Ga1 113.61(16) . 1_545 ?
Ga1 Ga4 Ga1 72.56(8) 25 1_545 ?
Ga1 Ga4 Ga1 72.56(8) 25_455 1_545 ?
Ga3 Ga4 Pr1 65.57(7) . 25_445 ?
Ga1 Ga4 Pr1 139.92(3) . 25_445 ?
Ga1 Ga4 Pr1 139.92(3) 25 25_445 ?
Ga1 Ga4 Pr1 71.80(2) 25_455 25_445 ?
Ga1 Ga4 Pr1 71.80(2) 1_545 25_445 ?
Ga3 Ga4 Pr1 65.57(7) . 25 ?
Ga1 Ga4 Pr1 71.80(2) . 25 ?
Ga1 Ga4 Pr1 71.80(2) 25 25 ?
Ga1 Ga4 Pr1 139.92(3) 25_455 25 ?
Ga1 Ga4 Pr1 139.92(3) 1_545 25 ?
Pr1 Ga4 Pr1 131.14(14) 25_445 25 ?
Ga3 Ga4 Pr1 65.57(7) . 25_455 ?
Ga1 Ga4 Pr1 71.80(2) . 25_455 ?
Ga1 Ga4 Pr1 139.92(3) 25 25_455 ?
Ga1 Ga4 Pr1 71.80(2) 25_455 25_455 ?
Ga1 Ga4 Pr1 139.92(3) 1_545 25_455 ?

Pr1 Ga4 Pr1 80.15(5) 25_445 25_455 ?
Pr1 Ga4 Pr1 80.15(5) 25 25_455 ?
Ga3 Ga4 Pr1 65.57(7) . 25_545 ?
Ga1 Ga4 Pr1 139.92(3) . 25_545 ?
Ga1 Ga4 Pr1 71.80(2) 25 25_545 ?
Ga1 Ga4 Pr1 139.92(3) 25_455 25_545 ?
Ga1 Ga4 Pr1 71.80(2) 1_545 25_545 ?
Pr1 Ga4 Pr1 80.15(5) 25_445 25_545 ?
Pr1 Ga4 Pr1 80.15(5) 25 25_545 ?
Pr1 Ga4 Pr1 131.14(14) 25_455 25_545 ?
Ga4 Ga3 Ga2 125.46(7) . 13_455 ?
Ga4 Ga3 Ga2 125.46(7) . 25_545 ?
Ga2 Ga3 Ga2 70.33(7) 13_455 25_545 ?
Ga4 Ga3 Ga2 125.46(7) . 13 ?
Ga2 Ga3 Ga2 109.08(15) 13_455 13 ?
Ga2 Ga3 Ga2 70.33(7) 25_545 13 ?
Ga4 Ga3 Ga2 125.46(7) . 25 ?
Ga2 Ga3 Ga2 70.33(7) 13_455 25 ?
Ga2 Ga3 Ga2 109.08(15) 25_545 25 ?
Ga2 Ga3 Ga2 70.33(7) 13 25 ?
Ga4 Ga3 Pr1 70.76(7) . 25 ?
Ga2 Ga3 Pr1 137.30(5) 13_455 25 ?
Ga2 Ga3 Pr1 137.30(5) 25_545 25 ?
Ga2 Ga3 Pr1 69.35(3) 13 25 ?
Ga2 Ga3 Pr1 69.35(4) 25 25 ?
Ga4 Ga3 Pr1 70.76(7) . 25_445 ?
Ga2 Ga3 Pr1 69.35(4) 13_455 25_445 ?
Ga2 Ga3 Pr1 69.35(4) 25_545 25_445 ?
Ga2 Ga3 Pr1 137.30(5) 13 25_445 ?
Ga2 Ga3 Pr1 137.30(5) 25 25_445 ?
Pr1 Ga3 Pr1 141.52(14) 25 25_445 ?
Ga4 Ga3 Pr1 70.76(7) . 25_455 ?
Ga2 Ga3 Pr1 69.35(3) 13_455 25_455 ?
Ga2 Ga3 Pr1 137.30(5) 25_545 25_455 ?
Ga2 Ga3 Pr1 137.30(5) 13 25_455 ?
Ga2 Ga3 Pr1 69.35(4) 25 25_455 ?
Pr1 Ga3 Pr1 83.77(4) 25 25_455 ?
Pr1 Ga3 Pr1 83.77(4) 25_445 25_455 ?
Ga4 Ga3 Pr1 70.76(7) . 25_545 ?
Ga2 Ga3 Pr1 137.30(5) 13_455 25_545 ?
Ga2 Ga3 Pr1 69.35(3) 25_545 25_545 ?
Ga2 Ga3 Pr1 69.35(4) 13 25_545 ?
Ga2 Ga3 Pr1 137.30(5) 25 25_545 ?
Pr1 Ga3 Pr1 83.77(4) 25 25_545 ?
Pr1 Ga3 Pr1 83.77(4) 25_445 25_545 ?
Pr1 Ga3 Pr1 141.52(14) 25_455 25_545 ?

_diffrn_measured_fraction_theta_max 0.992
_diffrn_reflns_theta_full 29.98
_diffrn_measured_fraction_theta_full 0.992
_refine_diff_density_max 8.914
_refine_diff_density_min -2.657
_refine_diff_density_rms 0.706

D.3. Ce_2NiGa_{12}

X-ray Filename: Jasmine28

```
data_Ce2NiGa12
_audit_creation_method           SHELXL-97
_chemical_name_systematic
;
 ?
;
_chemical_name_common             ?
_chemical_melting_point           ?
_chemical_formula_moiety          ?
_chemical_formula_sum
'Ce Ga20 Ni'
_chemical_formula_weight          1593.23

loop_
 _atom_type_symbol
 _atom_type_description
 _atom_type_scat_dispersion_real
 _atom_type_scat_dispersion_imag
 _atom_type_scat_source
'Ce'  'Ce'  -0.2486   2.6331
'International Tables Vol C Tables 4.2.6.8 and 6.1.1.4'
'Ni'  'Ni'   0.3393   1.1124
'International Tables Vol C Tables 4.2.6.8 and 6.1.1.4'
'Ga'  'Ga'   0.2307   1.6083
'International Tables Vol C Tables 4.2.6.8 and 6.1.1.4'

_symmetry_cell_setting            Tetragonal
_symmetry_space_group_name_H-M    P4/nbm

loop_
 _symmetry_equiv_pos_as_xyz
'x, y, z'
'-x+1/2, -y+1/2, z'
'x, -y+1/2, -z'
'-x+1/2, y, -z'
'-y+1/2, -x+1/2, -z'
'y, x, -z'
'y, -x+1/2, z'
'-y+1/2, x, z'
'-x, -y, -z'
'x-1/2, y-1/2, -z'
'-x, y-1/2, z'
'x-1/2, -y, z'
'y-1/2, x-1/2, z'
'-y, -x, z'
'-y, x-1/2, -z'
'y-1/2, -x, -z'

_cell_length_a                    6.0360(3)
_cell_length_b                    6.0360(3)
_cell_length_c                    15.5060(15)
```

```
_cell_angle_alpha                90.00
_cell_angle_beta                 90.00
_cell_angle_gamma                90.00
_cell_volume                     564.93(7)
_cell_formula_units_Z            2
_cell_measurement_temperature    293(2)
_cell_measurement_reflns_used    ?
_cell_measurement_theta_min      ?
_cell_measurement_theta_max      ?

_exptl_crystal_description       ?
_exptl_crystal_colour            ?
_exptl_crystal_size_max          ?
_exptl_crystal_size_mid          ?
_exptl_crystal_size_min          ?
_exptl_crystal_density_meas      ?
_exptl_crystal_density_diffrn    9.366
_exptl_crystal_density_method    'not measured'
_exptl_crystal_F_000             1412
_exptl_absorpt_coefficient_mu    52.279
_exptl_absorpt_correction_type   ?
_exptl_absorpt_correction_T_min  ?
_exptl_absorpt_correction_T_max  ?
_exptl_absorpt_process_details   ?

_exptl_special_details
;
 ?
;

_diffrn_ambient_temperature      293(2)
_diffrn_radiation_wavelength     0.71073
_diffrn_radiation_type           MoK\a
_diffrn_radiation_source         'fine-focus sealed tube'
_diffrn_radiation_monochromator  graphite
_diffrn_measurement_device_type  ?
_diffrn_measurement_method       ?
_diffrn_detector_area_resol_mean ?
_diffrn_standards_number         ?
_diffrn_standards_interval_count ?
_diffrn_standards_interval_time  ?
_diffrn_standards_decay_%        ?
_diffrn_reflns_number            1120
_diffrn_reflns_av_R_equivalents  0.0307
_diffrn_reflns_av_sigmaI/netI    0.0419
_diffrn_reflns_limit_h_min       -8
_diffrn_reflns_limit_h_max       8
_diffrn_reflns_limit_k_min       -6
_diffrn_reflns_limit_k_max       6
_diffrn_reflns_limit_l_min       -21
_diffrn_reflns_limit_l_max       11
_diffrn_reflns_theta_min         4.78
_diffrn_reflns_theta_max         30.01
_reflns_number_total             456
_reflns_number_gt                375
_reflns_threshold_expression     >2sigma(I)
```

```
_computing_data_collection       ?
_computing_cell_refinement       ?
_computing_data_reduction        ?
_computing_structure_solution    'SHELXS-97 (Sheldrick, 1990)'
_computing_structure_refinement  'SHELXL-97 (Sheldrick, 1997)'
_computing_molecular_graphics    ?
_computing_publication_material  ?

_refine_special_details
;
 Refinement of F^2^ against ALL reflections.  The weighted R-factor wR and
 goodness of fit S are based on F^2^, conventional R-factors R are based
 on F, with F set to zero for negative F^2^. The threshold expression of
 F^2^ > 2sigma(F^2^) is used only for calculating R-factors(gt) etc. and is
 not relevant to the choice of reflections for refinement.  R-factors based
 on F^2^ are statistically about twice as large as those based on F, and R-
 factors based on ALL data will be even larger.
;

_refine_ls_structure_factor_coef  Fsqd
_refine_ls_matrix_type           full
_refine_ls_weighting_scheme      calc
_refine_ls_weighting_details
 'calc w=1/[\s^2^(Fo^2^)+(0.0283P)^2^+0.7799P] where P=(Fo^2^+2Fc^2^)/3'
_atom_sites_solution_primary     direct
_atom_sites_solution_secondary   difmap
_atom_sites_solution_hydrogens   geom
_refine_ls_hydrogen_treatment    mixed
_refine_ls_extinction_method     SHELXL
_refine_ls_extinction_coef       0.0010(2)
_refine_ls_extinction_expression
 'Fc^*^=kFc[1+0.001xFc^2^\l^3^/sin(2\q)]^-1/4^'
_refine_ls_number_reflns         456
_refine_ls_number_parameters     26
_refine_ls_number_restraints     0
_refine_ls_R_factor_all          0.0406
_refine_ls_R_factor_gt           0.0301
_refine_ls_wR_factor_ref         0.0710
_refine_ls_wR_factor_gt          0.0667
_refine_ls_goodness_of_fit_ref   1.114
_refine_ls_restrained_S_all      1.114
_refine_ls_shift/su_max          0.000
_refine_ls_shift/su_mean         0.000

loop_
 _atom_site_label
 _atom_site_type_symbol
 _atom_site_fract_x
 _atom_site_fract_y
 _atom_site_fract_z
 _atom_site_U_iso_or_equiv
 _atom_site_adp_type
 _atom_site_occupancy
 _atom_site_symmetry_multiplicity
 _atom_site_calc_flag
```

```
 _atom_site_refinement_flags
 _atom_site_disorder_assembly
 _atom_site_disorder_group
Ce1 Ce 0.7500 0.2500 0.24439(4) 0.0074(2) Uani 1 4 d S . .
Ni2 Ni 0.7500 0.2500 0.0000 0.0079(4) Uani 1 8 d S . .
Ga3 Ga 0.50023(8) 0.00023(8) -0.08340(5) 0.0093(2) Uani 1 2 d S . .
Ga1 Ga 0.7500 0.7500 0.18143(8) 0.0087(3) Uani 1 4 d S . .
Ga2 Ga 0.7500 0.7500 0.33955(9) 0.0119(3) Uani 1 4 d S . .
Ga4 Ga 0.57027(11) 0.07027(11) 0.42816(7) 0.0212(3) Uani 1 2 d S . .

loop_
 _atom_site_aniso_label
 _atom_site_aniso_U_11
 _atom_site_aniso_U_22
 _atom_site_aniso_U_33
 _atom_site_aniso_U_23
 _atom_site_aniso_U_13
 _atom_site_aniso_U_12
Ce1 0.0066(2) 0.0066(2) 0.0090(4) 0.000 0.000 -0.0005(2)
Ni2 0.0072(6) 0.0072(6) 0.0092(10) 0.000 0.000 0.000
Ga3 0.0097(3) 0.0097(3) 0.0084(5) 0.0000(2) 0.0000(2) -0.0007(3)
Ga1 0.0084(4) 0.0084(4) 0.0093(7) 0.000 0.000 0.000
Ga2 0.0124(4) 0.0124(4) 0.0108(7) 0.000 0.000 0.000
Ga4 0.0243(4) 0.0243(4) 0.0149(5) 0.0052(3) 0.0052(3) 0.0091(4)

_geom_special_details
;
 All esds (except the esd in the dihedral angle between two l.s. planes)
 are estimated using the full covariance matrix.  The cell esds are taken
 into account individually in the estimation of esds in distances, angles
 and torsion angles; correlations between esds in cell parameters are only
 used when they are defined by crystal symmetry.  An approximate (isotropic)
 treatment of cell esds is used for estimating esds involving l.s. planes.
;

loop_
 _geom_bond_atom_site_label_1
 _geom_bond_atom_site_label_2
 _geom_bond_distance
 _geom_bond_site_symmetry_2
 _geom_bond_publ_flag
Ce1 Ga1 3.1720(5) 11_655 ?
Ce1 Ga1 3.1720(5) 1_545 ?
Ce1 Ga1 3.1720(5) 11_755 ?
Ce1 Ga1 3.1720(5) . ?
Ce1 Ga4 3.2361(11) 2_655 ?
Ce1 Ga4 3.2362(11) . ?
Ce1 Ga3 3.2830(9) 3 ?
Ce1 Ga3 3.2830(9) 4_655 ?
Ce1 Ga3 3.2855(9) 9_655 ?
Ce1 Ga3 3.2855(9) 10_665 ?
Ce1 Ga2 3.3593(7) 11_655 ?
Ce1 Ga2 3.3593(7) 1_545 ?
Ni2 Ga3 2.4936(8) 4_655 ?
Ni2 Ga3 2.4936(8) 3 ?
Ni2 Ga3 2.4936(8) . ?
```

Ni2 Ga3 2.4936(8) 2_655 ?
Ni2 Ga3 2.4969(8) 9_655 ?
Ni2 Ga3 2.4970(8) 10_665 ?
Ni2 Ga3 2.4970(8) 12_655 ?
Ni2 Ga3 2.4970(8) 11_665 ?
Ga3 Ni2 2.4970(8) 9_655 ?
Ga3 Ga3 2.5863(16) 9_655 ?
Ga3 Ga1 2.6200(9) 3 ?
Ga3 Ga1 2.6200(9) 9_665 ?
Ga3 Ga3 3.01800(15) 12_655 ?
Ga3 Ga3 3.01800(15) 11_655 ?
Ga3 Ga3 3.01800(15) 11_665 ?
Ga3 Ga3 3.01800(15) 12 ?
Ga3 Ce1 3.2830(9) 3 ?
Ga3 Ce1 3.2855(9) 9_655 ?
Ga1 Ga2 2.4518(18) . ?
Ga1 Ga3 2.6201(9) 3 ?
Ga1 Ga3 2.6201(9) 10_665 ?
Ga1 Ga3 2.6201(9) 9_665 ?
Ga1 Ga3 2.6201(9) 4_665 ?
Ga1 Ce1 3.1720(5) 11_665 ?
Ga1 Ce1 3.1720(5) 11_765 ?
Ga1 Ce1 3.1720(5) 1_565 ?
Ga2 Ga4 2.6080(9) 12_665 ?
Ga2 Ga4 2.6080(9) 1_565 ?
Ga2 Ga4 2.6080(9) 2_655 ?
Ga2 Ga4 2.6080(9) 11_665 ?
Ga2 Ce1 3.3593(7) 11_665 ?
Ga2 Ce1 3.3594(7) 1_565 ?
Ga2 Ce1 3.3594(7) 11_765 ?
Ga4 Ga4 2.531(2) 9_656 ?
Ga4 Ga2 2.6080(9) 11_655 ?
Ga4 Ga2 2.6080(9) 1_545 ?

loop_
 _geom_angle_atom_site_label_1
 _geom_angle_atom_site_label_2
 _geom_angle_atom_site_label_3
 _geom_angle
 _geom_angle_site_symmetry_1
 _geom_angle_site_symmetry_3
 _geom_angle_publ_flag
Ga1 Ce1 Ga1 84.564(14) 11_655 1_545 ?
Ga1 Ce1 Ga1 144.15(5) 11_655 11_755 ?
Ga1 Ce1 Ga1 84.564(14) 1_545 11_755 ?
Ga1 Ce1 Ga1 84.563(14) 11_655 . ?
Ga1 Ce1 Ga1 144.15(5) 1_545 . ?
Ga1 Ce1 Ga1 84.563(14) 11_755 . ?
Ga1 Ce1 Ga4 126.15(3) 11_655 2_655 ?
Ga1 Ce1 Ga4 126.15(3) 1_545 2_655 ?
Ga1 Ce1 Ga4 87.25(2) 11_755 2_655 ?
Ga1 Ce1 Ga4 87.25(2) . 2_655 ?
Ga1 Ce1 Ga4 87.25(2) 11_655 . ?
Ga1 Ce1 Ga4 87.25(2) 1_545 . ?
Ga1 Ce1 Ga4 126.15(3) 11_755 . ?
Ga1 Ce1 Ga4 126.15(3) . . ?

Ga4 Ce1 Ga4 56.60(4) 2_655 . ?
Ga1 Ce1 Ga3 47.857(19) 11_655 3 ?
Ga1 Ce1 Ga3 101.71(3) 1_545 3 ?
Ga1 Ce1 Ga3 101.70(3) 11_755 3 ?
Ga1 Ce1 Ga3 47.857(19) . 3 ?
Ga4 Ce1 Ga3 132.031(14) 2_655 3 ?
Ga4 Ce1 Ga3 132.032(14) . 3 ?
Ga1 Ce1 Ga3 101.71(3) 11_655 4_655 ?
Ga1 Ce1 Ga3 47.857(19) 1_545 4_655 ?
Ga1 Ce1 Ga3 47.857(19) 11_755 4_655 ?
Ga1 Ce1 Ga3 101.70(3) . 4_655 ?
Ga4 Ce1 Ga3 132.031(14) 2_655 4_655 ?
Ga4 Ce1 Ga3 132.031(14) . 4_655 ?
Ga3 Ce1 Ga3 81.00(3) 3 4_655 ?
Ga1 Ce1 Ga3 47.836(19) 11_655 9_655 ?
Ga1 Ce1 Ga3 47.836(19) 1_545 9_655 ?
Ga1 Ce1 Ga3 101.74(3) 11_755 9_655 ?
Ga1 Ce1 Ga3 101.74(3) . 9_655 ?
Ga4 Ce1 Ga3 167.75(3) 2_655 9_655 ?
Ga4 Ce1 Ga3 111.15(2) . 9_655 ?
Ga3 Ce1 Ga3 54.705(14) 3 9_655 ?
Ga3 Ce1 Ga3 54.705(14) 4_655 9_655 ?
Ga1 Ce1 Ga3 101.74(3) 11_655 10_665 ?
Ga1 Ce1 Ga3 101.74(3) 1_545 10_665 ?
Ga1 Ce1 Ga3 47.835(19) 11_755 10_665 ?
Ga1 Ce1 Ga3 47.835(19) . 10_665 ?
Ga4 Ce1 Ga3 111.15(2) 2_655 10_665 ?
Ga4 Ce1 Ga3 167.75(3) . 10_665 ?
Ga3 Ce1 Ga3 54.705(14) 3 10_665 ?
Ga3 Ce1 Ga3 54.705(14) 4_655 10_665 ?
Ga3 Ce1 Ga3 81.10(3) 9_655 10_665 ?
Ga1 Ce1 Ga2 43.98(3) 11_655 11_655 ?
Ga1 Ce1 Ga2 97.770(11) 1_545 11_655 ?
Ga1 Ce1 Ga2 171.87(4) 11_755 11_655 ?
Ga1 Ce1 Ga2 97.769(11) . 11_655 ?
Ga4 Ce1 Ga2 85.09(3) 2_655 11_655 ?
Ga4 Ce1 Ga2 46.54(2) . 11_655 ?
Ga3 Ce1 Ga2 85.49(2) 3 11_655 ?
Ga3 Ce1 Ga2 138.292(18) 4_655 11_655 ?
Ga3 Ce1 Ga2 85.45(2) 9_655 11_655 ?
Ga3 Ce1 Ga2 138.307(18) 10_665 11_655 ?
Ga1 Ce1 Ga2 97.770(11) 11_655 1_545 ?
Ga1 Ce1 Ga2 43.98(3) 1_545 1_545 ?
Ga1 Ce1 Ga2 97.769(11) 11_755 1_545 ?
Ga1 Ce1 Ga2 171.87(4) . 1_545 ?
Ga4 Ce1 Ga2 85.09(3) 2_655 1_545 ?
Ga4 Ce1 Ga2 46.54(2) . 1_545 ?
Ga3 Ce1 Ga2 138.292(18) 3 1_545 ?
Ga3 Ce1 Ga2 85.49(2) 4_655 1_545 ?
Ga3 Ce1 Ga2 85.45(2) 9_655 1_545 ?
Ga3 Ce1 Ga2 138.307(18) 10_665 1_545 ?
Ga2 Ce1 Ga2 78.878(18) 11_655 1_545 ?
Ga3 Ni2 Ga3 117.52(4) 4_655 3 ?
Ga3 Ni2 Ga3 105.602(17) 4_655 . ?
Ga3 Ni2 Ga3 105.602(17) 3 . ?
Ga3 Ni2 Ga3 105.601(17) 4_655 2_655 ?

Ga3 Ni2 Ga3 105.601(17) 3 2_655 ?
Ga3 Ni2 Ga3 117.52(4) . 2_655 ?
Ga3 Ni2 Ga3 74.421(15) 4_655 9_655 ?
Ga3 Ni2 Ga3 74.421(15) 3 9_655 ?
Ga3 Ni2 Ga3 62.43(3) . 9_655 ?
Ga3 Ni2 Ga3 179.95(2) 2_655 9_655 ?
Ga3 Ni2 Ga3 74.420(15) 4_655 10_665 ?
Ga3 Ni2 Ga3 74.420(15) 3 10_665 ?
Ga3 Ni2 Ga3 179.95(2) . 10_665 ?
Ga3 Ni2 Ga3 62.43(3) 2_655 10_665 ?
Ga3 Ni2 Ga3 117.62(4) 9_655 10_665 ?
Ga3 Ni2 Ga3 62.43(3) 4_655 12_655 ?
Ga3 Ni2 Ga3 179.95(2) 3 12_655 ?
Ga3 Ni2 Ga3 74.420(15) . 12_655 ?
Ga3 Ni2 Ga3 74.420(15) 2_655 12_655 ?
Ga3 Ni2 Ga3 105.559(17) 9_655 12_655 ?
Ga3 Ni2 Ga3 105.558(17) 10_665 12_655 ?
Ga3 Ni2 Ga3 179.95(2) 4_655 11_665 ?
Ga3 Ni2 Ga3 62.43(3) 3 11_665 ?
Ga3 Ni2 Ga3 74.420(15) . 11_665 ?
Ga3 Ni2 Ga3 74.420(15) 2_655 11_665 ?
Ga3 Ni2 Ga3 105.559(17) 9_655 11_665 ?
Ga3 Ni2 Ga3 105.558(17) 10_665 11_665 ?
Ga3 Ni2 Ga3 117.62(4) 12_655 11_665 ?
Ni2 Ga3 Ni2 117.57(3) . 9_655 ?
Ni2 Ga3 Ga3 58.85(3) . 9_655 ?
Ni2 Ga3 Ga3 58.72(3) 9_655 9_655 ?
Ni2 Ga3 Ga1 107.55(2) . 3 ?
Ni2 Ga3 Ga1 107.45(2) 9_655 3 ?
Ga3 Ga3 Ga1 125.46(3) 9_655 3 ?
Ni2 Ga3 Ga1 107.55(2) . 9_665 ?
Ni2 Ga3 Ga1 107.45(2) 9_655 9_665 ?
Ga3 Ga3 Ga1 125.46(3) 9_655 9_665 ?
Ga1 Ga3 Ga1 109.08(5) 3 9_665 ?
Ni2 Ga3 Ga3 52.84(2) . 12_655 ?
Ni2 Ga3 Ga3 127.180(13) 9_655 12_655 ?
Ga3 Ga3 Ga3 90.06(2) 9_655 12_655 ?
Ga1 Ga3 Ga3 54.834(13) 3 12_655 ?
Ga1 Ga3 Ga3 125.24(3) 9_665 12_655 ?
Ni2 Ga3 Ga3 127.239(13) . 11_655 ?
Ni2 Ga3 Ga3 52.74(2) 9_655 11_655 ?
Ga3 Ga3 Ga3 89.94(2) 9_655 11_655 ?
Ga1 Ga3 Ga3 54.834(13) 3 11_655 ?
Ga1 Ga3 Ga3 125.09(3) 9_665 11_655 ?
Ga3 Ga3 Ga3 90.0 12_655 11_655 ?
Ni2 Ga3 Ga3 52.84(2) . 11_665 ?
Ni2 Ga3 Ga3 127.180(13) 9_655 11_665 ?
Ga3 Ga3 Ga3 90.06(2) 9_655 11_665 ?
Ga1 Ga3 Ga3 125.24(3) 3 11_665 ?
Ga1 Ga3 Ga3 54.834(13) 9_665 11_665 ?
Ga3 Ga3 Ga3 90.11(4) 12_655 11_665 ?
Ga3 Ga3 Ga3 179.89(5) 11_655 11_665 ?
Ni2 Ga3 Ga3 127.239(13) . 12 ?
Ni2 Ga3 Ga3 52.74(2) 9_655 12 ?
Ga3 Ga3 Ga3 89.94(2) 9_655 12 ?
Ga1 Ga3 Ga3 125.09(3) 3 12 ?

Ga1 Ga3 Ga3 54.834(13) 9_665 12 ?
Ga3 Ga3 Ga3 179.89(5) 12_655 12 ?
Ga3 Ga3 Ga3 89.89(4) 11_655 12 ?
Ga3 Ga3 Ga3 90.0 11_665 12 ?
Ni2 Ga3 Ce1 80.74(2) . 3 ?
Ni2 Ga3 Ce1 161.69(3) 9_655 3 ?
Ga3 Ga3 Ce1 139.59(4) 9_655 3 ?
Ga1 Ga3 Ce1 63.85(2) 3 3 ?
Ga1 Ga3 Ce1 63.85(2) 9_665 3 ?
Ga3 Ga3 Ce1 62.690(17) 12_655 3 ?
Ga3 Ga3 Ce1 117.364(8) 11_655 3 ?
Ga3 Ga3 Ce1 62.690(17) 11_665 3 ?
Ga3 Ga3 Ce1 117.364(8) 12 3 ?
Ni2 Ga3 Ce1 161.79(3) . 9_655 ?
Ni2 Ga3 Ce1 80.64(2) 9_655 9_655 ?
Ga3 Ga3 Ce1 139.36(4) 9_655 9_655 ?
Ga1 Ga3 Ce1 63.81(2) 3 9_655 ?
Ga1 Ga3 Ce1 63.81(2) 9_665 9_655 ?
Ga3 Ga3 Ce1 117.341(8) 12_655 9_655 ?
Ga3 Ga3 Ce1 62.604(17) 11_655 9_655 ?
Ga3 Ga3 Ce1 117.341(8) 11_665 9_655 ?
Ga3 Ga3 Ce1 62.604(17) 12 9_655 ?
Ce1 Ga3 Ce1 81.05(2) 3 9_655 ?
Ga2 Ga1 Ga3 125.46(3) . 3 ?
Ga2 Ga1 Ga3 125.46(3) . 10_665 ?
Ga3 Ga1 Ga3 70.33(3) 3 10_665 ?
Ga2 Ga1 Ga3 125.46(3) . 9_665 ?
Ga3 Ga1 Ga3 70.33(3) 3 9_665 ?
Ga3 Ga1 Ga3 109.08(5) 10_665 9_665 ?
Ga2 Ga1 Ga3 125.46(3) . 4_665 ?
Ga3 Ga1 Ga3 109.08(5) 3 4_665 ?
Ga3 Ga1 Ga3 70.33(3) 10_665 4_665 ?
Ga3 Ga1 Ga3 70.33(3) 9_665 4_665 ?
Ga2 Ga1 Ce1 72.07(2) . 11_665 ?
Ga3 Ga1 Ce1 68.353(17) 3 11_665 ?
Ga3 Ga1 Ce1 136.64(2) 10_665 11_665 ?
Ga3 Ga1 Ce1 68.290(17) 9_665 11_665 ?
Ga3 Ga1 Ce1 136.56(2) 4_665 11_665 ?
Ga2 Ga1 Ce1 72.07(2) . . ?
Ga3 Ga1 Ce1 68.290(17) 3 . ?
Ga3 Ga1 Ce1 68.353(17) 10_665 . ?
Ga3 Ga1 Ce1 136.56(2) 9_665 . ?
Ga3 Ga1 Ce1 136.64(2) 4_665 . ?
Ce1 Ga1 Ce1 84.564(14) 11_665 . ?
Ga2 Ga1 Ce1 72.07(2) . 11_765 ?
Ga3 Ga1 Ce1 136.56(2) 3 11_765 ?
Ga3 Ga1 Ce1 68.290(17) 10_665 11_765 ?
Ga3 Ga1 Ce1 136.64(2) 9_665 11_765 ?
Ga3 Ga1 Ce1 68.352(17) 4_665 11_765 ?
Ce1 Ga1 Ce1 144.15(5) 11_665 11_765 ?
Ce1 Ga1 Ce1 84.564(14) . 11_765 ?
Ga2 Ga1 Ce1 72.07(2) . 1_565 ?
Ga3 Ga1 Ce1 136.64(2) 3 1_565 ?
Ga3 Ga1 Ce1 136.56(2) 10_665 1_565 ?
Ga3 Ga1 Ce1 68.352(17) 9_665 1_565 ?
Ga3 Ga1 Ce1 68.290(17) 4_665 1_565 ?

Ce1 Ga1 Ce1 84.563(14) 11_665 1_565 ?
Ce1 Ga1 Ce1 144.15(5) . 1_565 ?
Ce1 Ga1 Ce1 84.563(14) 11_765 1_565 ?
Ga1 Ga2 Ga4 121.79(3) . 12_665 ?
Ga1 Ga2 Ga4 121.79(3) . 1_565 ?
Ga4 Ga2 Ga4 73.89(3) 12_665 1_565 ?
Ga1 Ga2 Ga4 121.79(3) . 2_655 ?
Ga4 Ga2 Ga4 73.89(3) 12_665 2_655 ?
Ga4 Ga2 Ga4 116.42(6) 1_565 2_655 ?
Ga1 Ga2 Ga4 121.79(3) . 11_665 ?
Ga4 Ga2 Ga4 116.42(6) 12_665 11_665 ?
Ga4 Ga2 Ga4 73.89(3) 1_565 11_665 ?
Ga4 Ga2 Ga4 73.89(3) 2_655 11_665 ?
Ga1 Ga2 Ce1 63.95(2) . 11_665 ?
Ga4 Ga2 Ce1 153.81(2) 12_665 11_665 ?
Ga4 Ga2 Ce1 81.82(2) 1_565 11_665 ?
Ga4 Ga2 Ce1 127.23(2) 2_655 11_665 ?
Ga4 Ga2 Ce1 64.24(2) 11_665 11_665 ?
Ga1 Ga2 Ce1 63.95(2) . . ?
Ga4 Ga2 Ce1 127.23(2) 12_665 . ?
Ga4 Ga2 Ce1 153.81(2) 1_565 . ?
Ga4 Ga2 Ce1 64.24(2) 2_655 . ?
Ga4 Ga2 Ce1 81.82(2) 11_665 . ?
Ce1 Ga2 Ce1 78.878(18) 11_665 . ?
Ga1 Ga2 Ce1 63.95(2) . 1_565 ?
Ga4 Ga2 Ce1 81.82(2) 12_665 1_565 ?
Ga4 Ga2 Ce1 64.24(2) 1_565 1_565 ?
Ga4 Ga2 Ce1 153.81(2) 2_655 1_565 ?
Ga4 Ga2 Ce1 127.23(2) 11_665 1_565 ?
Ce1 Ga2 Ce1 78.878(18) 11_665 1_565 ?
Ce1 Ga2 Ce1 127.89(5) . 1_565 ?
Ga1 Ga2 Ce1 63.95(2) . 11_765 ?
Ga4 Ga2 Ce1 64.24(2) 12_665 11_765 ?
Ga4 Ga2 Ce1 127.23(2) 1_565 11_765 ?
Ga4 Ga2 Ce1 81.82(2) 2_655 11_765 ?
Ga4 Ga2 Ce1 153.81(2) 11_665 11_765 ?
Ce1 Ga2 Ce1 127.89(5) 11_665 11_765 ?
Ce1 Ga2 Ce1 78.878(18) . 11_765 ?
Ce1 Ga2 Ce1 78.878(18) 1_565 11_765 ?
Ga4 Ga4 Ga2 110.78(4) 9_656 11_655 ?
Ga4 Ga4 Ga2 110.78(4) 9_656 1_545 ?
Ga2 Ga4 Ga2 109.82(6) 11_655 1_545 ?
Ga4 Ga4 Ce1 180.00(9) 9_656 . ?
Ga2 Ga4 Ce1 69.22(3) 11_655 . ?
Ga2 Ga4 Ce1 69.22(3) 1_545 . ?

_diffrn_measured_fraction_theta_max 0.958
_diffrn_reflns_theta_full 30.01
_diffrn_measured_fraction_theta_full 0.958
_refine_diff_density_max 2.480
_refine_diff_density_min -1.397
_refine_diff_density_rms 0.341

D.4. CIF for Pr_2NiGa_{12}

X-ray Filename: Jasmine21

data_shelxl

```
_audit_creation_method            SHELXL-97
_chemical_name_systematic
;
 ?
;
_chemical_name_common             ?
_chemical_melting_point           ?
_chemical_formula_moiety          ?
_chemical_formula_sum
 'Ga20 Ni Pr'
_chemical_formula_weight          1594.02

loop_
 _atom_type_symbol
 _atom_type_description
 _atom_type_scat_dispersion_real
 _atom_type_scat_dispersion_imag
 _atom_type_scat_source
 'Pr'  'Pr'  -0.2180   2.8214
 'International Tables Vol C Tables 4.2.6.8 and 6.1.1.4'
 'Ni'  'Ni'   0.3393   1.1124
 'International Tables Vol C Tables 4.2.6.8 and 6.1.1.4'
 'Ga'  'Ga'   0.2307   1.6083
 'International Tables Vol C Tables 4.2.6.8 and 6.1.1.4'

_symmetry_cell_setting            ?
_symmetry_space_group_name_H-M    ?

loop_
 _symmetry_equiv_pos_as_xyz
 'x, y, z'
 '-x+1/2, -y+1/2, z'
 'x, -y+1/2, -z'
 '-x+1/2, y, -z'
 '-y+1/2, -x+1/2, -z'
 'y, x, -z'
 'y, -x+1/2, z'
 '-y+1/2, x, z'
 '-x, -y, -z'
 'x-1/2, y-1/2, -z'
 '-x, y-1/2, z'
 'x-1/2, -y, z'
 'y-1/2, x-1/2, z'
 '-y, -x, z'
 '-y, x-1/2, -z'
 'y-1/2, -x, -z'

_cell_length_a                    6.0080(7)
_cell_length_b                    6.0080(7)
```

```
_cell_length_c                    15.454(3)
_cell_angle_alpha                 90.00
_cell_angle_beta                  90.00
_cell_angle_gamma                 90.00
_cell_volume                      557.83(13)
_cell_formula_units_Z             2
_cell_measurement_temperature     298(2)
_cell_measurement_reflns_used     ?
_cell_measurement_theta_min       ?
_cell_measurement_theta_max       ?

_exptl_crystal_description        ?
_exptl_crystal_colour             ?
_exptl_crystal_size_max           0.05
_exptl_crystal_size_mid           0.03
_exptl_crystal_size_min           0.03
_exptl_crystal_density_meas       ?
_exptl_crystal_density_diffrn     9.490
_exptl_crystal_density_method     'not measured'
_exptl_crystal_F_000              1414
_exptl_absorpt_coefficient_mu     53.231
_exptl_absorpt_correction_type    ?
_exptl_absorpt_correction_T_min   0.1761
_exptl_absorpt_correction_T_max   0.3496
_exptl_absorpt_process_details    ?

_exptl_special_details
;
 ?
;

_diffrn_ambient_temperature       298(2)
_diffrn_radiation_wavelength      0.71073
_diffrn_radiation_type            MoK\a
_diffrn_radiation_source          'fine-focus sealed tube'
_diffrn_radiation_monochromator   graphite
_diffrn_measurement_device_type   ?
_diffrn_measurement_method        ?
_diffrn_detector_area_resol_mean  ?
_diffrn_standards_number          ?
_diffrn_standards_interval_count  ?
_diffrn_standards_interval_time   ?
_diffrn_standards_decay_%         ?
_diffrn_reflns_number             933
_diffrn_reflns_av_R_equivalents   0.1161
_diffrn_reflns_av_sigmaI/netI     0.1079
_diffrn_reflns_limit_h_min        -7
_diffrn_reflns_limit_h_max        7
_diffrn_reflns_limit_k_min        -5
_diffrn_reflns_limit_k_max        5
_diffrn_reflns_limit_l_min        -17
_diffrn_reflns_limit_l_max        15
_diffrn_reflns_theta_min          3.96
_diffrn_reflns_theta_max          27.89
_reflns_number_total              346
_reflns_number_gt                 193
_reflns_threshold_expression      >2sigma(I)
```

```
_computing_data_collection        ?
_computing_cell_refinement        ?
_computing_data_reduction         ?
_computing_structure_solution     'SHELXS-97 (Sheldrick, 1990)'
_computing_structure_refinement   'SHELXL-97 (Sheldrick, 1997)'
_computing_molecular_graphics     ?
_computing_publication_material   ?

_refine_special_details
;
 Refinement of F^2^ against ALL reflections.  The weighted R-factor wR and
 goodness of fit S are based on F^2^, conventional R-factors R are based
 on F, with F set to zero for negative F^2^. The threshold expression of
 F^2^ > 2sigma(F^2^) is used only for calculating R-factors(gt) etc. and is
 not relevant to the choice of reflections for refinement.  R-factors based
 on F^2^ are statistically about twice as large as those based on F, and R-
 factors based on ALL data will be even larger.
;

_refine_ls_structure_factor_coef  Fsqd
_refine_ls_matrix_type            full
_refine_ls_weighting_scheme       calc
_refine_ls_weighting_details
 'calc w=1/[\s^2^(Fo^2^)+(0.0556P)^2^+0.0000P] where P=(Fo^2^+2Fc^2^)/3'
_atom_sites_solution_primary      direct
_atom_sites_solution_secondary    difmap
_atom_sites_solution_hydrogens    geom
_refine_ls_hydrogen_treatment     mixed
_refine_ls_extinction_method      SHELXL
_refine_ls_extinction_coef        0.0022(4)
_refine_ls_extinction_expression
 'Fc^*^=kFc[1+0.001xFc^2^\l^3^/sin(2\q)]^-1/4^'
_refine_ls_number_reflns          346
_refine_ls_number_parameters      26
_refine_ls_number_restraints      0
_refine_ls_R_factor_all           0.1105
_refine_ls_R_factor_gt            0.0493
_refine_ls_wR_factor_ref          0.1312
_refine_ls_wR_factor_gt           0.1063
_refine_ls_goodness_of_fit_ref    0.963
_refine_ls_restrained_S_all       0.963
_refine_ls_shift/su_max           0.000
_refine_ls_shift/su_mean          0.000

loop_
 _atom_site_label
 _atom_site_type_symbol
 _atom_site_fract_x
 _atom_site_fract_y
 _atom_site_fract_z
 _atom_site_U_iso_or_equiv
 _atom_site_adp_type
 _atom_site_occupancy
 _atom_site_symmetry_multiplicity
 _atom_site_calc_flag
 _atom_site_refinement_flags
```

```
 _atom_site_disorder_assembly
 _atom_site_disorder_group
Pr1 Pr 0.7500 0.2500 0.24459(11) 0.0067(6) Uani 1 4 d S . .
Ni2 Ni 0.7500 0.2500 0.0000 0.0047(13) Uani 1 8 d S . .
Ga3 Ga 0.5006(3) 0.0006(3) -0.08399(16) 0.0068(7) Uani 1 2 d S . .
Ga1 Ga 0.7500 0.7500 0.1816(2) 0.0088(10) Uani 1 4 d S . .
Ga2 Ga 0.7500 0.7500 0.3394(3) 0.0120(10) Uani 1 4 d S . .
Ga4 Ga 0.5697(4) 0.0697(4) 0.4281(2) 0.0219(10) Uani 1 2 d S . .

loop_
 _atom_site_aniso_label
 _atom_site_aniso_U_11
 _atom_site_aniso_U_22
 _atom_site_aniso_U_33
 _atom_site_aniso_U_23
 _atom_site_aniso_U_13
 _atom_site_aniso_U_12
Pr1 0.0062(8) 0.0062(8) 0.0077(11) 0.000 0.000 0.0006(11)
Ni2 0.005(2) 0.005(2) 0.004(3) 0.000 0.000 0.000
Ga3 0.0071(10) 0.0071(10) 0.0062(15) -0.0003(9) -0.0003(9) -0.0026(11)
Ga1 0.0091(14) 0.0091(14) 0.008(2) 0.000 0.000 0.000
Ga2 0.0137(15) 0.0137(15) 0.009(2) 0.000 0.000 0.000
Ga4 0.0255(13) 0.0255(13) 0.0147(17) 0.0082(12) 0.0082(12) 0.0115(17)

_geom_special_details
;
 All esds (except the esd in the dihedral angle between two l.s. planes)
 are estimated using the full covariance matrix.  The cell esds are taken
 into account individually in the estimation of esds in distances, angles
 and torsion angles; correlations between esds in cell parameters are only
 used when they are defined by crystal symmetry.  An approximate (isotropic)
 treatment of cell esds is used for estimating esds involving l.s. planes.
;

loop_
 _geom_bond_atom_site_label_1
 _geom_bond_atom_site_label_2
 _geom_bond_distance
 _geom_bond_site_symmetry_2
 _geom_bond_publ_flag
Pr1 Ga1 3.1577(13) 11_755 ?
Pr1 Ga1 3.1577(13) . ?
Pr1 Ga1 3.1577(13) 11_655 ?
Pr1 Ga1 3.1577(13) 1_545 ?
Pr1 Ga4 3.223(3) 2_655 ?
Pr1 Ga4 3.223(3) . ?
Pr1 Ga3 3.264(3) 3 ?
Pr1 Ga3 3.264(3) 4_655 ?
Pr1 Ga3 3.270(3) 10_665 ?
Pr1 Ga3 3.270(3) 9_655 ?
Pr1 Ga2 3.3420(19) 11_755 ?
Pr1 Ga2 3.3420(19) . ?
Ni2 Ga3 2.485(3) 2_655 ?
Ni2 Ga3 2.485(3) . ?
Ni2 Ga3 2.485(3) 4_655 ?
Ni2 Ga3 2.485(3) 3 ?
Ni2 Ga3 2.494(3) 12_655 ?
```

```
Ni2 Ga3 2.494(3) 11_665 ?
Ni2 Ga3 2.494(3) 10_665 ?
Ni2 Ga3 2.494(3) 9_655 ?
Ga3 Ni2 2.494(3) 9_655 ?
Ga3 Ga3 2.596(5) 9_655 ?
Ga3 Ga1 2.605(3) 3 ?
Ga3 Ga1 2.605(3) 9_665 ?
Ga3 Ga3 3.0040(4) 12_655 ?
Ga3 Ga3 3.0040(4) 11_655 ?
Ga3 Ga3 3.0040(4) 11_665 ?
Ga3 Ga3 3.0040(4) 12 ?
Ga3 Pr1 3.264(3) 3 ?
Ga3 Pr1 3.270(3) 9_655 ?
Ga1 Ga2 2.438(5) . ?
Ga1 Ga3 2.605(3) 4_665 ?
Ga1 Ga3 2.605(3) 10_665 ?
Ga1 Ga3 2.605(3) 9_665 ?
Ga1 Ga3 2.605(3) 3 ?
Ga1 Pr1 3.1577(13) 11_765 ?
Ga1 Pr1 3.1577(13) 1_565 ?
Ga1 Pr1 3.1577(13) 11_665 ?
Ga2 Ga4 2.597(3) 12_665 ?
Ga2 Ga4 2.597(3) 1_565 ?
Ga2 Ga4 2.597(3) 2_655 ?
Ga2 Ga4 2.597(3) 11_665 ?
Ga2 Pr1 3.3420(19) 11_765 ?
Ga2 Pr1 3.3420(19) 1_565 ?
Ga2 Pr1 3.3420(19) 11_665 ?
Ga4 Ga4 2.518(6) 9_656 ?
Ga4 Ga2 2.597(3) 11_655 ?
Ga4 Ga2 2.597(3) 1_545 ?

loop_
 _geom_angle_atom_site_label_1
 _geom_angle_atom_site_label_2
 _geom_angle_atom_site_label_3
 _geom_angle
 _geom_angle_site_symmetry_1
 _geom_angle_site_symmetry_3
 _geom_angle_publ_flag
Ga1 Pr1 Ga1 84.55(4) 11_755 . ?
Ga1 Pr1 Ga1 144.10(14) 11_755 11_655 ?
Ga1 Pr1 Ga1 84.55(4) . 11_655 ?
Ga1 Pr1 Ga1 84.55(4) 11_755 1_545 ?
Ga1 Pr1 Ga1 144.10(14) . 1_545 ?
Ga1 Pr1 Ga1 84.55(4) 11_655 1_545 ?
Ga1 Pr1 Ga4 87.22(8) 11_755 2_655 ?
Ga1 Pr1 Ga4 87.22(8) . 2_655 ?
Ga1 Pr1 Ga4 126.22(8) 11_655 2_655 ?
Ga1 Pr1 Ga4 126.22(8) 1_545 2_655 ?
Ga1 Pr1 Ga4 126.22(8) 11_755 . ?
Ga1 Pr1 Ga4 126.22(8) . . ?
Ga1 Pr1 Ga4 87.22(8) 11_655 . ?
Ga1 Pr1 Ga4 87.22(8) 1_545 . ?
Ga4 Pr1 Ga4 56.76(14) 2_655 . ?
Ga1 Pr1 Ga3 101.68(8) 11_755 3 ?
Ga1 Pr1 Ga3 47.84(6) . 3 ?
```

```
Ga1 Pr1 Ga3 47.84(6) 11_655 3 ?
Ga1 Pr1 Ga3 101.68(8) 1_545 3 ?
Ga4 Pr1 Ga3 132.00(5) 2_655 3 ?
Ga4 Pr1 Ga3 132.00(5) . 3 ?
Ga1 Pr1 Ga3 47.84(6) 11_755 4_655 ?
Ga1 Pr1 Ga3 101.68(8) . 4_655 ?
Ga1 Pr1 Ga3 101.68(8) 11_655 4_655 ?
Ga1 Pr1 Ga3 47.84(6) 1_545 4_655 ?
Ga4 Pr1 Ga3 132.00(5) 2_655 4_655 ?
Ga4 Pr1 Ga3 132.00(5) . 4_655 ?
Ga3 Pr1 Ga3 80.99(10) 3 4_655 ?
Ga1 Pr1 Ga3 47.78(6) 11_755 10_665 ?
Ga1 Pr1 Ga3 47.78(6) . 10_665 ?
Ga1 Pr1 Ga3 101.77(8) 11_655 10_665 ?
Ga1 Pr1 Ga3 101.77(8) 1_545 10_665 ?
Ga4 Pr1 Ga3 110.99(8) 2_655 10_665 ?
Ga4 Pr1 Ga3 167.76(9) . 10_665 ?
Ga3 Pr1 Ga3 54.75(4) 3 10_665 ?
Ga3 Pr1 Ga3 54.75(4) 4_655 10_665 ?
Ga1 Pr1 Ga3 101.77(8) 11_755 9_655 ?
Ga1 Pr1 Ga3 101.77(8) . 9_655 ?
Ga1 Pr1 Ga3 47.78(6) 11_655 9_655 ?
Ga1 Pr1 Ga3 47.78(6) 1_545 9_655 ?
Ga4 Pr1 Ga3 167.76(9) 2_655 9_655 ?
Ga4 Pr1 Ga3 110.99(8) . 9_655 ?
Ga3 Pr1 Ga3 54.75(4) 3 9_655 ?
Ga3 Pr1 Ga3 54.75(4) 4_655 9_655 ?
Ga3 Pr1 Ga3 81.25(10) 10_665 9_655 ?
Ga1 Pr1 Ga2 43.94(9) 11_755 11_755 ?
Ga1 Pr1 Ga2 97.76(3) . 11_755 ?
Ga1 Pr1 Ga2 171.96(11) 11_655 11_755 ?
Ga1 Pr1 Ga2 97.76(3) 1_545 11_755 ?
Ga4 Pr1 Ga2 46.55(6) 2_655 11_755 ?
Ga4 Pr1 Ga2 85.22(9) . 11_755 ?
Ga3 Pr1 Ga2 138.24(5) 3 11_755 ?
Ga3 Pr1 Ga2 85.44(6) 4_655 11_755 ?
Ga3 Pr1 Ga2 85.34(6) 10_665 11_755 ?
Ga3 Pr1 Ga2 138.28(5) 9_655 11_755 ?
Ga1 Pr1 Ga2 97.76(3) 11_755 . ?
Ga1 Pr1 Ga2 43.94(9) . . ?
Ga1 Pr1 Ga2 97.76(3) 11_655 . ?
Ga1 Pr1 Ga2 171.96(11) 1_545 . ?
Ga4 Pr1 Ga2 46.55(6) 2_655 . ?
Ga4 Pr1 Ga2 85.22(9) . . ?
Ga3 Pr1 Ga2 85.44(6) 3 . ?
Ga3 Pr1 Ga2 138.24(5) 4_655 . ?
Ga3 Pr1 Ga2 85.34(6) 10_665 . ?
Ga3 Pr1 Ga2 138.28(5) 9_655 . ?
Ga2 Pr1 Ga2 78.93(5) 11_755 . ?
Ga3 Ni2 Ga3 117.03(12) 2_655 . ?
Ga3 Ni2 Ga3 105.83(5) 2_655 4_655 ?
Ga3 Ni2 Ga3 105.83(5) . 4_655 ?
Ga3 Ni2 Ga3 105.83(5) 2_655 3 ?
Ga3 Ni2 Ga3 105.83(5) . 3 ?
Ga3 Ni2 Ga3 117.02(12) 4_655 3 ?
Ga3 Ni2 Ga3 74.22(5) 2_655 12_655 ?
Ga3 Ni2 Ga3 74.22(5) . 12_655 ?
```

```
Ga3 Ni2 Ga3 62.86(10) 4_655 12_655 ?
Ga3 Ni2 Ga3 179.88(8) 3 12_655 ?
Ga3 Ni2 Ga3 74.22(5) 2_655 11_665 ?
Ga3 Ni2 Ga3 74.22(5) . 11_665 ?
Ga3 Ni2 Ga3 179.88(8) 4_655 11_665 ?
Ga3 Ni2 Ga3 62.86(10) 3 11_665 ?
Ga3 Ni2 Ga3 117.26(12) 12_655 11_665 ?
Ga3 Ni2 Ga3 62.86(10) 2_655 10_665 ?
Ga3 Ni2 Ga3 179.88(8) . 10_665 ?
Ga3 Ni2 Ga3 74.22(5) 4_655 10_665 ?
Ga3 Ni2 Ga3 74.22(5) 3 10_665 ?
Ga3 Ni2 Ga3 105.72(5) 12_655 10_665 ?
Ga3 Ni2 Ga3 105.72(5) 11_665 10_665 ?
Ga3 Ni2 Ga3 179.88(8) 2_655 9_655 ?
Ga3 Ni2 Ga3 62.86(10) . 9_655 ?
Ga3 Ni2 Ga3 74.22(5) 4_655 9_655 ?
Ga3 Ni2 Ga3 74.22(5) 3 9_655 ?
Ga3 Ni2 Ga3 105.72(5) 12_655 9_655 ?
Ga3 Ni2 Ga3 105.72(5) 11_665 9_655 ?
Ga3 Ni2 Ga3 117.26(12) 10_665 9_655 ?
Ni2 Ga3 Ni2 117.14(10) . 9_655 ?
Ni2 Ga3 Ga3 58.73(10) . 9_655 ?
Ni2 Ga3 Ga3 58.41(10) 9_655 9_655 ?
Ni2 Ga3 Ga1 107.70(8) . 3 ?
Ni2 Ga3 Ga1 107.45(8) 9_655 3 ?
Ga3 Ga3 Ga1 125.38(8) 9_655 3 ?
Ni2 Ga3 Ga1 107.70(8) . 9_665 ?
Ni2 Ga3 Ga1 107.45(8) 9_655 9_665 ?
Ga3 Ga3 Ga1 125.38(8) 9_655 9_665 ?
Ga1 Ga3 Ga1 109.23(16) 3 9_665 ?
Ni2 Ga3 Ga3 53.02(7) . 12_655 ?
Ni2 Ga3 Ga3 127.04(5) 9_655 12_655 ?
Ga3 Ga3 Ga3 90.15(8) 9_655 12_655 ?
Ga1 Ga3 Ga3 54.80(4) 3 12_655 ?
Ga1 Ga3 Ga3 125.39(11) 9_665 12_655 ?
Ni2 Ga3 Ga3 127.19(5) . 11_655 ?
Ni2 Ga3 Ga3 52.76(7) 9_655 11_655 ?
Ga3 Ga3 Ga3 89.85(8) 9_655 11_655 ?
Ga1 Ga3 Ga3 54.80(4) 3 11_655 ?
Ga1 Ga3 Ga3 125.02(11) 9_665 11_655 ?
Ga3 Ga3 Ga3 90.0 12_655 11_655 ?
Ni2 Ga3 Ga3 53.02(7) . 11_665 ?
Ni2 Ga3 Ga3 127.04(5) 9_655 11_665 ?
Ga3 Ga3 Ga3 90.15(8) 9_655 11_665 ?
Ga1 Ga3 Ga3 125.39(11) 3 11_665 ?
Ga1 Ga3 Ga3 54.80(4) 9_665 11_665 ?
Ga3 Ga3 Ga3 90.27(14) 12_655 11_665 ?
Ga3 Ga3 Ga3 179.73(15) 11_655 11_665 ?
Ni2 Ga3 Ga3 127.19(5) . 12 ?
Ni2 Ga3 Ga3 52.76(7) 9_655 12 ?
Ga3 Ga3 Ga3 89.85(8) 9_655 12 ?
Ga1 Ga3 Ga3 125.02(11) 3 12 ?
Ga1 Ga3 Ga3 54.80(4) 9_665 12 ?
Ga3 Ga3 Ga3 179.73(15) 12_655 12 ?
Ga3 Ga3 Ga3 89.73(14) 11_655 12 ?
Ga3 Ga3 Ga3 90.0 11_665 12 ?
Ni2 Ga3 Pr1 80.99(7) . 3 ?
```

```
Ni2 Ga3 Pr1 161.86(10) 9_655 3 ?
Ga3 Ga3 Pr1 139.72(16) 9_655 3 ?
Ga1 Ga3 Pr1 63.95(7) 3 3 ?
Ga1 Ga3 Pr1 63.95(7) 9_665 3 ?
Ga3 Ga3 Pr1 62.74(6) 12_655 3 ?
Ga3 Ga3 Pr1 117.40(3) 11_655 3 ?
Ga3 Ga3 Pr1 62.74(6) 11_665 3 ?
Ga3 Ga3 Pr1 117.40(3) 12 3 ?
Ni2 Ga3 Pr1 162.11(11) . 9_655 ?
Ni2 Ga3 Pr1 80.74(7) 9_655 9_655 ?
Ga3 Ga3 Pr1 139.16(16) 9_655 9_655 ?
Ga1 Ga3 Pr1 63.85(7) 3 9_655 ?
Ga1 Ga3 Pr1 63.85(7) 9_665 9_655 ?
Ga3 Ga3 Pr1 117.34(3) 12_655 9_655 ?
Ga3 Ga3 Pr1 62.52(6) 11_655 9_655 ?
Ga3 Ga3 Pr1 117.34(3) 11_665 9_655 ?
Ga3 Ga3 Pr1 62.52(6) 12 9_655 ?
Pr1 Ga3 Pr1 81.12(7) 3 9_655 ?
Ga2 Ga1 Ga3 125.38(8) . 4_665 ?
Ga2 Ga1 Ga3 125.38(8) . 10_665 ?
Ga3 Ga1 Ga3 70.41(8) 4_665 10_665 ?
Ga2 Ga1 Ga3 125.38(8) . 9_665 ?
Ga3 Ga1 Ga3 70.41(8) 4_665 9_665 ?
Ga3 Ga1 Ga3 109.23(16) 10_665 9_665 ?
Ga2 Ga1 Ga3 125.38(8) . 3 ?
Ga3 Ga1 Ga3 109.23(16) 4_665 3 ?
Ga3 Ga1 Ga3 70.41(8) 10_665 3 ?
Ga3 Ga1 Ga3 70.41(8) 9_665 3 ?
Ga2 Ga1 Pr1 72.05(7) . 11_765 ?
Ga3 Ga1 Pr1 68.37(6) 4_665 11_765 ?
Ga3 Ga1 Pr1 68.21(6) 10_665 11_765 ?
Ga3 Ga1 Pr1 136.73(8) 9_665 11_765 ?
Ga3 Ga1 Pr1 136.52(8) 3 11_765 ?
Ga2 Ga1 Pr1 72.05(7) . 1_565 ?
Ga3 Ga1 Pr1 68.21(6) 4_665 1_565 ?
Ga3 Ga1 Pr1 136.52(8) 10_665 1_565 ?
Ga3 Ga1 Pr1 68.37(6) 9_665 1_565 ?
Ga3 Ga1 Pr1 136.73(8) 3 1_565 ?
Pr1 Ga1 Pr1 84.55(4) 11_765 1_565 ?
Ga2 Ga1 Pr1 72.05(7) . . ?
Ga3 Ga1 Pr1 136.73(8) 4_665 . ?
Ga3 Ga1 Pr1 68.36(6) 10_665 . ?
Ga3 Ga1 Pr1 136.52(8) 9_665 . ?
Ga3 Ga1 Pr1 68.21(6) 3 . ?
Pr1 Ga1 Pr1 84.55(4) 11_765 . ?
Pr1 Ga1 Pr1 144.10(14) 1_565 . ?
Ga2 Ga1 Pr1 72.05(7) . 11_665 ?
Ga3 Ga1 Pr1 136.52(8) 4_665 11_665 ?
Ga3 Ga1 Pr1 136.73(8) 10_665 11_665 ?
Ga3 Ga1 Pr1 68.21(6) 9_665 11_665 ?
Ga3 Ga1 Pr1 68.36(6) 3 11_665 ?
Pr1 Ga1 Pr1 144.10(14) 11_765 11_665 ?
Pr1 Ga1 Pr1 84.55(4) 1_565 11_665 ?
Pr1 Ga1 Pr1 84.55(4) . 11_665 ?
Ga1 Ga2 Ga4 121.88(9) . 12_665 ?
Ga1 Ga2 Ga4 121.88(9) . 1_565 ?
Ga4 Ga2 Ga4 73.81(9) 12_665 1_565 ?
```

```
Ga1 Ga2 Ga4 121.88(9) . 2_655 ?
Ga4 Ga2 Ga4 73.81(9) 12_665 2_655 ?
Ga4 Ga2 Ga4 116.24(19) 1_565 2_655 ?
Ga1 Ga2 Ga4 121.88(9) . 11_665 ?
Ga4 Ga2 Ga4 116.25(19) 12_665 11_665 ?
Ga4 Ga2 Ga4 73.81(9) 1_565 11_665 ?
Ga4 Ga2 Ga4 73.81(9) 2_655 11_665 ?
Ga1 Ga2 Pr1 64.01(7) . 11_765 ?
Ga4 Ga2 Pr1 64.32(7) 12_665 11_765 ?
Ga4 Ga2 Pr1 127.33(8) 1_565 11_765 ?
Ga4 Ga2 Pr1 81.74(7) 2_655 11_765 ?
Ga4 Ga2 Pr1 153.67(9) 11_665 11_765 ?
Ga1 Ga2 Pr1 64.01(7) . 1_565 ?
Ga4 Ga2 Pr1 81.74(7) 12_665 1_565 ?
Ga4 Ga2 Pr1 64.32(7) 1_565 1_565 ?
Ga4 Ga2 Pr1 153.67(9) 2_655 1_565 ?
Ga4 Ga2 Pr1 127.33(8) 11_665 1_565 ?
Pr1 Ga2 Pr1 78.93(5) 11_765 1_565 ?
Ga1 Ga2 Pr1 64.01(7) . . ?
Ga4 Ga2 Pr1 127.33(8) 12_665 . ?
Ga4 Ga2 Pr1 153.67(9) 1_565 . ?
Ga4 Ga2 Pr1 64.32(7) 2_655 . ?
Ga4 Ga2 Pr1 81.74(7) 11_665 . ?
Pr1 Ga2 Pr1 78.93(5) 11_765 . ?
Pr1 Ga2 Pr1 128.02(13) 1_565 . ?
Ga1 Ga2 Pr1 64.01(7) . 11_665 ?
Ga4 Ga2 Pr1 153.67(9) 12_665 11_665 ?
Ga4 Ga2 Pr1 81.74(7) 1_565 11_665 ?
Ga4 Ga2 Pr1 127.33(8) 2_655 11_665 ?
Ga4 Ga2 Pr1 64.32(7) 11_665 11_665 ?
Pr1 Ga2 Pr1 128.02(13) 11_765 11_665 ?
Pr1 Ga2 Pr1 78.93(5) 1_565 11_665 ?
Pr1 Ga2 Pr1 78.93(5) . 11_665 ?
Ga4 Ga4 Ga2 111.03(14) 9_656 11_655 ?
Ga4 Ga4 Ga2 111.03(14) 9_656 1_545 ?
Ga2 Ga4 Ga2 109.77(18) 11_655 1_545 ?
Ga4 Ga4 Pr1 179.7(3) 9_656 . ?
Ga2 Ga4 Pr1 69.13(9) 11_655 . ?
Ga2 Ga4 Pr1 69.13(9) 1_545 . ?

_diffrn_measured_fraction_theta_max    0.896
_diffrn_reflns_theta_full              27.89
_diffrn_measured_fraction_theta_full   0.896
_refine_diff_density_max    4.359
_refine_diff_density_min   -2.889
_refine_diff_density_rms    0.687
```

APPENDIX E: LETTERS OF PERMISSION

Dear Jasmine N Millican
We hereby grant you permission to reprint the material detailed below at no charge in your thesis subject to the following conditions:

1. If any part of the material to be used (for example, figures) has appeared in our publication with credit or acknowledgement to another source, permission must also be sought from that source. If such permission is not obtained then that material may not be included in your publication/copies.

2. Suitable acknowledgment to the source must be made, either as a footnote or in a reference list at the end of your publication, as follows:

"Reprinted from Publication title, Vol number, Author(s), Title of article, Pages No., Copyright (Year), with permission from Elsevier".

3. Your thesis may be submitted to your institution in either print or electronic form.

4. Reproduction of this material is confined to the purpose for which permission is hereby given.

5. This permission is granted for non-exclusive world English rights only. For other languages please reapply separately for each one required. permission excludes use in an electronic form other than submission. Should you have a specific electronic project in mind please reapply for permission

6. This includes permission for UMI to supply single copies, on demand, of the complete thesis. Should your thesis be published commercially, please reapply for permission.

Yours sincerely

Jennifer Jones
Rights Assistant

Dear Jasmine N Millican

We hereby grant you permission to reprint the material detailed below at no charge **in your thesis** subject to the following conditions:

1. If any part of the material to be used (for example, figures) has appeared in our publication with credit or acknowledgement to another source, permission must also be sought from that source. If such permission is not obtained then that material may not be included in your publication/copies.

2. Suitable acknowledgment to the source must be made, either as a footnote or in a reference list at the end of your publication, as follows:

   "Reprinted from Publication title, Vol number, Author(s), Title of article, Pages No., Copyright (Year), with permission from Elsevier".

3. Your thesis may be submitted to your institution in either print or electronic form.

4. Reproduction of this material is confined to the purpose for which permission is hereby given.

5. This permission is granted for non-exclusive world **English** rights only. For other languages please reapply separately for each one required. Permission excludes use in an electronic form other than submission. Should you have a specific electronic project in mind please reapply for permission

6. This includes permission for UMI to supply single copies, on demand, of the complete thesis. Should your thesis be published commercially, please reapply for permission.

Yours sincerely

Jennifer Jones
Rights Assistant

Taylor & Francis Group
an **informa** business

Taylor & Francis' position on Copyright and Author Rights

Introduction

For over two hundred years, Taylor & Francis have sought to achieve the widest dissemination of new research knowledge via our scholarly journals. We continue to support the widest possible access to the scientific, scholarly and medical literature through innovative and creative publishing policy and practice, founded on the highest standards of peer review.

Taylor & Francis, and the scholarly and professional associations with whom we work, are committed to good stewardship of the scholarly record, and to managing authors' Intellectual Property Rights (IPR) as these are associated with their article. Such articles are normally the primary written report of the results of a scientific research project. Such research may be supported by funding from Government or commercial sources. It may be conducted by a single research group from a single institution, or may be the outcome of collaborative working between institutions on a global scale. Such research in its written form, has been submitted for consideration to a Taylor & Francis journal, and is then subject to that journals rigorous peer review. If acceptable after revision in the light of referees' comments, then that research is published in its final and definitive form, for the first time, by Taylor & Francis in a Taylor & Francis journal, or in a journal published by Taylor & Francis on behalf of a scholarly or professional association.

This is the version of scholarly record, and in its online form will be fully reference-linked. Taylor & Francis has added value to this version – editing to a style consistent with linking conventions, converting to a suitable digital form, putting in the digital reference links and meta-tags for feeds to abstracting and indexing services, registering the digital object identifier (DOI), and monitoring electronic usage.

In all our activities, we are working for the benefit of authors to ensure maximum access to and use of their articles, and to ensure that authors may gain from the goodwill associated with publishing in a Taylor & Francis journal. Yet we are also seeking to enhance the reputation and prestige of the Journal, its editors and editorial board, its peer review processes, and the added value brought by the journal and its publisher.

The rights that you retain as Author

In assigning Taylor & Francis or the journal proprietor copyright, or granting an exclusive licence to publish, you retain:

1. the right to be identified as the Author of an article whenever and wherever the Article is published;

2. patent rights, trademark rights, or rights to any process, product or procedure described in an article;

3. the right to share with colleagues print or electronic 'preprints' (i.e., versions of the article created prior to peer review) of an unpublished Article, perhaps in the form and content as submitted for publication;

4. always providing that the editorial policy of the journal concerned allows this within its policies on prior publication, the right to post such a 'preprint' on your own website, or on your institution's intranet, or within the Institutional Repository of your institution or company of employment, on the following condition, and with the following acknowledgement: This is a preprint of an article submitted for consideration in the [JOURNAL TITLE] © [year of publication] [copyright Taylor & Francis]; [JOURNAL TITLE} is available online at: **http://www.informaworld.com/** with the open URL of your article, which would be the following address:

   http://www.informaworld.com/openurl?genre=article&issn=[paper issn]&volume=[volume number]&issue=[issue number]&spage=[starting page of article]

10. the right to include an article in a thesis or dissertation that is not to be published commercially, provided that acknowledgement to prior publication in the relevant Taylor & Francis journal is made explicit;

AMERICAN PHYSICAL SOCIETY
One Physics Ellipse, College Park, MD 20740 - http://www.aps.org

February 20, 2007

Jasmine Millican
jnmillican@gmail.com

Ref #4704

Thank you for your permission request dated February 18, 2007. We are pleased to grant you non-exclusive, non-transferable permission, English rights, but limited to **print format** only, provided you meet the criteria outlined below. Permission is for one-time use and does not include permission for future editions, additional printings, updates, any electronic forms, databases, translations, or any other matters. Permission must be sought for each additional use. This permission does not include the right to modify APS material.

Please print the required copyright credit line on the first page that the material appears: "Reprinted (abstract/excerpt/figure) with permission from [FULL REFERENCE CITATION] as follows: authors names, journal title, volume number, page number and year of publication. Copyright (YEAR) by the American Physical Society.

You must also obtain permission from at least one of the authors for each separate work, if you haven't done so already. The author's name and address can be found on the first page of the published Article.

Use of the APS material must not imply any endorsement by the American Physical Society.

Permission is granted for use of the following APS material only:

- Phys. Rev. Lett. Vol. 74, 224431 (2006)

Permission is limited to the single title specified or single edition of the publication as follows:

- Dissertation by Jasmine Millican

If you have any questions, please refer to the Copyright FAQ at: http://forms.aps.org/author/copyfaq.html or contact me at assocpub@aps.org.

Sincerely,

Eileen LaManca

Eileen LaManca
Marketing Assistant

VITA

Jasmine N. Millican was born on August 5, 1980, in Baton Rouge, Louisiana, and raised under the guidance of her parents Shermaine Millican Thomas and Kemp Thomas, III. She is the oldest of two siblings, Kandace R. Thomas and Angela C. Thomas. She graduated from Scotlandville Magnet High School in June of 1998. In the Fall of 1998, Jasmine attended Southern University and Agricultural and Mechanical College, where she received various academic honors and was a Timbuktu Scholar, LAMP Scholar, and an Honors student. She received her Bachelor of Science Degree in chemistry from Southern University and Agricultural and Mechanical College on July 27, 2002.

In the Fall of 2002, Jasmine began her graduate career at Louisiana State University and Agricultural and Mechanical College. Under the tutelage of her advisor, Dr. Julia Y. Chan, Jasmine's graduate studies concentrated on the growth and characterization of novel intermetallic materials with exotic physical behavior. During Jasmine's 4 ½ year period in Dr. Julia Y. Chan's solid state research group, she was first author of 3 peer-reviewed publications and co-author of 5 peer-reviewed publications. Jasmine received various awards and honors, such as the Procter and Gamble research award in 2004, American Crystallographic Association Travel Award in 2005, and the Coates Travel Award in September of 2006. Jasmine was selected to present at the XX Congress of the International Union of Crystallography (IUCr) Meeting held in Florence, Italy, in August 2005. Jasmine also presented her scientific research at several national conferences, such as the Materials Research Society Meeting held in Boston, Massachusetts, in November of 2004 and the American Chemical Society Meeting held in San Francisco, California, in September of 2006. During a two week period from August 13-27 in 2006, Jasmine was also selected to participate in the National School on Neutron and X-ray

Scattering at Argonne National Laboratory in Chicago, Illinois. During her reign at Louisiana State University and Agricultural and Mechanical College, Jasmine also enjoyed community service projects, such as performing chemistry demonstrations at various local elementary schools.